DYNAMIC RESPONSE OF BRIDGES TO NEAR-FAULT, FORWARD DIRECTIVITY GROUND MOTIONS

WA-RD 689.1

Research Report
April 2008

Washington State
Department of Transportation

Research Report
Agreement 355270, Task 6
Near-Fault Ground Motions

DYNAMIC RESPONSE OF BRIDGES TO NEAR-FAULT, FORWARD DIRECTIVITY GROUND MOTIONS

by

Adrian Rodriguez-Marek
Associate Professor

William Cofer
Professor

Civil and Environmental Engineering Department
Washington State University
Pullman, WA 99164

Washington State Transportation Center (TRAC)
Washington State University
Civil & Environmental Engineering
PO Box 642910
Pullman, WA 99164-2910

Washington State Department of Transportation Technical Monitor
Kim Willoughby
Research Manager Materials and Construction, Bridges and Structures and Maintenance

Prepared for

Washington State Transportation Commission
Department of Transportation
and in cooperation with
U.S. Department of Transportation
Federal Highway Administration

December 2007

1. REPORT NO.	2. GOVERNMENT ACCESSION NO.	3. RECIPIENT'S CATALOG NO.
WA-RD 689.1		

4. TITLE AND SUBTITLE	5. REPORT DATE
DYNAMIC RESPONSE OF BRIDGES TO NEAR-FAULT, FORWARD DIRECTIVITY GROUND MOTIONS	December 2007
	6. PERFORMING ORGANIZATION CODE
7. AUTHOR(S)	8. PERFORMING ORGANIZATION REPORT NO.
Adrian Rodriguez-Marek and William Cofer	
9. PERFORMING ORGANIZATION NAME AND ADDRESS	10. WORK UNIT NO.
Washington State Transportation Center (TRAC) Washington State University, Civil & Environmental Engineering PO Box 642910 Pullman, WA 99164-2910	11. CONTRACT OR GRANT NO. WSDOT 355270, Task 6
12. SPONSORING AGENCY NAME AND ADDRESS	13. TYPE OF REPORT AND PERIOD COVERED
Research Office Washington State Department of Transportation Transportation Building, MS 47372 Olympia, Washington 98504-7372	Research Report
	14. SPONSORING AGENCY CODE

15. SUPPLEMENTARY NOTES

This study was conducted in cooperation with the U.S. Department of Transportation, Federal Highway Administration.

16. ABSTRACT

Research over the last decade has shown that pulse-type earthquake ground motions that result from forward-directivity (FD) effects can result in significant damage to structures. Three typical post-1990 Washington State Department of Transportation (WSDOT) monolithic concrete bridges were chosen to investigate their nonlinear response to FD ground motions (FDGMs) and non-FDGMs. Results showed that significant seismic damage may occur if the structural response is in tune with the period of the velocity pulse of the FDGM. This velocity pulse is a result of fault propagation effects in the near-fault, and occurs when the direction of slip and rupture propagation coincide. The period of the velocity pulse is proportional to the magnitude of the earthquake. The severity of the demand is controlled by the ratio of the pulse period to bridge fundamental periods. As a consequence of this, damage in a bridge with moderate periods (T=0.1s to 1.0s) may be more significant in smaller magnitude earthquakes where the pulse period is closer to the fundamental period of the structure. This was the case for both the MDOF and SDOF analyses of all three bridges in this research. The results showed also that the occurrence of high PGA and/or PGV is only one of several conditions that can cause high demand on the bridges.

Of the three bridges considered, all typical concrete overpasses ranging from 50 m to 91 m in length, all generally survived the earthquake motions with only minor damage to their columns. However, column flexural failure was predicted for one model when subjected to two of the forward directivity ground motions.

SDOF bridge models for preliminary analyses were found to yield slightly unconservative base shears and displacements compared to that of the full bridge models under non-FDGM. For FDGM, the results of a simple SDOF bridge model ranged from very conservative to slightly unconservative. Therefore, nonlinear SDOF analyses are specifically not recommended in the case of FDGM since the results were not consistent. A more detailed MDOF model should be used to assess bridge seismic performance so that SSI and the interaction of the longitudinal and transverse responses of the bridges can be included, particularly if a performance based design or assessment of the bridge is required.

17. KEY WORDS	18. DISTRIBUTION STATEMENT
Earthquakes, Ground Motions, Near-Fault, Forward-Directivity, Dynamic Response, Bridges	No restrictions. This document is available to the public through the National Technical Information Service, Springfield, VA 22616

19. SECURITY CLASSIF. (of this report)	20. SECURITY CLASSIF. (of this page)	21. NO. OF PAGES	22. PRICE
None	None	84	

DISCLAIMER

The contents of this report reflect the views of the authors, who are responsible for the facts and the accuracy of the data presented herein. The contents do not necessarily reflect the official views or policies of the Washington State Transportation Commmission, Department of Transportation, or the Federal Highway Administration. This report does not constitute a standard, specification, or regulation.

CONTENTS

FIGURES

TABLES

EXECUTIVE SUMMARY

Research over the last decade has shown that pulse-type earthquake ground motions that result from forward-directivity effects can result in significant damage to structures. Furthermore, analytical models indicate that traditional analysis methods are insufficient to capture the full effects of pulse-type ground motions. Fortunately, the recent increase in the number of recorded ground motions has allowed a better characterization of these near-fault, forward-directivity ground motions (FDGMs). The objective of this research is to use the wealth of recent ground motion data to improve the understanding of the response of typical reinforced concrete and precast concrete bridges to pulse-type ground motions that result from forward-directivity effects.

Three typical post-1990 Washington State Department of Transportation (WSDOT) monolithic concrete bridges were chosen to investigate their nonlinear response to FDGMs and non-FDGMs. Results showed that significant seismic damage may occur if the structural response is in tune with the period of the velocity pulse of the FDGM. This velocity pulse is a result of fault propagation effects in the near-fault, and occurs when the direction of slip and rupture propagation coincide. The period of the velocity pulse is proportional to the magnitude of the earthquake. The severity of the demand is controlled by the ratio of the pulse period to bridge fundamental periods. As a consequence of this, damage in a bridge with moderate periods (T=0.1s to 1.0s) may be more significant in smaller magnitude earthquakes where the pulse period is closer to the fundamental period of the structure. This was the case for both the MDOF and SDOF analyses of all three bridges in this research. The results showed also that the occurrence of high PGA and/or PGV is only one of several conditions that can cause high demand on the bridges.

The nonlinear time history analyses results from ABAQUS showed that most of the damage in the bridge columns during FDGMs occurred at the beginning of the record in response to the double-sided velocity pulse. Therefore, a simple ground motion consisting of a sinusoidal single pulse may be sufficient to evaluate bridge performance for FDGMs.

The three bridges considered, Bridge 90, Bridge 405, and Bridge 520, all typical concrete overpasses ranging from 50 m to 91 m in length, generally survived the earthquake motions with only minor damage to their columns. However, column flexural failure was predicted for the Bridge 90 model

when subjected to two of the forward directivity ground motions. The maximum curvature capacity of one of the four columns was reached. The bridge models often indicated distress at the abutments, including pounding, violation of abutment strength limits, and significant movement at the bearing pads. The risk of the deck exceeding the abutment bearing pad displacement capacity was high for Bridge 90 under forward directivity ground motion. The abutment strength limit was often reached, corresponding to an excessive pressure from the abutment on its surrounding soil.

The use of the acceleration response spectra to compute the expected response of the bridges in terms of maximum base shears and relative displacements was found to yield mixed responses for non-FD and FDGMs. Care must be taken in the choice of the response modification factor (or R-Factor) to include the inelasticity effect on the maximum base shear in the columns. The performance of the nonlinear SDOF bridge models were always slightly unconservative compared to that of the full bridge models under non-FDGM. The results of a simple SDOF bridge model to predict the response of a bridge under FDGM ranged from very conservative for some ground motions, to slightly unconservative for other GM. Therefore, nonlinear SDOF analyses are specifically not recommended in the case of FDGM since the results were not consistent. A more detailed MDOF model should be used to assess bridge seismic performance so that SSI and the interaction of the longitudinal and transverse responses of the bridges can be included, particularly if a performance based design or assessment of the bridge is required.

INTRODUCTION

Research over the last decade has shown that pulse-type earthquake ground motions that result from forward-directivity effects can result in significant damage to structures. Both experimental evidence (Makley 2001) and observations in recent earthquakes (e.g. the 1994 Northridge earthquake and the 1995 Kobe earthquake, Alavi and Krawinkler 2000) support this assessment. Furthermore, analytical models (e.g. Krawinkler and Alavi 1998) indicate that traditional analysis methods are insufficient to capture the full effects of pulse-type ground motions. Fortunately, the recent increase in the number of recorded ground motions has allowed a better characterization of these near-fault, forward-directivity ground motions (FDGMs) (Mavroeidis and Papageorgiou 2003, Bray and Rodriguez-Marek 2004). The objective of this research was to use the wealth of recent ground motion data to improve the understanding of the response of typical reinforced concrete and precast concrete bridges to pulse-type ground motions that result from forward-directivity effects. Increased clarity concerning FDGMs and the structural response to this type of ground motion will result in direct benefits to communities across the United States exposed to nearby faults, thus resulting in reduced seismic risk as well as the opportunity for improved resource allocation.

BACKGROUND

In the near-fault region, ground motions at a particular site are significantly influenced by the rupture mechanism and the rupture direction relative to the site, as well as the permanent ground displacement at the site resulting from tectonic movement. Depending on the first two factors, ground motions in the near-fault zone can exhibit the dynamic consequences of "forward-directivity," "neutral-directivity," or "backward-directivity." Depending on the last factor, ground motions close to the rupture surface may contain a significant permanent static displacement, which is termed "fling-step" (Bray and Rodriguez-Marek 2004). The estimation of ground motions for a project site close to an active fault should account for these special aspects of near-fault ground motions. The "fling-step" usually induces only limited inertial demands on structures due to the long-period nature of the static displacement. On the other hand, ground motions that are influenced by forward-directivity effects can be very damaging to structures. Forward-directivity effects are seen when the rupture direction is aligned with the direction of slip, and the

rupture front moves towards a given site (Bray and Rodriguez-Marek 2004). These conditions occur readily in strike-slip earthquakes when the rupture propagates horizontally towards a given site. Forward-directivity conditions are also met for dip-slip faulting at sites that are located close to the surface projection of the fault. Whereas in a strike slip earthquake forward-directivity effects can be observed at all locations along the fault away from the hypocenter, in dip-slip earthquakes forward directivity effects are concentrated in a limited region up-dip from the hypocenter (Somerville 2003). FDGMs typically contain very few long period, high intensity ground motion pulses that are best observed in velocity time histories. Due to the radiation pattern of the fault, these pulses are typically aligned with the fault normal direction. However, strong pulses may be present in the fault parallel direction as well (Bray and Rodriguez-Marek 2004). These motions typically have a short duration with amplitudes larger than those of generic motions, and with a strong preferential fault-normal orientation.

The effects of FDGMs on structures were first recognized in the 1970's (Bertero 1976), however, engineers largely ignored FDGMs in structural design until after the 1994 Northridge earthquake. Since then, a number of studies have been directed at the effect of near-fault ground motions on structural response, prompting revision of design codes. In current practice, rupture directivity effects are generally taken into account by modifications to the elastic acceleration response spectrum at 5% damping (Somerville et al. 1997, Somerville 2003).

However, recent research has found that a time-domain representation of FDGMs is preferable over frequency-domain representations (Krawinkler and Alavi 1998). This is because traditional response spectrum representations of ground motions do not adequately represent the demand for a high rate of energy absorption presented by near-fault pulses. More specifically, when the high intensity levels of these motions drive structures into the nonlinear range, the linear-elastic assumption underlying the response spectrum concept is invalidated (Somerville 2003).

Although FDGMs pose a significant threat to structures, this threat is not equal for all structures. For example, coincidence of the structure and pulse period intuitively leads to the largest structural response for a given earthquake. However, the period of the structure and the pulse period can vary significantly. The FDGM pulse period is proportional to the earthquake magnitude, lengthening as the

earthquake magnitude increases. As a result, damage due to smaller magnitude earthquakes can be more significant for short period structures than damage due to larger magnitude earthquakes, since the near-fault pulse period is closer to the fundamental period of the structure in the smaller magnitude earthquake. This contradicts conventional engineering intuition that directly correlates damage potential with earthquake magnitude, thus highlighting the need for a unique way to accurately assess the potential for structural damage due to FDGMs. The near-fault pulse can impose an additional damage variable on structures: large residual deformations. Although consisting only of a few cycles, the pulses can impose large inelastic drift on structures, resulting in significant permanent deformations. Not only are conventional damage indices such as maximum displacement and energy absorbed important for assessing the response of structures, alternatives including residual displacement are necessary as well (Priestley, 2003).

PROJECT OBJECTIVES AND RESEARCH SCOPE

The overall goal of this research was to evaluate the response of bridge structures to near-fault FDGMs. In order to obtain results that are applicable to realistic structures, three bridges in Washington State were selected for the structural analyses. The objectives of the research were:

1. Select three bridge structures in Washington State that have the potential to experience a near-fault earthquake.
2. Compile an updated database of near-fault, FDGMs and select from this database ground motions for use in the structural analyses of the bridges.
3. Develop finite element models of the bridges
4. Determine the effect of the FDGM on the bridge structures, including the effects of site response and soil-structure interaction.
5. Provide FHWA and WSDOT with design and assessment recommendations for bridges likely to be affected by near fault, FDGMs.

REPORT ORGANIZATION

This report summarizes the research performed for FHWA for the project titled *Dynamic Response of Bridges to Near-Fault, Forward Directivity Ground Motions*. First, the compilation of a

database of near-fault ground motions and the selection of ground motion for time history analyses of the selected bridges are described. The structural models of the selected bridges are then presented, along with the results of the analyses and relevant conclusions.

GROUND MOTION SELECTION

Time domain analysis of non-linear structures requires the use of earthquake acceleration time histories as input. Current practice for ground motion selection includes the determination of a target elastic response spectrum, usually obtained from probabilistic or deterministic seismic hazard analyses (or prescribed by appropriate codes), and the selection of a set of ground motions that match, in general, the characteristic of the seismic events controlling the hazard. This set of ground motions can be selected such that, on average, they match the target spectrum or they can be modified by appropriate codes (e.g. Abrahamson 1998) such that each motion matches the target spectrum. This process, however, is not necessarily appropriate for FDGMs because of the particularities of these motions. More specifically, the pulse-type characteristics of the motions are not well reflected in ground motion selection procedures that are based on a target spectrum. For this reason, the ground motion selection for the analyses of the three selected bridges was targeted at the selection of FDGMs that reflect the characteristics of an earthquake in the Seattle Fault, adjacent to the selected bridges. Here, a process for selecting a comprehensive database of FDGMs that enhances an existing database compiled by Rodriguez-Marek (Bray and Rodriguez-Marek 2004) is described. In addition, a set of non forward-directivity ground motions that can be used as a control group was also created. The selection of a set of FDGMs for the analyses of three bridges in Washington State is then discussed.

GROUND MOTION DATABASES

FDGM database

A ground motion is considered to be a FDGM if it is recorded within 20 km of a fault, and is located in a region that is prone to forward directivity effects according to the definition of Somerville et al. (1997). In addition, the velocity time history of the ground motion must show a polarization in the fault normal direction and must have a clear pulse in the fault normal direction. For brevity, the detailed

requirements for forward directivity are not included herein but are discussed at length elsewhere (Rodriguez-Marek 2000, Bray and Rodriguez-Marek 2004, Gillie 2005).

A current database of 54 forward-directivity ground motions (FDGM) from 13 different earthquakes up to the 1999 Chi-Chi earthquake was complied by Rodriguez-Marek (2000, Bray & Rodriguez-Marek 2004). The task of updating the database involved collecting and processing several records from earthquakes since 1999.

Time domain parameters for each FDGM were obtained. This involved simplifying the FDGM into pulses, a concept first utilized extensively by Alavi and Krawinkler (1998). This project fitted a series of half-sine pulses to the train of pulses at the beginning of both the fault normal and fault parallel components of each record using a method presented by Rodriguez-Marek (2000, Bray and Rodriguez-Marek 2004). Each half-sine pulse in both the fault-normal and fault-parallel directions is completely described by the pulse period and the amplitude. The time offset between the beginnings of the pulses in the fault normal versus the fault parallel directions is also computed. These parameters are then used in a statistical analysis to find a correlation between ground motion parameters and structural response.

The complete FDGM data base is presented in a table in Appendix A. Details of the compilation of the database are given by Gillie (2005). Time domain parameters for the selected FDGMs were extracted using the procedure described by Bray and Rodriguez-Marek (2004). This procedure consists of fitting half-sine pulses to the velocity time histories of the ground motions. The ground motions can then be characterized by the amplitude and the period of the dominant pulse. These parameters are also listed in Appendix A. A set of motions from the 2004 Parkfield earthquake did not satisfy the geometric conditions for forward directivity (e.g. the motions were not located in an area prone to FD according to the criteria of Somerville et al. 1997), yet these motions had all other characteristics of NFGMs. These motions are also listed in a separate table in Appendix A.

Non-FDGM Database

The database of non-FDGMs was required to have similar characteristics to the FDGM database. To achieve this, motions were taken from the same earthquake events as the FDGMs. Distance to the fault of non-FDGMs were restricted to 30 km or less. The extension of the distance requirement was needed to

increase the number of motions available because most records within 20 km of the fault rupture display some pulse-type characteristics. PGA and spectral acceleration at short periods would ideally be the same for both sets of motions. PGV and peak spectral velocity values for the FDGM would be inherently greater than those of the non-FDGM. The number of motions in the database also needed to be approximately equal to the number of FDGMs to allow for a statistical comparison between the two sets. The non-FDGM database consists of 63 records from eleven different events, which are listed in Appendix A. The PGA and spectral accelerations of the non-FDGM database were lower on average than those of the FDGM database (see Appendix A).

GROUND MOTION SELECTION

This section describes the selection of ground motions for the structural analyses of three bridges. The representative bridges were selected based on their location with respect to the Seattle Fault (Figure 1). The bridges are all located in the Puget Lowlands, designated as *Bridge 90/26A*, *Bridge 405/46NE*, and *Bridge 520/19EN*. This section describes the tectonic and geotechnical characteristics of the bridge sites, and presents the criteria utilized for selecting ground motion for time domain analyses of the sites.

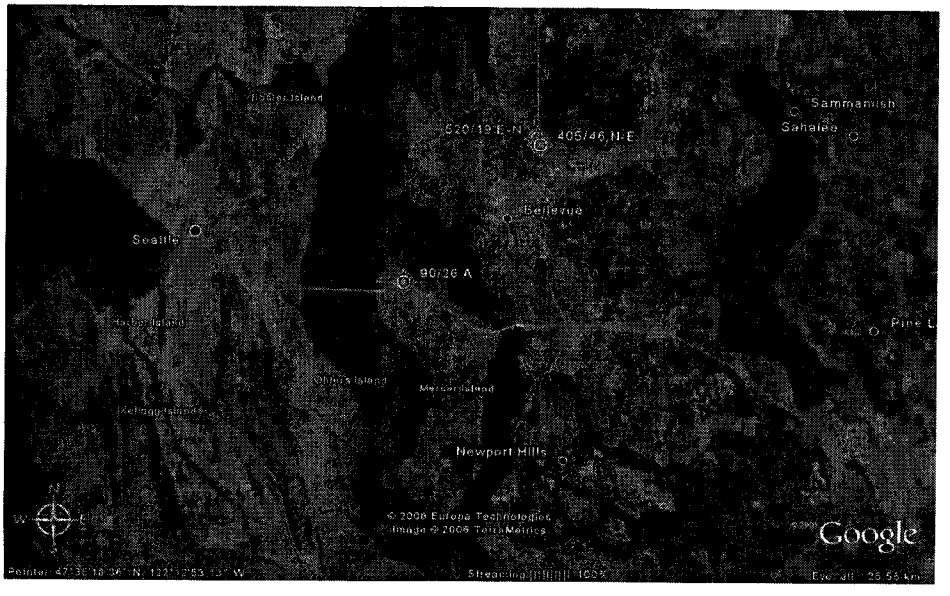

Figure 1. Bridge locations.

The Seattle area bridges chosen by the structural engineers for analysis are all located in the eastern portion of the Puget Lowlands and are located within the Seattle Fault Zone. Johnson et al. (1999) defines the Seattle Fault as a 4 to 6 km-wide west-trending zone of three or more south-dipping reverse faults. The fault has a dip of 20° in the first 3-4 km and 45° thereafter (Pratt et al. 1997) and extends from the Kitsap peninsula to the Cascade foothills with a maximum rupture length of approximately 65 km. Located between Seattle and Tacoma is the geological structure known as the Seattle Uplift (see Figure 2). Quaternary sediments are folded and faulted in the Seattle uplift zone. The most pronounced folding occurs along the northernmost published fault trace, which defines the edge of the Seattle Uplift and the Seattle Basin (Johnson et al. 1999). This location of the Seattle Fault places the bridges from 2 to 7 km north of the northernmost fault trace.

New data presented by Brocher et al. (2004) indicates that the Seattle Uplift is a passive roof duplex. A passive uplift is bounded both at the top and bottom by oppositely dipping thrust faults that form a triangular zone at the leading edge of the advancing thrust sheet (Figure 2). Brocher et al. (2004) propose that the active tip of this triangular region extends underneath the Seattle Basin 3 km farther north than previously recognized. This new location places Bridge 90 26A on the hanging wall of the fault. At the 520 and 405 bridges sites, the precise location of the fault is not known; these sites could potentially be on the hanging wall. Sites that are on the hanging wall have the potential for experiencing source fling in addition to FD effects, which must be taken into consideration in seismic analysis. Consideration of fling is beyond the scope of this project.

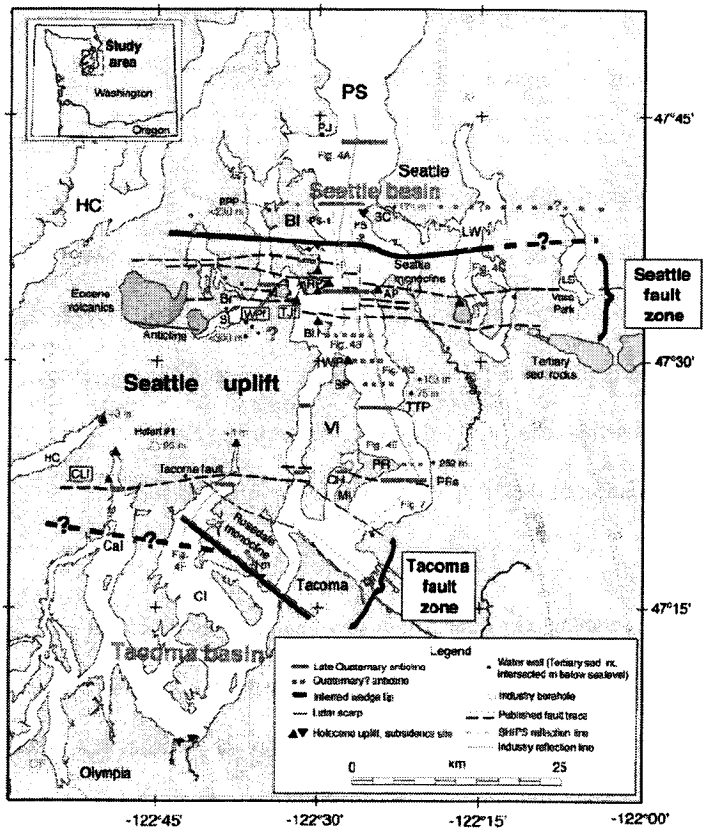

Figure 2. Seattle Area Map showing the Seattle fault zone (Brocher et al., 2004).

Site descriptions

All three bridge sites are in the Puget Lowlands, a depression bounded by the Cascades on the east and the Olympics on the west. North-south trending ridges and valleys characterize the Lowlands; a result of the erosion and deposition caused by repeated glaciation in the Puget Sound area (Roger Assoc. 1980). Uplands in the Puget Lowlands generally expose sediments associated with Vashon Ice from the most recent glaciation known as the Vashon Stade of the Fraser Glaciation, which ended approximately 10,000 to 13,000 years ago (WSDOT 1990). Underneath the Vashon sediments are deep deposits of Pleistocene glacial and interglacial sediments up to 670 m thick (Hall and Othberg 1974), which overly tertiary bedrock. More recently deposited alluvial and lacustrine sediments overlie the Pleistocene glacial deposits (WSDOT 1990). Site explorations at the different sites give evidence of these glacial depositions.

Ground Motion Selection Process

The structural engineer required a comprehensive set of ground motions that represent *FDGMs* and non-FDGMs expected to occur at the bridge sites. The analysis involved the following tasks:

1. Perform a probabilistic seismic hazard analysis (PSHA) for each bridge site.
2. Obtain target design spectra for each bridge from the PSHA based on a Uniform Hazard Spectrum (UHS) with a probability of exceedance of 2% in 50 years.
3. Select 5-10 non-FDGMs that best match the UHS.
4. Apply spectral matching to the ground motions from (3) to fit the target spectra obtained from (2).
5. Determine time domain parameters for FDGMs produced by (a) the characteristic EQ of the Seattle fault, and (b) an earthquake that produces a pulse period close to the structural period of the bridges.
6. Use the parameters from (5) to select 2 sets of FDGM records, one set with pulse period similar to that of the bridges and one set to represent motions expected from the Seattle Fault Zone;
7. Convert the equivalent non-FDGMs to motions that will be applied at the foundation level of the bridges using one-dimensional site response analysis for each bridge site.

Probabilistic Seismic Hazard Analysis (PSHA)

The PSHA analyses were conducted using the tools provided by the USGS (http://eqint.cr.usgs.gov/eq-men/html/deaggint2002.html). For details on the methodology, see the USGS website. The methodology has also been summarized by Gillie (2005). A return period (RP) of 2475 years was selected for developing the UHS, which, in turn will be used as the target spectrum for design. The RP of 2475 years corresponds to a probability of exceedance of 2% in 50 years. This probability level is adopted by the 2003 IBC as a "collapse level" motion. Design motions are taken as 2/3 of the collapse level motion. Given that the motions are required for research rather than design, the RP corresponding to "collapse level" was selected (ICC 2003). The UHS for the 3 bridge sites are shown in Figure 3. Results of

hazard deaggregation show that earthquakes at distances of 0-20 km and magnitudes of Mw 6.0 – 7.5 contribute approximately 80% of the hazard for each bridge site (Gillie 2005).

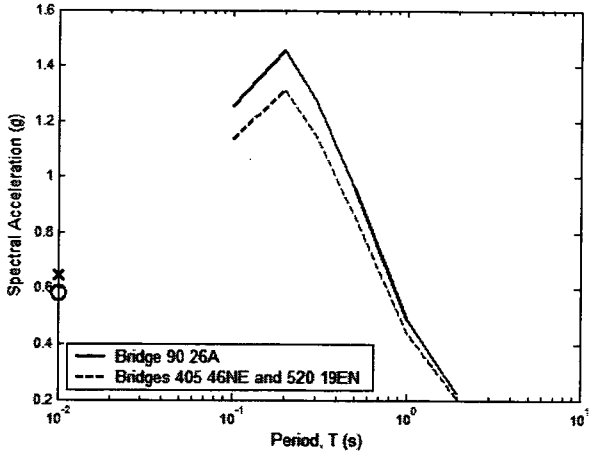

Figure 3, Equal Hazard Spectra for the three bridges sites for a return period of 2475 years.

Trends in the data show that the most common sources having more than 10% contribution for the bridge sites include (1) Western U.S. (WUS) shallow gridded seismicity; (2) intraplate events (40 – 70) km gridded seismicity; (3) Puget Lowlands gridded seismicity; and (4) Washington and Oregon faults. The only analysis for which the Mw9.0 Cascadia subduction zone scenario contributed a significant portion of hazard was at a spectral acceleration of 2 s, with contributions of 11%, 13% and 13% of the total hazard for the 90 26A, 405 46NE, and 520 19EN bridge sites, respectively. The faults contributing to the Washington and Oregon regional faults were, in most cases, the three Seattle fault traces.

Non-FDGM Selection and Processing

The structural engineer required that 5-10 motions be selected for analysis of the WSDOT bridges. Ground motion selection involved determining the R and Mw pairs that contributed the most to the seismic hazard for the selected RP. Once the ranges of magnitude and distance were determined, all ground motions that satisfied these requirements were selected for further analysis from the PEER database (PEER 2000). In some cases the distance and magnitudes were expanded to obtain motions that best satisfied the following criteria:

(1) similar faulting type,

(2) recorded on rock,

(3) response spectra matching the shape of the target spectra, and

(4) no FD characteristics.

After the ground motions were selected, spectral matching was performed using the target spectra obtained from the UHS. Before spectral matching could be performed the USGS UHS needed to be extended to periods from 2 s to 5 s. This should be done within the PSHA calculations, but extending the USGS PSHA was deemed to be outside the scope of this project. Extension of the UHS was done using Abrahamson and Silva (1997) spectral attenuation relationship for periods greater than 2 s with magnitude and distance applied according to the site and the earthquake contributing the most to the hazard at 2.0 s (e.g. the Seattle Fault). For details see Gillie (2005). The target spectra for the three bridges are displayed in Figure 3, which shows that the hazard spectra for the three sites are within 10 percent of each other. The decision was made to use the same target spectra for all three sites. The site with the largest UHS, the spectra at the 90 26A site, was used to be conservative.

Once the UHS was extended, RSPMATCH (Abrahamson 1998) was used to match the ground motion spectra to that of the PSHA for the bridge sites. RSPMATCH matches the response spectra by using adjustment functions to modify the reference time history in the time domain. RSPMATCH is run for three to four passes. For this project, each pass consisted of 10 iterations. For the first pass, model 6, the tapered cosine adjustment function, was used. Model 1, the reverse of the oscillator function, was used in all subsequent passes. The time history is scaled only once at the start of the first pass. No scaling was applied for subsequent passes. Each ground motion was run until the error between the target spectra and the matched spectra was less than 5 percent.

Seven non-FDGMs were selected for the bridge analyses. The parameters of the selected motions are displayed in Table 1. Notice that of these motions, four are recorded in thrust fault events; one is a strike-slip event; one is from a deep, intraplate event; and one is from a subduction zone type event. The record from the strike-slip event was chosen because it satisfied the magnitude and distance ranges from the PSHA not satisfied by any non-FDGMs recorded in thrust or reverse type earthquakes.

Table 1 – Parameters of the 7 non-FDGMs selected using probabilistic seismic hazard analysis parameters.

Station	Agency	Earthquake	M_w	Mechanism	R (km)	PGA (g)	PGV (cm/s)
Sun Valley	USC	Northridge	6.7	Reverse	10.05	0.39	32.67
Pacoima Kagel Canyon	CDMG	Northridge	6.7	Reverse	7.26	0.18	10.48
Santa Susana	USGS	Northridge	6.7	Reverse	16.74	0.53	55.97
Izmit	ERD	Kocaeli	7.4	Strike-Slip	4.80	0.22	29.77
TCU-071	CWB	Chi-Chi	7.6	Reverse	5.30	0.65	69.42
Fire Station #28	USGS	Nisqually	6.8	Normal	49.95	0.084	5.28
Moquegua	CISMID	Peru	8.4	Thrust	100.0	0.30	29.9

FDGM Selection

Forward-directivity motions were also selected for analysis of the WSDOT bridges. Time history parameters for FDGM were obtained to serve as a guide in selecting records most appropriate for the types of events predicted for the Seattle Fault and motions that would be critical to the bridges. This portion of the seismic hazard analysis follows a deterministic seismic hazard analysis approach. It is assumed that the controlling event will be a rupture of the Seattle Fault. The characteristic event used by the USGS for the Seattle Fault is Mw7.2. The pulse period for an Mw7.2 event is predicted to be approximately 2.5 s. However, the structural period of the bridges is approximately 0.5 s, which means an event with a lower magnitude, in the range of Mw6.0-6.5, could be more damaging than a larger event. Two sets of two motions each were selected to incorporate both events. One set had a pulse period near the pulse period of a characteristic earthquake for the Seattle Fault and the second set had a pulse period near the structural period of the bridges.

Time domain parameters and spectral acceleration values were obtained using various attenuation relationships. Parameters and their respective values are listed in Tables 2 and 3. The attenuation relationship used for pulse period, T_p, is given by Bray and Rodriguez-Marek (2004) for rock sites:

$$\ln(T_p) = -8.6 + 1.32M_w \pm \sigma_{total} \quad (1)$$

where σ_{total} = 0.40. The period with maximum spectral velocity, T_{RSV}, was given by Alavi and Krawinkler (2004):

$$\log_{10} T_{RSV} = -1.76 + 0.31M_w \quad (2)$$

The fault normal component for PGV was predicted using data from Bray and Rodriguez-Marek (2004) for rock sites:

$$\ln(PGV) = 4.46 + 0.34M_w - 0.58\ln(R^2 + 7.00^2) \pm \sigma_{total} \quad (3)$$

with σ_{total}=0.39. Bray and Rodriguez-Marek (2004) also present ratios that predict the fault parallel PGV from the fault normal component. The PGA, which is the same in the fault normal and fault parallel components, is obtained from Abrahamson and Silva (1997). PGA is not affected by near-fault effects and is not considered in the selection of FDGM. Spectral acceleration values at T = 3 s and T = 0.5 s are taken from Abrahamson and Silva (1997) with modifications for FD by Somerville et al. (1997). Arias duration was computed using Abrahamson and Silva (1996, see also Gillie 2005)

The forward directivity motions were selected from the FDGM database used in this research. Motions were selected based on the following criteria (in order of importance):

(1) Existence of distinct forward directivity pulses;

(2) Correspondence of the desired pulse period;

(3) Similarity of faulting, magnitude, and distance to the site; and

(4) Correspondence of PGV, maximum period of the velocity spectra, and spectral acceleration at the structural period or the target pulse period.

The set of FDGMs selected for the Mw 7.2 characteristic earthquake on the Seattle Fault are listed in Table 2 along with their corresponding parameters. The set of FDGMs selected to correspond with the structural period of 0.5 s are presented with their parameters in Table 3. The motions that match the pulse period of the characteristic Seattle Fault rupture event are the TCU-075 record from the 1999 Chi-Chi earthquake and the Sylmar Converter Station East, referred to as Sylmar, from the 1994 Northridge earthquake. Both the Chi-Chi and Northridge earthquakes have a faulting style similar to that of the Seattle Fault. The parameters of closest distance to the fault and PGV were well matched between the chosen motions and the characteristic event on the Seattle Fault, so the decision was made to reduce to a minimum any modification of the two motions. Arguments could be made to scale both to match the target PGV and the target spectral acceleration at T = 2.5 s. Due to the consideration to limit modification, it was decided to scale the motion up if required to match the PGV. If scaling to PGV reduced the motion, then it was left

unscaled. These considerations resulted in scaling of the Chi-Chi motion by 1.26 when applied to bridge 90 26A. No scaling was necessary when TCU-075 was applied to the 405 and 520 bridges. The Sylmar record was left unscaled because scaling to PGV reduced the motion.

Table 2 – Target forward-directivity ground motion parameter values for a characteristic earthquake of M_w = 7.2 on the Seattle Fault

	Bridge	Record	Record	Bridges	Record	Record
	90 26A	TCU-075	Sylmar	405 & 520	TCU-075	Sylmar
Earthquake (date)	Target Values (Seattle Fault Characteristic EQ)	Chi-Chi	North-ridge	Target Values (Seattle Fault Characteristic EQ)	Chi-Chi	North-ridge
M_w	7.2	7.6	6.7	7.2	7.6	6.7
Fault Type	Reverse	Thrust	Reverse	Reverse	Thrust	Reverse
Closest Distance	2.8 km	1.5 km	6.1 km	6.5 km	1.5 km	6.1 km
Pulse Period[a]	2.5 s [1.7 - 3.7]	2.3 s	2.87 s	2.5 s [1.7 - 3.7]	2.3 s	2.87 s
Period for maximum spectral velocity[b]	3.0 s	2.03 s	2.92 s	3.0 s	2.03 s	2.92 s
PGV (fault normal)[c]	96.0 cm/s [65.0 – 141.8]	76.1 cm/s	116.4 cm/s	73.0 cm/s [49.4 – 107.8]	76.1 cm/s	116.4 cm/s
PGV (fault parallel)[d]	≈38 cm/s	33.4 cm/s	78.3 cm/s	≈36 cm/s	33.4 cm/s	78.3 cm/s
PGA (fault normal)[e]	0.93 g	0.31 g	0.84 g	0.86 g	0.31 g	0.84 g
PGA (fault parallel)[e]	0.93 g	0.28 g	0.5 g	0.83 g	0.28 g	0.5 g
Fault-normal S_a[f]	1.19 g	0.59 g	1.04 g	1.07 g	0.59 g	1.04 g
Arias Duration[g]	16.6 s	26.4 s	12.2 s	16.6 s	26.4 s	12.2 s
SCALING (for PGV)		**1.26**	**0.82**		**0.96**	**0.63**
SCALING Used		**1.26**	**1.00**		**1.00**	**1.00**

[a] Obtained from Bray and Rodriguez-Marek (2004) using the coefficients given for rock sites (Eq. 1)
[b] Obtained from Krawinkler and Alavi (1998) using the following equation (Eq. 2).
[c] Obtained from Bray and Rodriguez-Marek (2004) using the coefficients given for rock sites (Eq. 3).
[d] Obtained from Bray and Rodriguez-Marek (2004) from relationship of fault normal to fault parallel.
[e] Obtained from Abrahamson and Silva (1997) assuming bridges are on the hanging wall, a reverse style of faulting and rock site condition.
[f] Obtained from Somerville et al. (1997) assuming $Y\cos\phi = 0.9$.
[g] Obtained from Abrahamson and Silva (1996) for I = 0.95.

The motions chosen to represent the Mw 6.1 event are the Pacoima Dam record from the 1994 Northridge earthquake and the Cholame 3W record from the 2004 Parkfield event. The restriction of pulse period to Tp ≈ 0.5 s reduced the number of available motions, so style of faulting, PGV, and closest distance to the fault did not match as well as for the Mw7.2 event. Note that the pulse period of the Pacoima Dam motion is 0.61 s, greater than the expected period of the structure; however, it was included because nonlinear response of the structure could lead to an increase in the period of the structure. Each

motion required increased scaling to match the predicted PGV for 90 26A bridge site for the Mw6.1 event, with a value of 1.32 for the Pacoima Dam record and 1.53 for the Cholame 3W record. The Pacoima Dam motion did not require scaling for the 405 and 520 bridge sites, while the Cholame 3W record was multiplied by 1.16 to match the predicted PGV.

Figure 4 displays the response spectra of the unscaled FD motions selected to apply to the bridge models. Observe that all the FD motions have spectral values greater than the UHS at the pulse period of the motion. This shows that the FD motion controls the spectral response in a SDOF system at the pulse period. Notice also that the Cholame 3W motion, which is from the lowest magnitude earthquake (Mw = 6.0), dominates the response of all the motions for periods between 0.6 and 0.7 s. This means that a lower magnitude earthquake could cause greater damage than a larger earthquake if the structural period matches the pulse period of the motion.

The selected motions were used in site response analyses to account for the effects of local geology. For brevity, these analyses are not described in this report but are described in detail by Gillie (2005). A sample of the site response analyses results is shown in Figure 5. This figure presents the input and output response spectra for the site response analyses of the I-90 bridge site. Results show that the site deamplifies short period motions from 0.03 to 0.2 s, but amplifies motions from periods of 0.3 to 1 s, with the peak occurring around 0.5 s. Results also show that site response resulted in amplification for all periods from 0.03 s to 1 s for the 405 and 520 bridge sites, nearly doubling the response at a period of 0.5 s from approximately 1.4 g to 2.6 g (Gillie 2005).

Table 3 – Target forward-directivity ground motion parameter values for a characteristic earthquake of M_w = 6.0

	Bridge	Record	Record	Bridges	Record	Record
	90 26A	Pacoima	Cholame 3W	405 & 520	Pacoima	Cholame 3W
Earthquake (date)	Target Values (Pulse Period = 0.5)	North-ridge	Parkfield	Target Values (Pulse Period = 0.5)	North-ridge	Parkfield (9/28/04)
M_w	6.0	6.7	6.0	6.0	6.7	6.0
Fault Type	Reverse	Reverse	Strike-Slip	Reverse	Reverse	Strike-Slip
Closest Distance	2.8 km	6.1 km	7.2 km	6.5 km	6.1 km	7.2 km
Pulse Period*	0.5 s [0.3 - 0.8]	0.61 s	0.52 s	0.5 s [0.3 - 0.8]	0.61 s	0.52 s
Period for maximum spectral velocity*	1.3 s	0.44 s	0.42 s	1.3 s	0.44 s	0.42 s
PGV (fault normal)*	66.1 cm/s [44.7-97.6]	49.9 cm/s	43.22 cm/s	50.2 cm/s [34.0 – 74.2]	49.9 cm/s	43.22 cm/s
PGV (fault parallel)*	≈36 cm/s	23.1 cm/s	16.7 cm/s	≈30 cm/s	23.1 cm/s	16.
PGA (fault normal)*	0.51 g	0.48 g	0.44 g	0.40 g	0.48 g	0.
PGA (fault parallel)*	0.51 g	0.31 g	0.36 g	0.40 g	0.31 g	0.
Fault-normal S_a*	0.48 g	1.25 g	0.82 g	0.36 g	1.25 g	0.
Arias Duration*	6.49 s	3.82 s	5.68 s	6.49 s	3.82 s	5.
SCALING (for PGV)		**1.32**	**1.53**		**1.01**	**1**
SCALING Used		**1.32**	**1.53**		**1.00**	**1**

* See notes in Table 2.2

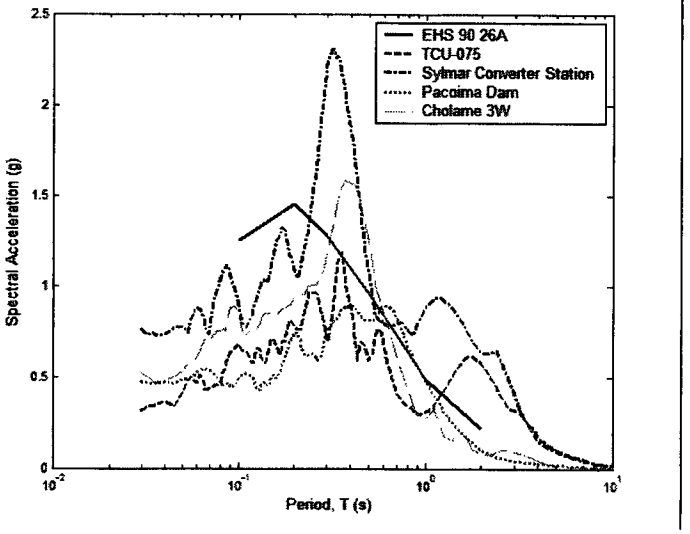

Figure 4 – Response spectra of FD motions in comparison with the USGS Equal Hazard Spectra.

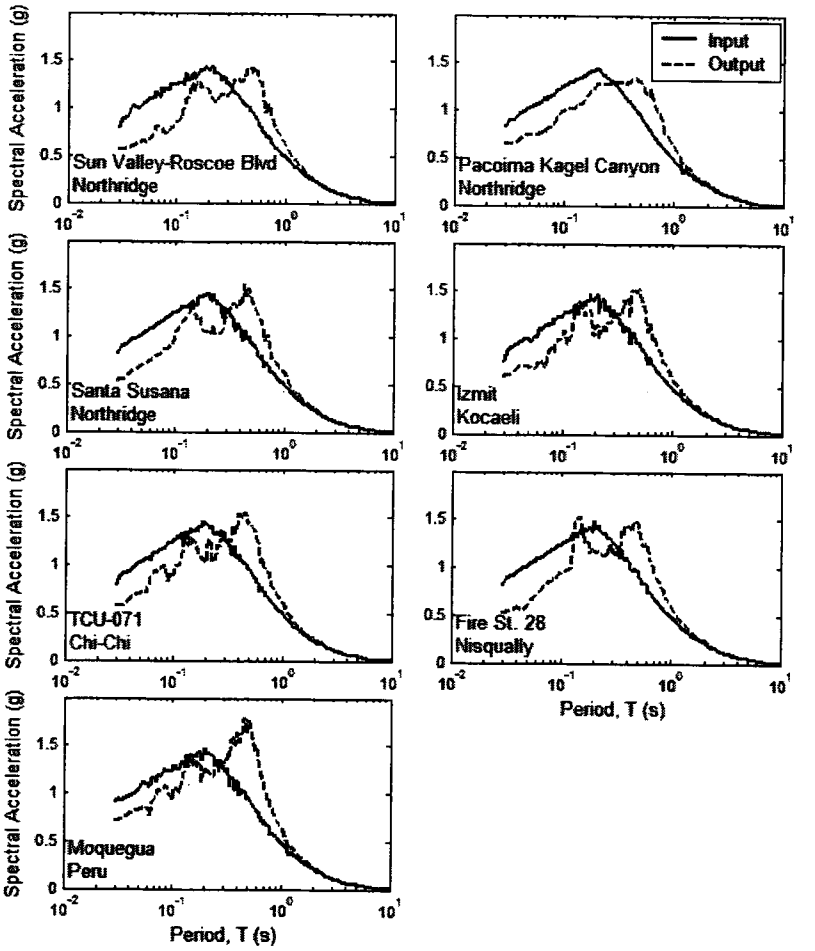

Figure 5 – Input response spectra from spectral matching and output spectra from SHAKE analyses of site response for the 90 26A bridge site.

STRUCTURAL ANALYSIS

This section describes the structural models used to simulate the dynamic response of the selected bridges to the input earthquake ground motions. Each bridge is discussed separately

WSDOT BRIDGE 405/46N-E

Geometry and reinforcement

Bridge 405/46N-E is an overpass located at 116th Avenue N. E. in Bellevue, Washington. In 1993, the bridge was built to service traffic on SR 405 at the junction with SR 520. By today's standards, the columns are considered well-reinforced, well-confined and adequately lap-spliced. The bridge length is

50.3 m (165 ft) back to back of pavement seats and consists of three spans. The western and eastern ramps are 15.85 m (52 ft) long with the center ramp measuring 18.6 m (61 ft) in length. The bridge has no skew to it.

The deck is composed of pre-tensioned concrete beams. Each span includes three girders spaced 2.90 m (114.4 in.) on center. Overlaid on top of the girders is a 17.8 cm (7 in.) thick, 8.46 m (27.75 ft.) wide reinforced concrete deck slab .At each of the two bents, a 1.22x1.22 m (4x4 ft.) crossbeam transversely connects the two columns. Each crossbeam extends 7 m (23 ft) in length. The steel reinforcement consists of five No. 9 bars located at the top and five No. 8 bars at the bottom of each crossbeam. Four No. 6 bars are located at the side edges and run longitudinally along the crossbeam. For shear reinforcement, No. 5 stirrups are spaced evenly along each member. The columns and crossbeam were cast monolithically adding considerable rigidity to each bent. The I-girders rest upon laminated elastomeric bearing pads located on top of the abutment seats. They are restrained in the transverse direction by girder stops.

At each bent, the bridge deck is monolithically constructed. The height of the columns at both bents is approximately 8.53 m (28 ft). The clear column height is about 6.7 m (22 ft). The columns are spaced at 3.96 m (13 ft) centerline to centerline. Each column has a cross-sectional diameter of 0.91 m (3 ft). Twelve evenly spaced No. 9 bars provide the longitudinal reinforcement within each column. This provides a longitudinal reinforcing ratio of 1.18%. The clear cover measures 3.8 cm (1.5 in.). Transverse reinforcement is provided by No. 5 bars spaced at 6.35 cm (2.5 in.) on center resulting in a transverse reinforcement ratio of 1.50%. Supporting each column is a spread footing. The length, width and depth of the spread footings are 7.92 m (26 ft), 4.27 m (14 ft), and 0.91 m (3 ft), respectively.

Abutments at both ends are approximately 3 m (10 ft) deep. Due to no endwall being on the abutments, there is no transverse resistance in the event of an earthquake. A footing measuring 8.6 m (28.1 ft) in length, 1.92 m (6.3 ft) in width, and 0.46 m (1.5 ft) in depth is located directly beneath the abutment-deck seating block. The footings and abutment walls were constructed with WSDOT Class 4000 mix concrete providing a compressive strength of f'c = 27.6 MPa (4 ksi). The concrete in the prestressed girders was specified to be class 6000. The concrete in the columns, crossbeam, diaphragms, and slabs was

specified to be class 5000. The reinforcing steel conforms to ASSHTO M31 Grade 60 with a yield strength of fy = 413.6 MPa (60 ksi).

Structural Model

Finite Element nonlinear dynamic implicit analysis was performed on ABAQUS/Standard with a 3D model. The bridge was discretized by 3-node quadratic Timoshenko (shear flexible) beam elements, resulting in a so-called spine model, as shown in Figure 6.

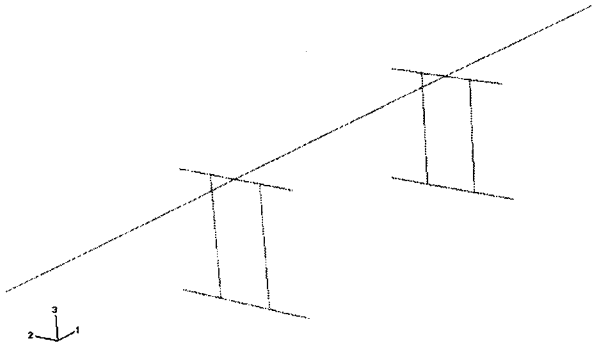

Figure 6. Bridge 405 spine model.

To get the equivalent beam properties of the deck, a two dimensional cross section analysis was performed. Figure 7 shows the deck cross section that was considered. For the torsional rigidity, the two dimensional region was meshed with warping elements. In the elastic range, however, warping is small and ABAQUS assumes that warping prevention at the ends can be neglected. The axial warping stresses are therefore assumed to be negligible, but the torsional shear stresses are assumed to be of the same order of magnitude as the stresses due to axial forces and bending moments.

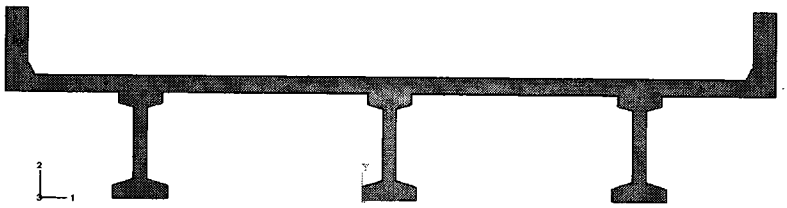

Figure 7. Bridge 405 deck cross section.

A solid Finite Element Model (FEM) of the Bridge 405 deck was therefore created to investigate the validity of these assumptions. A simple model, based on a cantilever beam under flexure or torsion, was also modeled with a single beam element, as shown in Figure 8. From the analysis, a modified equivalent torsional stiffness value was obtained and bending stiffness was verified. Figure 9 shows the cross section profiles for the different bridge elements.

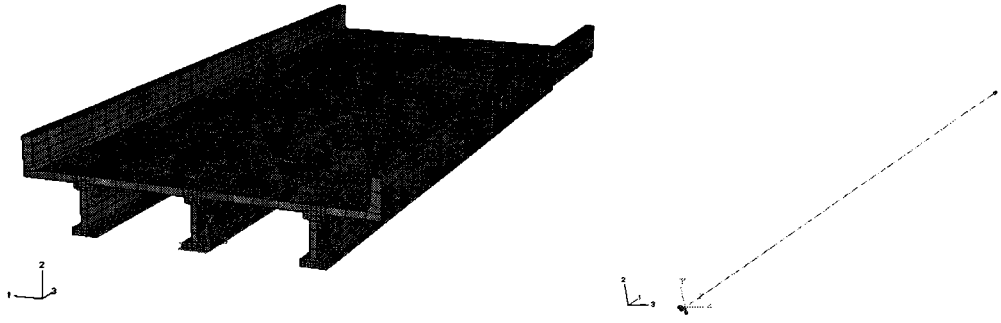

Figure 8. Bridge 405 deck solid and equivalent spine models.

There is no fixity assumed between the girders and the cap beam where the deck meets each bent. Therefore, the internal transverse moment was released at the crossbeam to model a hinge boundary condition.

Linear springs were used to connect the deck to the abutments. These springs represent the bearing pads. There was one bearing pad spring at each abutment. The abutments were modeled as a single node with a lumped mass. Linear springs connected the soil to the abutments to represent the Soil-Structure Interaction (SSI). The SSI characteristics were determined following the FEMA 356 (2000) procedure, based on the geometric properties of the abutment footing. Figure 10 shows the model that was used.

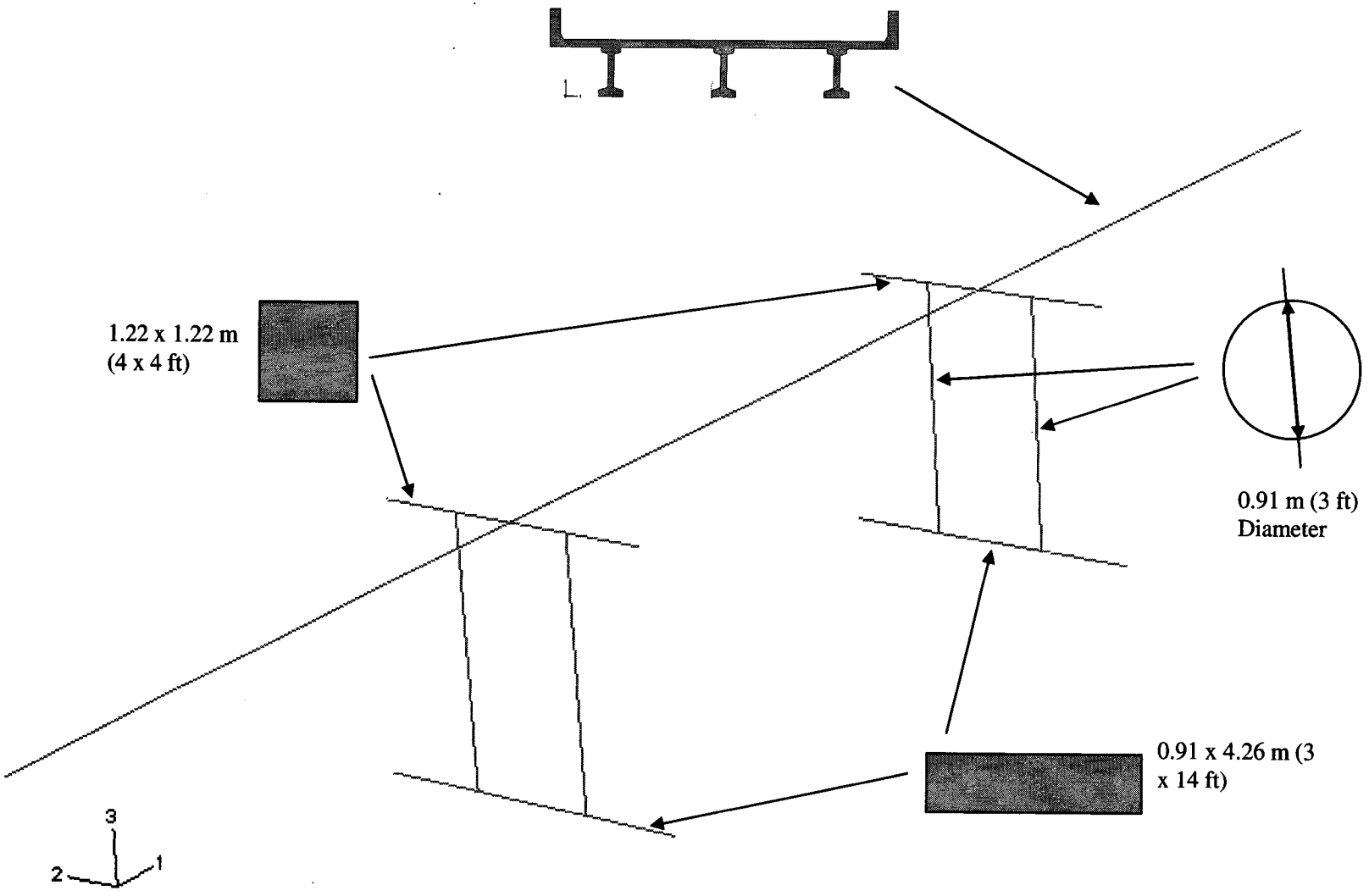

Figure 9. Bridge 405 cross sections.

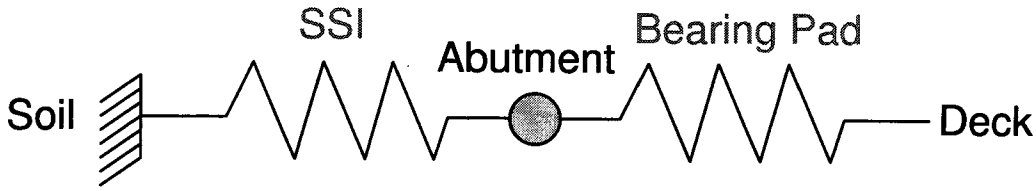

Figure 10. Model of the soil, abutment, and deck interaction in the transverse direction.

The longitudinal stiffness of the bearing pads was based on:

$$k = \frac{GA}{h} \tag{4}$$

where G is the shear modulus, A is the cross sectional area, and h is the height of the pad.

The other stiffness values of the bearing pads were set relatively high to model the resistance of the girder stops in the transverse and rotational degrees of freedom of the bridge. In the longitudinal direction, a nonlinear gap spring and a connector element were added in parallel to the bearing pad spring to model the 5 cm (2 in) gap between the abutment and the deck (see Figure 11). The connector was defined as a nonlinear spring that includes the plasticity effect to model the damage of the abutment resulting from pounding. The connector force-displacement curve was determined following the Caltrans – Seismic Design Criteria procedure. The resulting gap-spring element curve is shown in Figure 12.

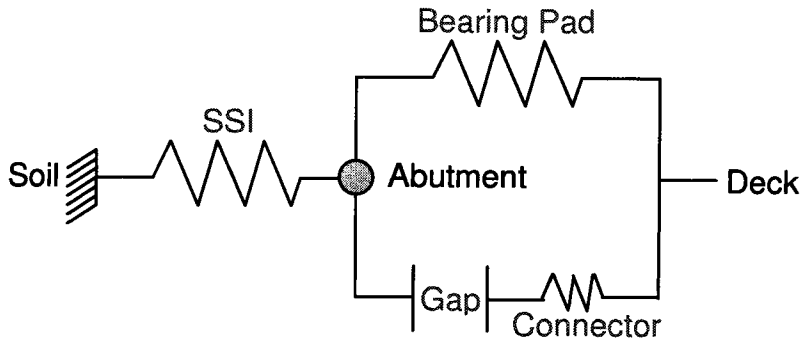

Figure 11. Model of the soil, abutment, and deck interaction, in the longitudinal direction.

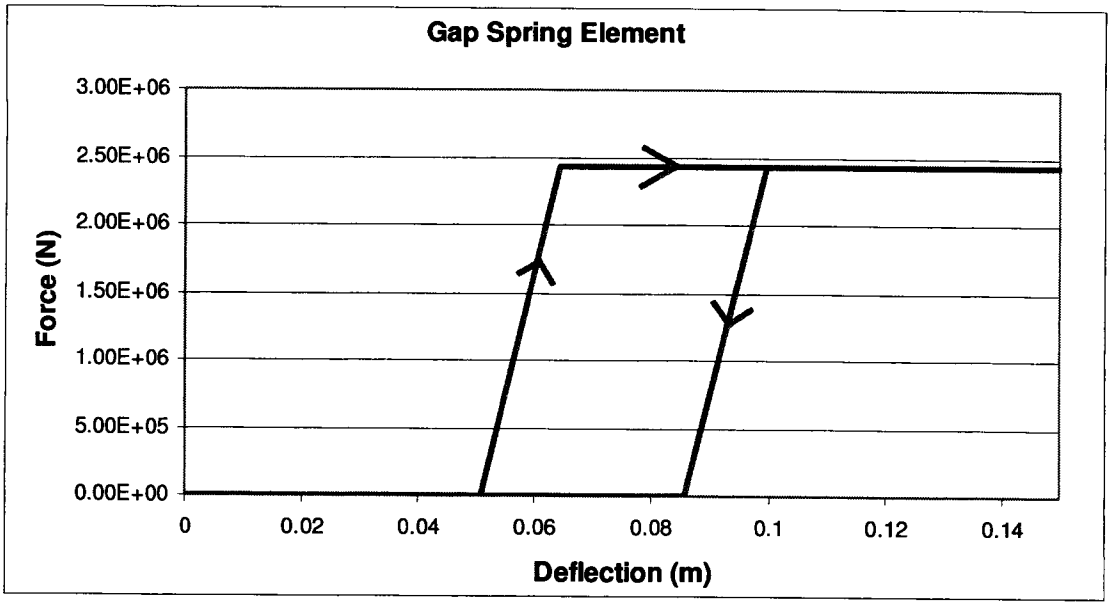

Figure 12. Force-displacement curve for the abutment gap spring and connector in series.

At the bottom and top of the columns, rigid connections were used to simulate the effect of the stiff foundation and crossbeam, respectively. The abutment and column footing soil springs were applied at the abutment and column footing nodes. Figure 13 shows a summary of the different applied boundary and connection conditions.

The ground motions were applied at the foundation nodes in the transverse, vertical and longitudinal directions. If not known, the vertical component of the ground motions was taken as 66% of the fault normal component. The gravity load was applied to the whole model. Rayleigh damping was specified for all bridge models. For all analyses, the damping ratio was specified as 5%.

ABAQUS, through a frequency extraction procedure, performs eigenvalue extraction to calculate the natural frequencies and the corresponding mode shapes of the bridge model. It includes initial stress and load stiffness effects due to preloads and initial conditions. Table 4 summarizes the frequency content of bridge 405. The first mode of vibration of bridge 405 is in its longitudinal direction with a frequency of 1.52 Hz (period, T = 0.65 sec). The bridge transverse direction is excited by the third mode of vibration with a frequency of 5.57 Hz (T = 0.18 sec).

Table 4 Frequency content of Bridge 405

Eigenvalue Output					
Mode No	Eigenvalue	Frequency		Generalized Mass	Governing DOF
		(Rad/Time)	(Cycles/Time)		
1	91.619	9.5718	1.5234	4.40E+05	**X-Component**
2	869.5	29.487	4.6931	1.10E+07	X-Rotation
3	1224.3	34.989	5.5687	2.65E+05	**Y-Component**
4	1236.7	35.166	5.5969	1.68E+07	
5	1278.8	35.76	5.6913	2.91E+06	

WSDOT BRIDGE 520/19E-N

Geometry and reinforcement

Bridge 520/19E-N is an overpass located at Northup way in Bellevue, Washington. In 1993, the bridge was built to service traffic on SR 405 at the junction with SR 520. By today's standards, the columns are considered well-reinforced, well-confined and adequately lap-spliced. The bridge length is 50 m (162 ft) back to back of pavement seats and consists of three spans. The southern and northern ramps are 13.4 m and 16.5 m (44 ft and 54 ft) long, respectively, with the center ramp measuring 19.5 m (64 ft) in length. The bridge has no skew to it.

The deck is composed of pre-tensioned concrete beams. Each span includes three girders spaced 2.90 m (114.4 in) on center. Overlaid on top of the girders is a 17.8 cm (7 in) thick, 8.46 m (27.75 ft) wide reinforced concrete deck slab. At each of the two bents, a 1.22x1.22 m (4x4 ft) crossbeam transversely connects the two columns. Each crossbeam extends 7 m (23 ft) in length. The steel reinforcement consists of six No. 9 bars located at the top and four No. 9 bars at the bottom of each crossbeam. For shear reinforcement, No. 5 stirrups are spaced evenly along each member. The columns and crossbeam were cast monolithically, adding considerable rigidity to each bent.

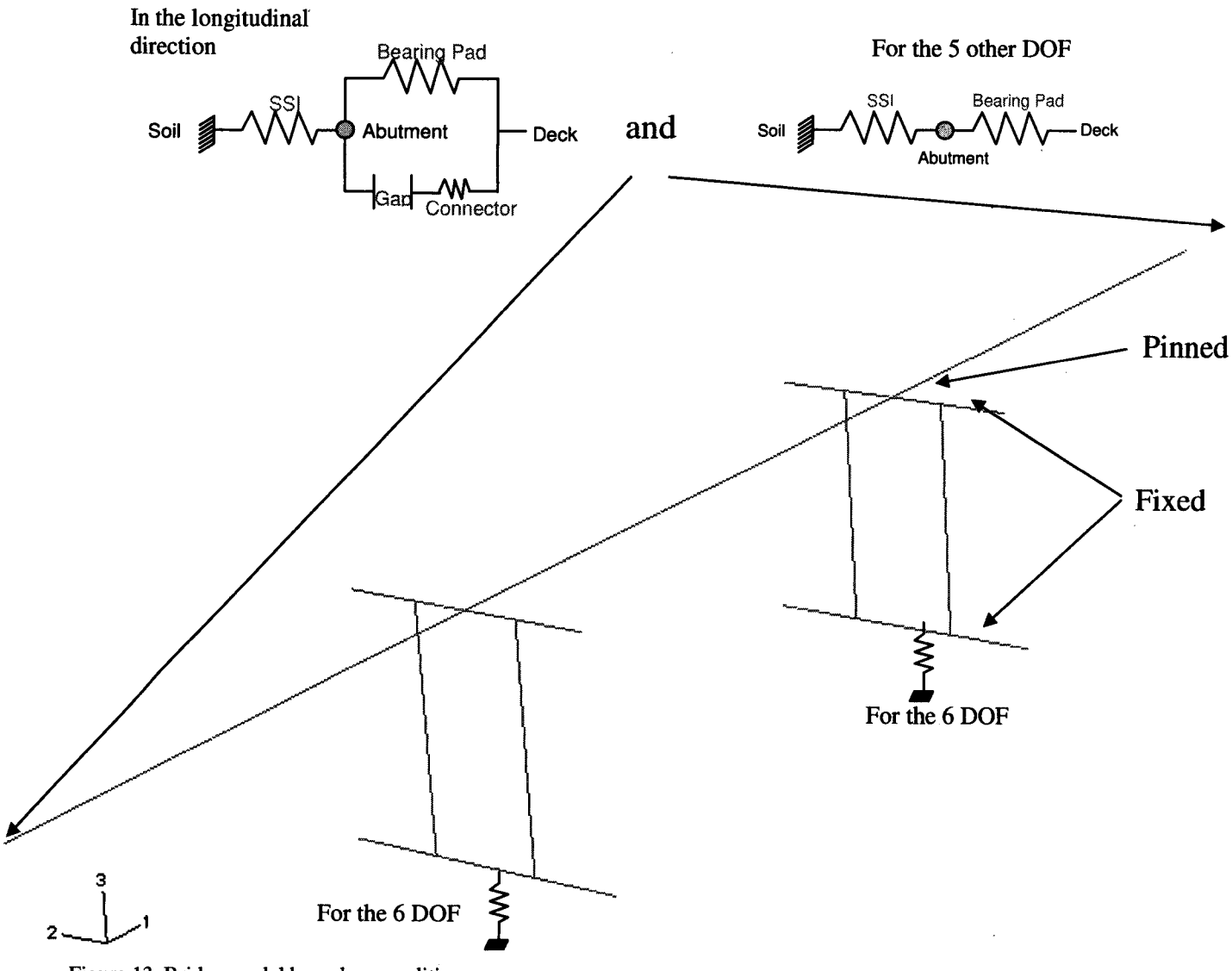

Figure 13. Bridge model boundary conditions.

The I-girders rest upon laminated elastomeric bearing pads located on top of the abutment seats. They are restrained in the transverse direction by girder stops. At each bent, the bridge deck is monolithically constructed. The height of the columns at both bents is approximately 10.6 m (34.7 ft). The clear column height is about 8.58 m (28.14 ft). The columns are spaced at 3.96 m (13 ft) centerline to centerline. Each column has a cross-sectional diameter of 0.91 m (3 ft). Fourteen evenly spaced No. 9 bars provide the longitudinal reinforcement within each column. This provides a longitudinal reinforcing ratio of 1.37%. The clear cover measures 3.8 cm (1.5 in.). Transverse reinforcement is provided by No. 5 bars spaced at 6.35 cm (2.5 in.) on center resulting in a transverse reinforcement ratio of 1.50%. Supporting each column is a spread footing.

The length, width and depth of the spread footings are 7.92 m (26 ft), 4.57 m (15 ft), and 0.91 m (3 ft), respectively. The footings are reinforced at the bottom with twenty one No. 7 bars and at the top with fifteen No. 6 bars in the direction of the width. In the length direction, they are reinforced with twenty five No. 6 bars at the top and thirty four No. 7 bars at the bottom.

Both abutments are approximately 6 m (20 ft) deep. Due to no endwall being on the abutments, there is no transverse resistance in the event of an earthquake. A footing measuring 8.84 m (29 ft) in length, 5.48 m (18 ft) in width, and 0.76 m (2.5 ft) in depth is located directly beneath the abutment-deck seating block. The footings and abutment walls were constructed with WSDOT Class 4000 mix concrete providing a compressive strength of f'_c = 27.6 MPa (4 ksi). The concrete in the prestressed girders, columns, crossbeam, diaphragms, and slabs was specified to be class 5000. The reinforcing steel conforms to AASHTO M31 Grade 60 with a yield strength of f_y = 413.6 MPa (60 ksi).

The Finite Element Model was built similarly to that of Bridge 405. Table 5 summarizes the frequency content of Bridge 520. The first mode of vibration of Bridge 520 is in its longitudinal direction with a frequency of 1.25 Hz (period, T = 0.8 sec). The bridge transverse direction is excited by the fourth mode of vibration with a frequency of 6.03 Hz (T = 0.165 sec).

Table 5. Frequency content of Bridge 520

Eigenvalue Output					
Mode No	Eigenvalue	Frequency		Generalized Mass	Governing DOF
		(Rad/Time)	(Cycles/Time)		
1	61.88	7.8664	1.252	4.36E+05	**X-Component**
2	869.69	29.491	4.6936	1.01E+07	X,Z-Rotation
3	1237.8	35.182	5.5994	9.92E+06	X,Z-Rotation
4	1434.8	37.879	6.0287	2.46E+05	**Y-Component**
5	1844.5	42.948	6.8354	1.28E+07	
6	3163.8	56.248	8.9522	97266	

WSDOT BRIDGE 90/26A

Geometry and reinforcement

Bridge 90/26A is an overpass located on Mercer Island near Seattle, Washington. In 1992, the bridge was built to service traffic on 72nd avenue SE. The I-90 underground Express Lane passes under the bridge. By today's standards, the columns are considered well-reinforced, well-confined and adequately lap-spliced.

The bridge length is 91 m (298 ft) back to back of pavement seats and consists of five spans. The ramps are 16.3 m (52 ft), 19.35 m (52 ft), 16 m (52 ft), 24 m (52 ft), and 15 m (52 ft) long from South to North, respectively. The bridge has no skew to it.

The deck is composed of a reinforced concrete box girder. The width of the deck is 10.2 m (33.5 ft) and the depth is 1.37 m (4.5 ft). The columns and concrete box girder were cast monolithically. The concrete box rests upon laminated elastomeric fixed and guided bearing pads located on top of the North and South abutment seats, respectively. They are restrained in the transverse direction by wing and retaining walls, respectively.

At each bent, the bridge deck is monolithically constructed. The clear height of the columns is 6.10 m (20 ft), 7.21 m (23.6 ft), 5.97 m (19.7 ft), and 4.33 m (14.2 ft), from South to North, respectively. Each column has a rectangular cross-section, 0.61x1.22 m (2x4 ft). Twenty two No. 11 bars provide the longitudinal reinforcement within each column. This provides a longitudinal reinforcing ratio of 3%. The clear cover measures 3.8 cm (1.5 in.). Transverse reinforcement is provided by No. 4 bars spaced at 30.5 cm (12 in.) on center. Supporting each column is

a pile shaft. The pile shaft lengths are respectively 16.15 m (53 ft), 15.5 m (50.8 ft), 16 m (52.5 ft), and 14.4 m (47.25 ft) from south to north. At the bottom of each pile shaft is a spread footing.

The pile shafts have the same longitudinal reinforcement and the same cross-section as those of the columns, although the transverse reinforcement is made up of No. 5 and 6 rebars. The south abutment is about 6 m (20 ft) deep. It is restrained transversely by retaining walls. A footing measuring 9.7 m (32 ft) in length, 3.8 m (12 ft) in width, and 0.91 m (3 ft) in depth is located directly beneath the abutment-deck seating block.

The north abutment is approximately 2.4 m (8 ft) deep. It is restrained transversely by wing walls. A footing measuring 9.7 m (32 ft) in length, 4.8 m (16 ft) in width, and 0.91 m (3 ft) in depth is located directly beneath the abutment-deck seating block. The footings, wing walls, and abutment walls were constructed with WSDOT Class "B" mix concrete providing a compressive strength of f'_c = 20.7 MPa (3 ksi). The concrete for the superstructure (Slabs, Girders, Diaphragms, and Barriers) was class AX, providing a compressive strength of f'_c = 27.6 MPa (4 ksi). The concrete in the columns was specified to be class RC, providing a compressive strength of f'_c = 34.47 MPa (5 ksi). The reinforcing steel conforms to AASHTO M31 Grade 60 with a yield strength of f_y = 413.6 MPa (60 ksi).

Structural model

As with the previous models, this bridge was discretized by 3-node quadratic Timoshenko (shear flexible) beam elements, resulting in a so-called spine model, as shown in Figure 14.

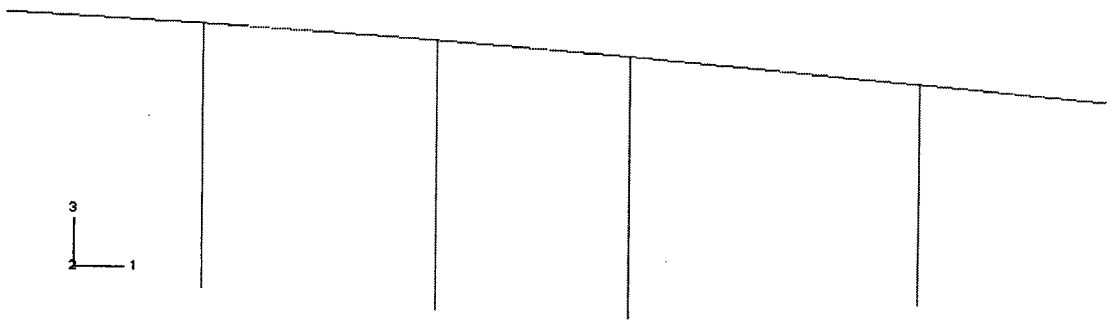

Figure 14. Bridge 90 spine model.

Figure 15 shows the assigned deck cross-section, for the computation of cross sectional properties. A solid finite element model of the bridge deck was created to confirm the torsional properties. As expected for a closed cross section, the warping effects were much less significant than for the previous two bridge decks. Thus, the torsional stiffness that was used for the spine model of Bridge 90 was taken as the original torsional stiffness value computed by ABAQUS.

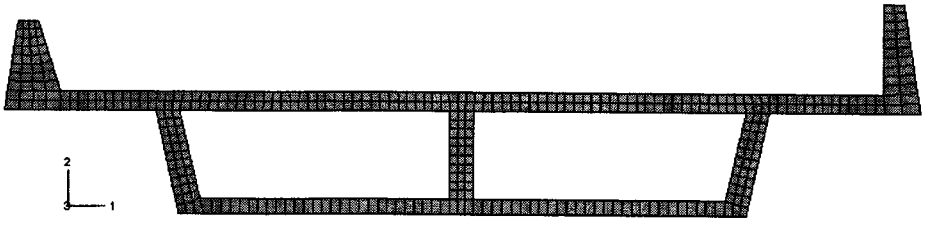

Figure 15. Bridge 90 meshed deck cross section.

The Bridge 90 north abutment is connected to the deck with a compression seal and fixed bearings, restraining the longitudinal deck movement. The south abutment is connected to the deck with a strip seal (gap = 7 cm) and guided bearings, allowing longitudinal deck movement. Each abutment was modeled as a single node with a lumped mass. Linear springs connected the soil to the abutments to represent the Soil-Structure Interaction (SSI). The SSI characteristics were determined following the FEMA 356 (2000) procedure based on the geometric properties of the abutment footing.

The longitudinal stiffness of the bearing pads was based on Equation 4. In the longitudinal direction, a nonlinear gap spring and a connector element were added in parallel to the bearing pad spring to model the 7.6 cm (3 in) gap between the south abutment and the deck. The north abutment was modeled similarly, but did not have a bearing pad spring in parallel (see Figure 16). The connector was defined as a nonlinear spring including the plasticity effect to model the damage of the abutment resulting from pounding. The connector force-displacement curve was determined following the Caltrans – Seismic Design Criteria – procedure.

Figure 16. FE model of the soil, abutments, and deck interaction in the longitudinal direction.

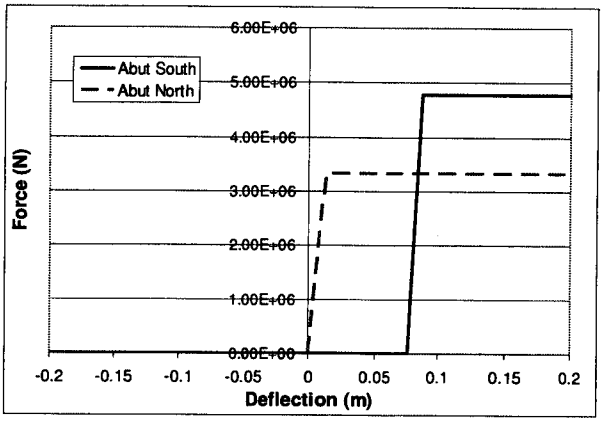

Figure 17. Abutment force-displacement curves.

The columns were considered fixed with the deck. The abutment and column footing soil springs were applied at the abutment and column footing nodes. Nonlinear springs along the pile shafts were used to model the resistance provided by the surrounding ground. The L-Pile software (ENSOFT 2002) was used to compute the *P-Y* curves, based on the stiff clay soil model without free water at 6 depths. The results were verified and compared to the procedure of Welch and Reese (1972). Figure 18 shows a summary of the different applied boundary conditions.

The ground motions were applied at the foundation nodes in the transverse, vertical and longitudinal directions. If not known, the vertical component of the ground motions was taken as 66% of the fault normal component. Figure 19 shows the points of application of the earthquake to the model, including SSI.

Table 6 summarizes the frequency content of Bridge 90. The first mode of vibration of Bridge 90 is in its longitudinal direction with a frequency of 1.22 Hz (period, T = 0.82 sec.). The bridge transverse direction is excited by its second mode of vibration with a frequency of 2.11 Hz (T = 0.47 sec.).

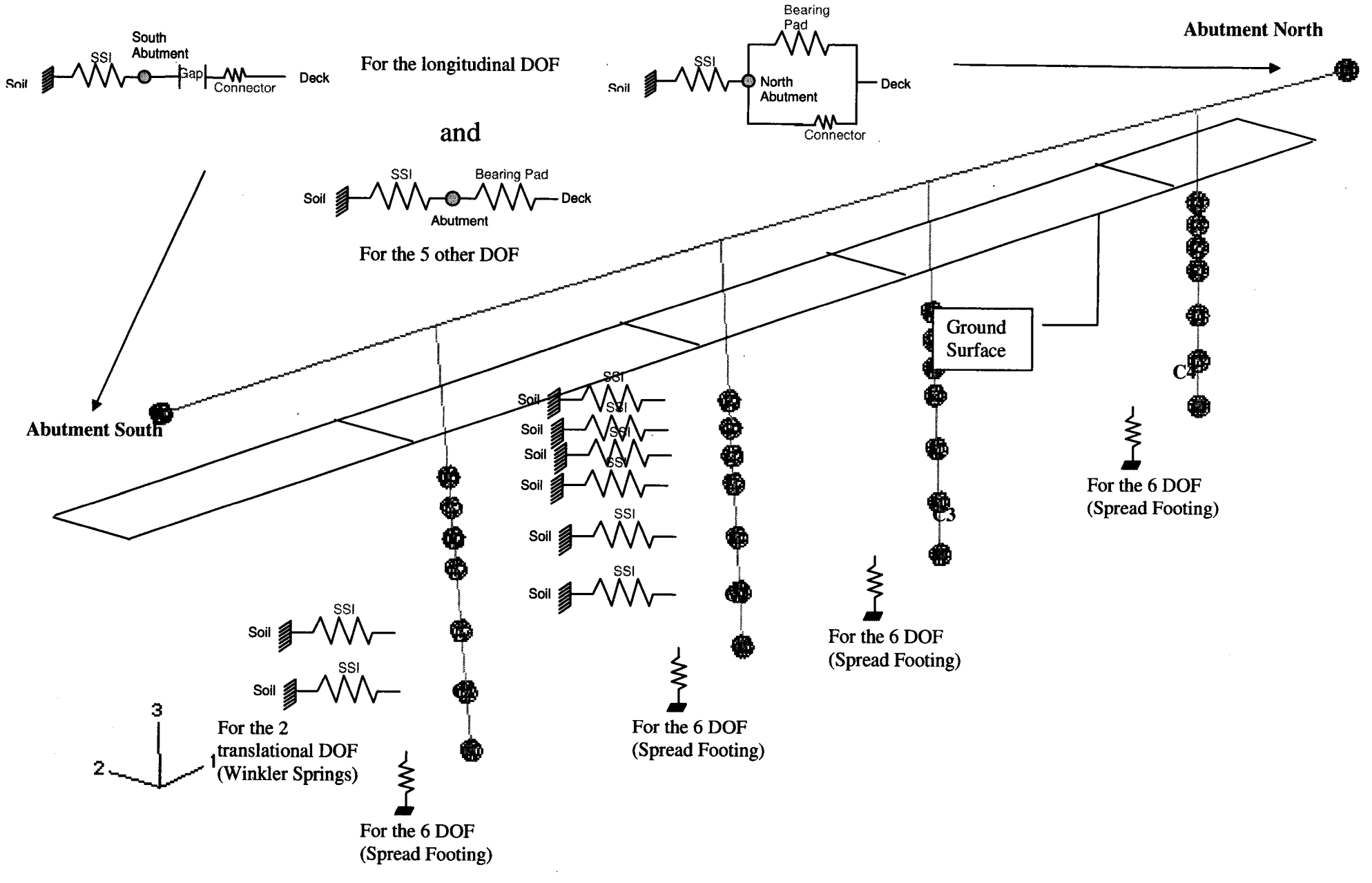

Figure 3.33. Boundary conditions for the Bridge 90 structural model.

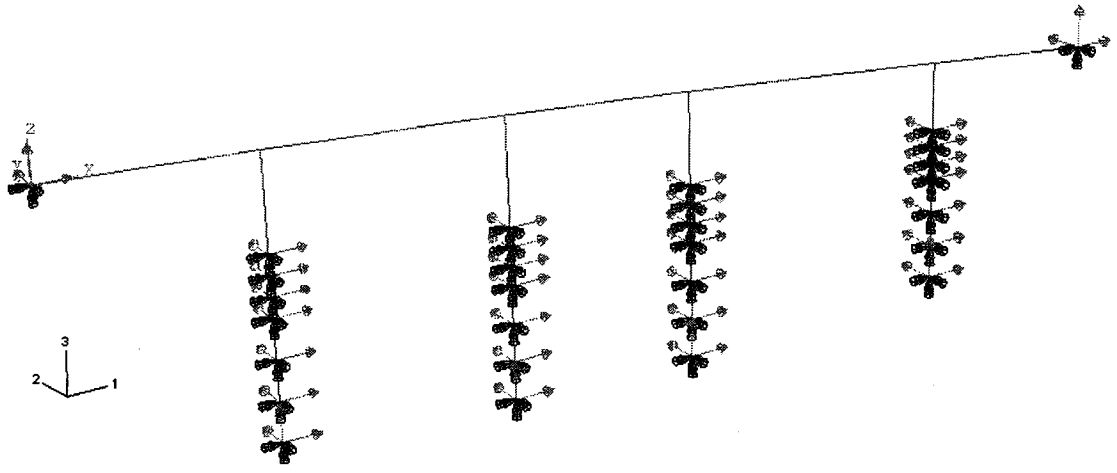

Figure 19. Points of application of the earthquake at the foundation nodes.

Table 6. Frequency content of Bridge 90

Eigenvalue Output					
Mode No	Eigenvalue	Frequency		Generalized Mass	Governing DOF
		(Rad/Time)	(Cycles/Time)		
1	58.485	7.6476	1.2171	1.05E+06	**X-Component**
2	176.4	13.281	2.1138	5.97E+05	**Y-Component**
3	906.86	30.114	4.7928	1.13E+06	
4	1544.7	39.302	6.2552	1.11E+06	
5	1616.4	40.204	6.3987	1.60E+05	
6	2545.6	50.454	8.0301	1.76E+05	

ANALYSIS RESULTS

Presented here are results from the nonlinear finite element time-history analyses of the three bridges. The terms "Regular" and "Inverse" refer to how the two ground motion components were applied to the bridge. "Regular" means that the FN and FP components were applied to the bridge transverse and longitudinal directions, respectively, and vice versa for "Inverse". Results are analyzed by describing the general behavior of the bridges and the effect of forward directivity and the velocity pulse period. Comparisons with the provisions of the AASHTO design methods and with those of a SDOF system are also presented.

GENERAL BRIDGE BEHAVIOR

Bridges 405 and 520

The behavior of Bridge 405 is described through its response to the non-FDGM recorded at Moquegua City during the southern Peru earthquake of June 23, 2001 (M_w = 8.4). The ground motion lasted about 2 minutes.

The bridge, due to the boundary conditions and to its geometry, showed different responses in its transverse and longitudinal directions. The bridge was very stiff in its transverse direction because of the high resistance provided by the bents. The moment-curvature relationship for the southwest column is shown in Figure 20. One can observe the pinching behavior and the decreasing stiffness of the column in the longitudinal direction. For comparison purposes, the backbone curve (in dashed green) was computed from a freeware program (USC_RC, Asadollah Esmaeily) which is based on the analysis of a cross-section fiber model. The computed curve closely matches the backbone curve from the ABAQUS model.

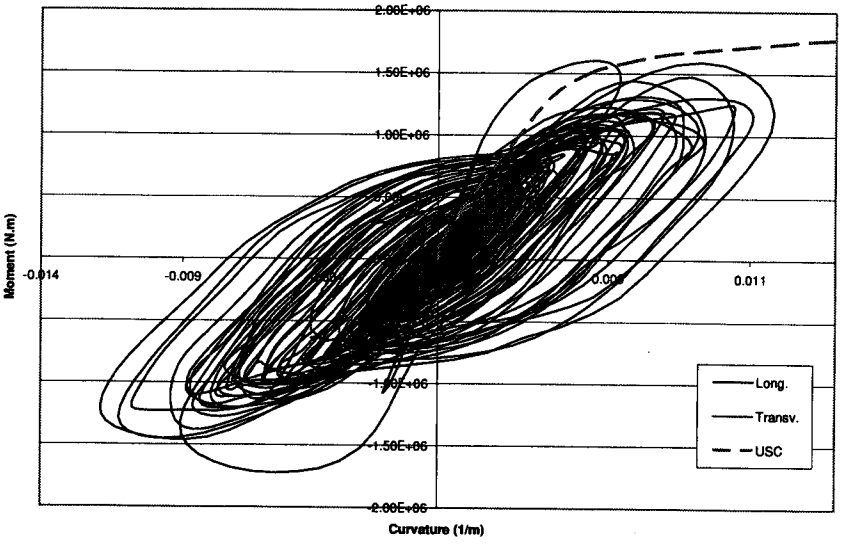

Figure 20. Moment-curvature hysteresis curves in the transverse (red) and longitudinal (black) column direction.

The columns were in double curvature in the transverse direction due to the two columns per bent and single curvature in the longitudinal direction. A plot of lateral force versus relative displacement for the southwest column is shown in Figure 21. The longitudinal component of the column relative

displacement was higher than the transverse one, as shown in Figure 21; however the column base shears were of similar amplitude.

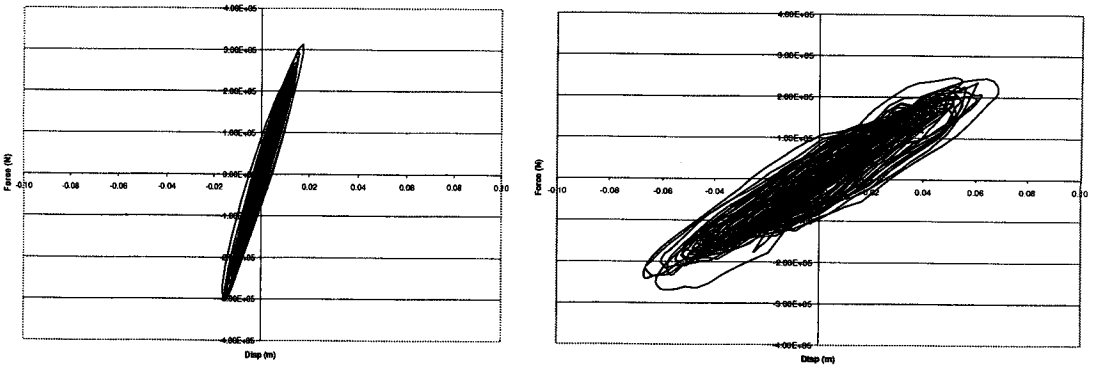

Figure 21. Force-displacement hysteresis curves in the transverse (left) and longitudinal (right) directions.

A plot of force versus displacement is shown in Figure 22 for Bridge 405. In dashed green, the shear capacity envelope proposed by Kowalsky and Priestley (2000) is shown. The column base shears never cross the shear capacity envelope. There is, therefore, very little risk of brittle shear failure in the columns. The ABAQUS output variable defined as the internal energy sums the total strain energy, energy dissipated by plastic deformation, and the kinetic energy. The internal energy in the system increases gradually during the earthquake (see Figure 23).

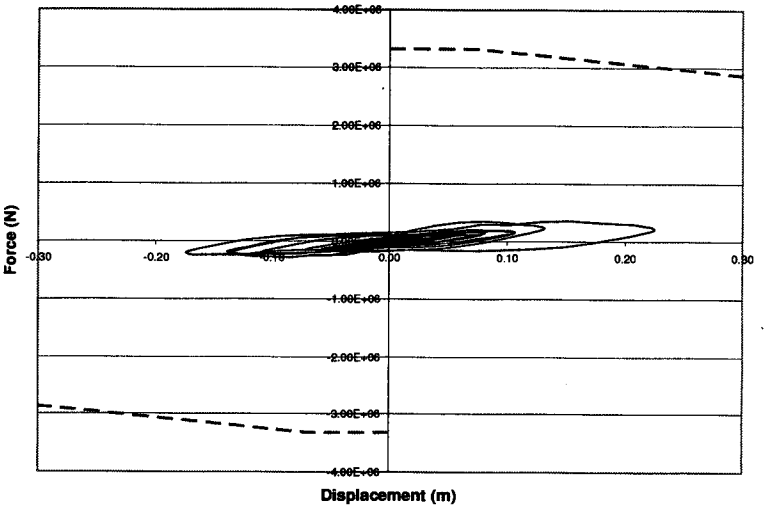

Figure 22. Bridge 405 force-displacement curve in the longitudinal direction, with column shear capacity

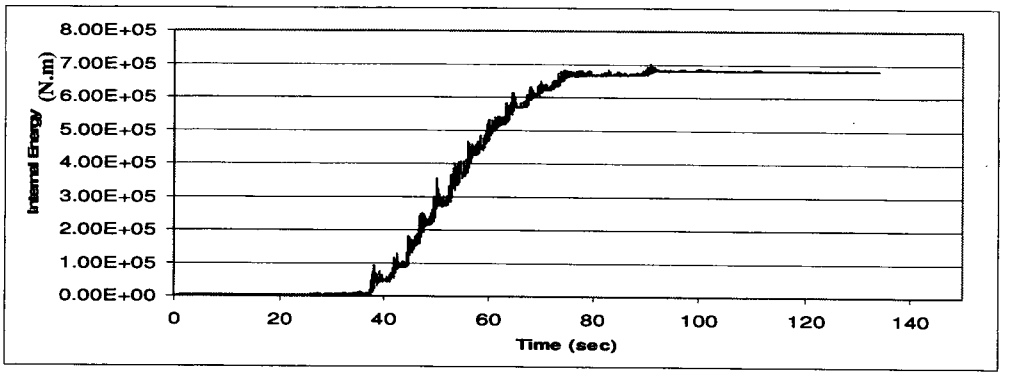

Figure 23. Internal energy in the system.

Figure 24 shows the longitudinal force response of the abutments from the Moquegua ground motion. At abutments, the deck was restrained only by the bearing pad's shear resistance when pushed toward the soil (negative displacement value on the Force-Displacement curve). But, when pushed in the opposite direction, one can see the high stiffness provided by the abutment when the 5 cm. (2 in.) gap closes (positive displacement value on the Force-Displacement curve). The north and south abutments experience pounding several times (Figure to the right), but do not reach their maximum allowable compressive force.

The general behavior of Bridge 520 was similar to that of Bridge 405 since the geometry and the boundary conditions were similar.

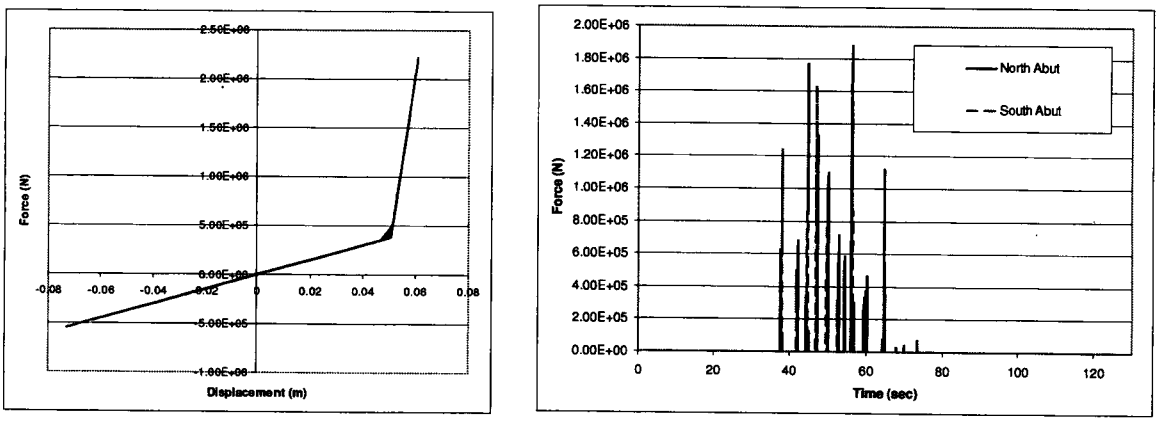

Figure 24. Abutment hysteresis force-displacement curve (left) and force time history curve (right).

Bridge 90

The behavior of Bridge 90 is described through its response to the non FDGM recorded in the Izmit Gulf during the M_w = 7.4 Kocaeli, Turkey, earthquake of August 17, 1999.

The longitudinal moment-curvature relationship at two locations of the northern column is shown in Figure 25. The moment-curvature seen at the top of the column is shown in blue and the moment-curvature seen at about 3 m (10 ft) below the ground level is shown in red where the maximum moment and curvature were recorded.

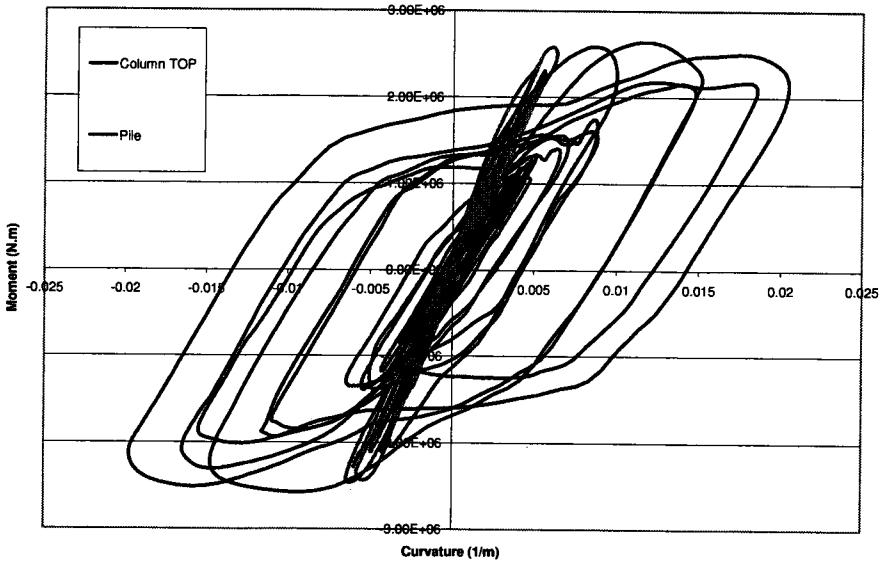

Figure 25. Moment-curvature hysteresis curves at the column top (blue) and at the pile (red) in the longitudinal direction.

A plot of lateral force versus relative displacement for the four columns is shown on Figure 26. The maximum forces were experienced at the column tops. The relative displacements were computed between the column top and the ground level. The four columns did not have the same response to the ground motions since they have different heights and Bridge 90 is not symmetric. The column C1 is the southern column, C4 is the northern one. The tallest column (C2, in green) experienced the highest relative displacement and the lowest resisting force. Conversely, the smallest column (C4, in red) experienced the lowest relative displacement and the highest resisting force.

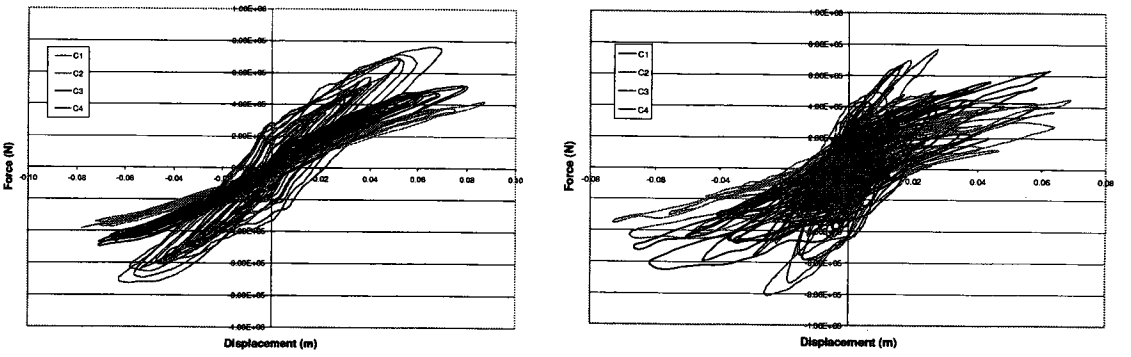

Figure 26. Column force-displacement hysteresis curves in the longitudinal (left) and transverse (right) direction.

A plot of force versus displacement is shown in Figure 27 for Bridge 90. In purple, the shear capacity envelope proposed by Kowalsky and Priestley (2000) is shown. The column base shears never cross their shear capacity envelope. There is no risk of brittle shear failure in the columns. The internal energy in the system increases gradually during the earthquake due to the energy dissipated by the columns (see Figure 28).

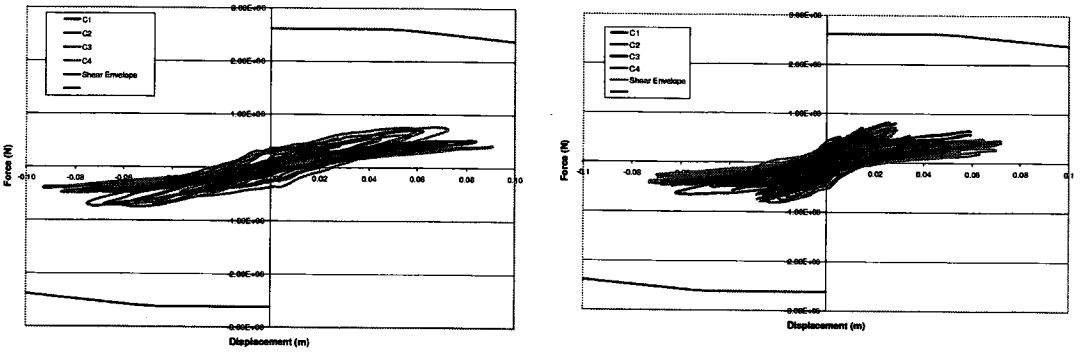

Figure 27. Force–displacement hysteresis curves in the longitudinal (left) and transverse (right) directions.

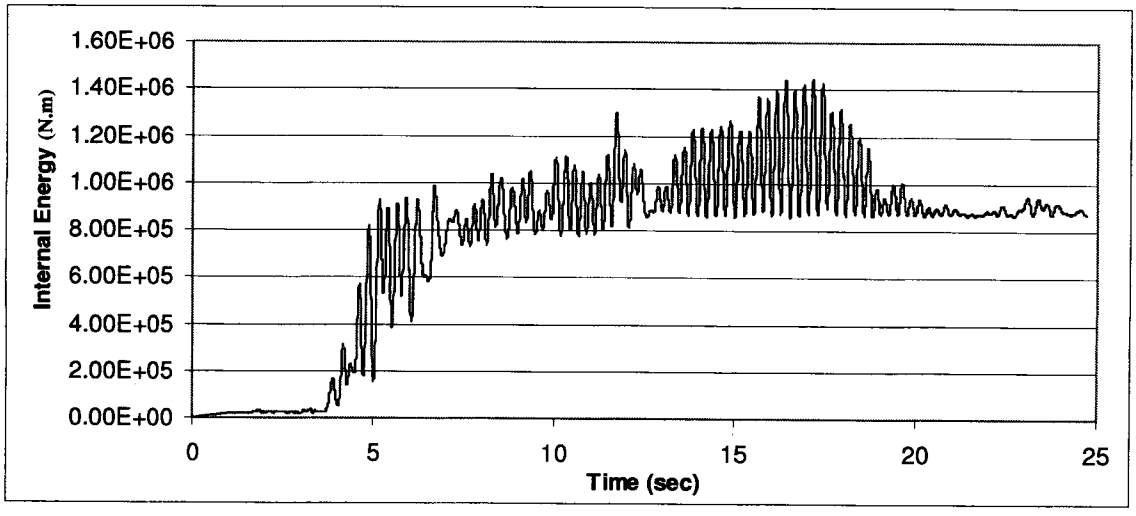

Figure 28. Internal energy in the system.

Figure 29 shows the longitudinal force response of the abutments from the Izmit ground motion. The abutments experienced pounding several times. Note also that they reached their maximum allowable compression force and experienced several cycles of plastic behavior.

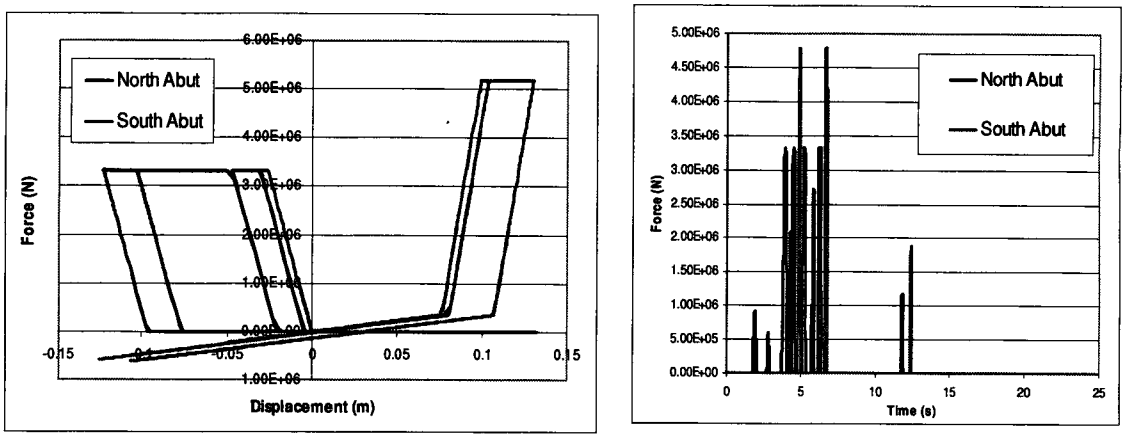

Figure 29. Abutment hysteresis force-displacement curve (left) and force time history curve (right).

FORWARD DIRECTIVITY EFFECTS – FREQUENCY CONTENT

Significant seismic damage may occur if the structure response is 'in tune' with components of the ground motion (resonance), which may be identified from the response spectrum. Figures 30 to 32 show

the acceleration response spectra (ARS) of the FN ground motion's component for each bridge. The blue and red vertical dashed lines are, respectively, the transverse and longitudinal mode shape periods. The forward directivity "bump" effect is visible on the acceleration response spectra (ARS) of the FN ground motion components. It is created by the velocity pulse, typical of a forward directivity ground motion (Somerville et al., 1997). The ARS show only one curve for each bridge for the non-FD ground motions since they have approximately the same frequency content. The ABAQUS output results (max displacement, max base shear, energy dissipated) as a function of the spectral acceleration value (S_a) are included in Appendix C.

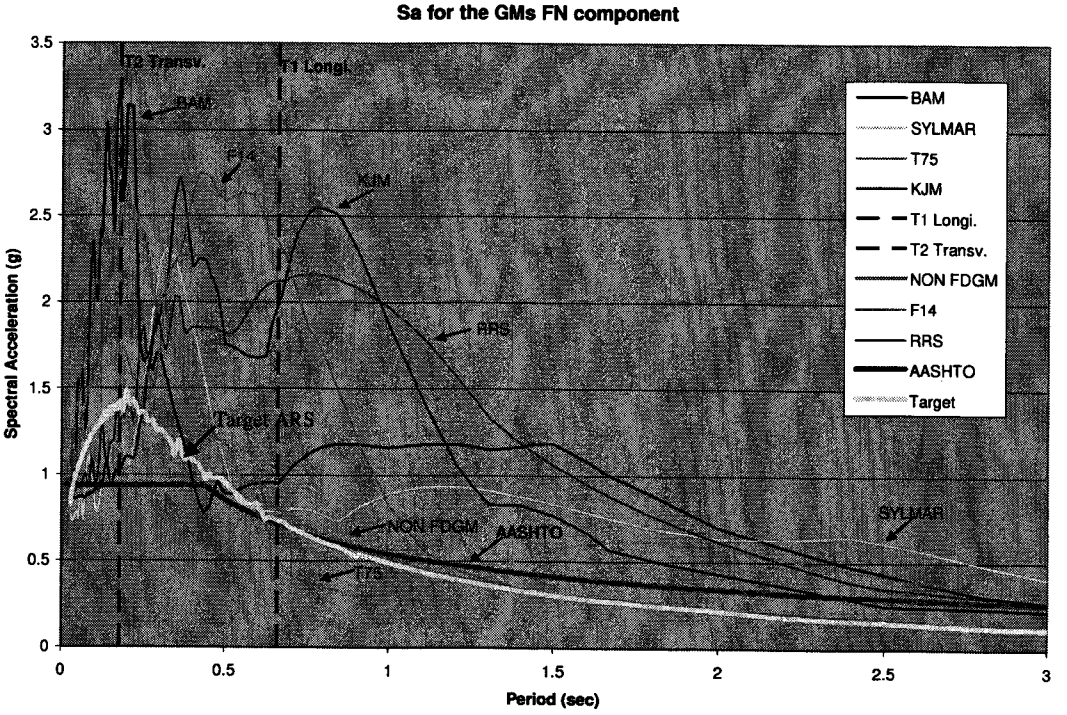

Figure 30. Bridge 405 ARS of the FN components of the ground motions.

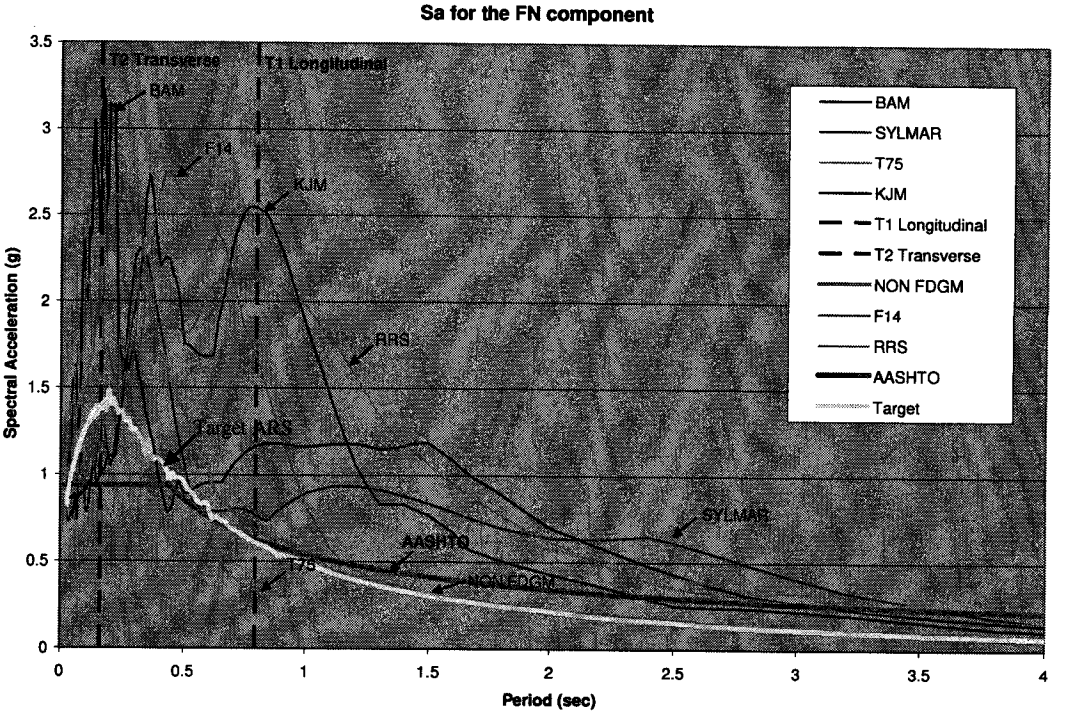

Figure 31. Bridge 520 ARS of the FN components of the ground motions.

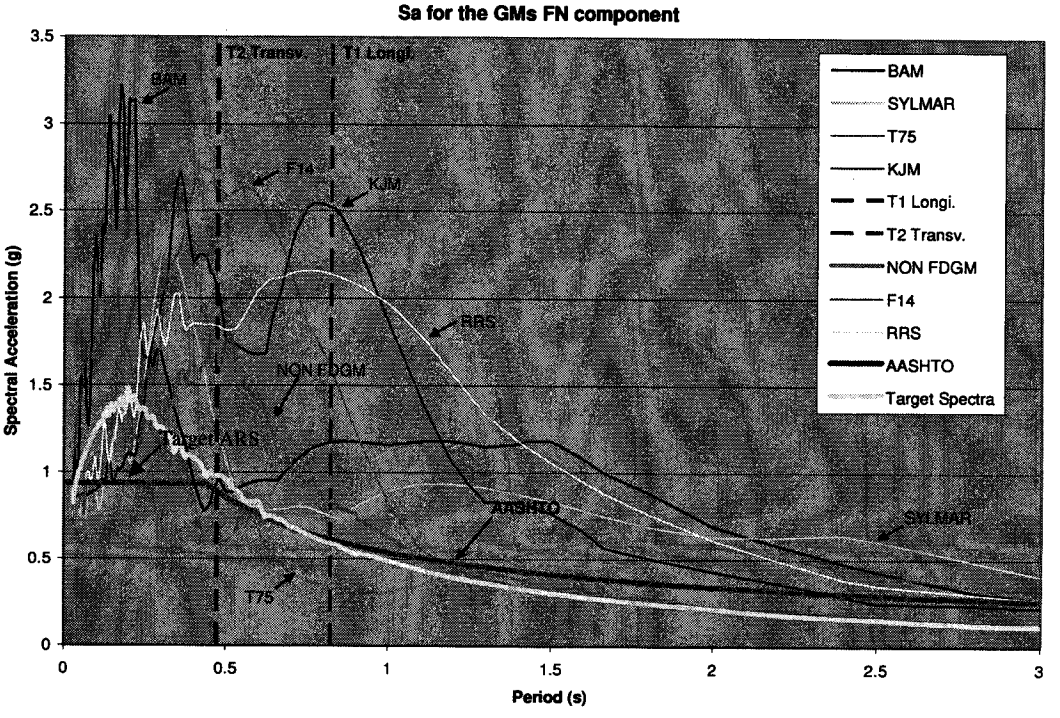

Figure 32. Bridge 90 ARS of the FN components of the ground motions.

Longitudinal Response

Figures 33 to 38 below show the effect of the spectral acceleration at the bridge fundamental longitudinal frequency on the peak column response in the longitudinal direction. The pink triangles represent the response from the FDGMs and the blue diamonds represent the response from the Non-FDGMs. For the "Regular" plots (on the figure's left), the FP ground motion component was applied to the bridge longitudinal direction, and for the "Inverse" plots (on the figure's right), the FN ground motion component was applied to the bridge longitudinal direction. Consequently, the range of ARS values (x-axis) was higher for "Inverse" than for "Regular" since the FD effect is seen only in the FN ground motion component.

In nearly all cases, there is a direct correlation between S_a and maximum base shear. Interestingly, the correlation appears to be similar for FDGMs and non-FDGMs and, with the exception of Bridge 405, the correlation between maximum shear and S_a applies to the FN and FP directions.

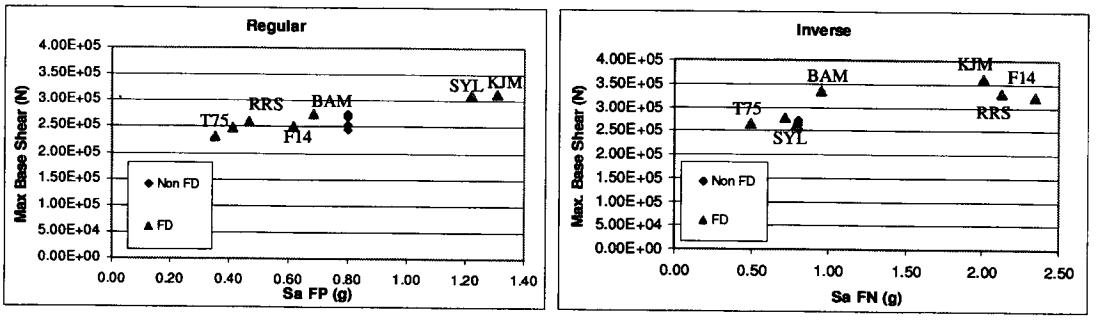

Figure 33. Bridge 405 max longitudinal base shear, S_a's at $T_l = 0.65$ sec.

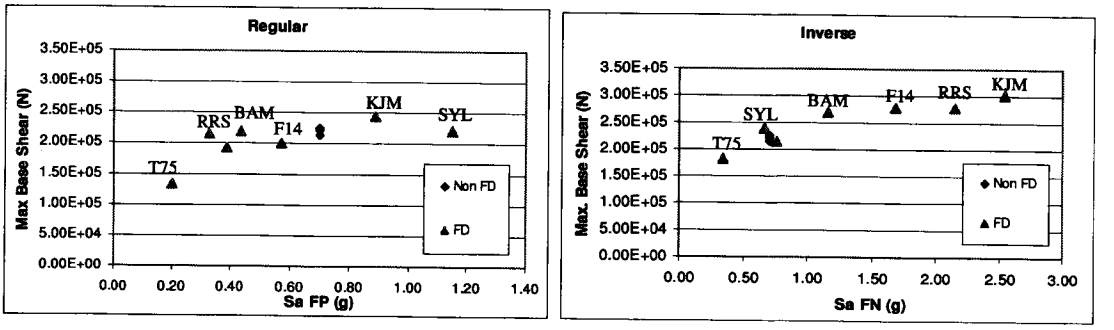

Figure 34. Bridge 520 max longitudinal base shear, S_a's at $T_l = 0.80$ sec.

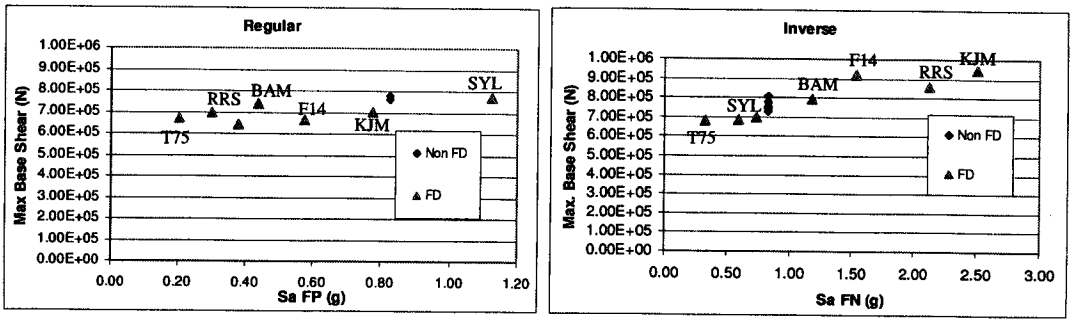

Figure 35. Bridge 90 max longitudinal column shear, S_a's at $T_1 = 0.82$ sec.

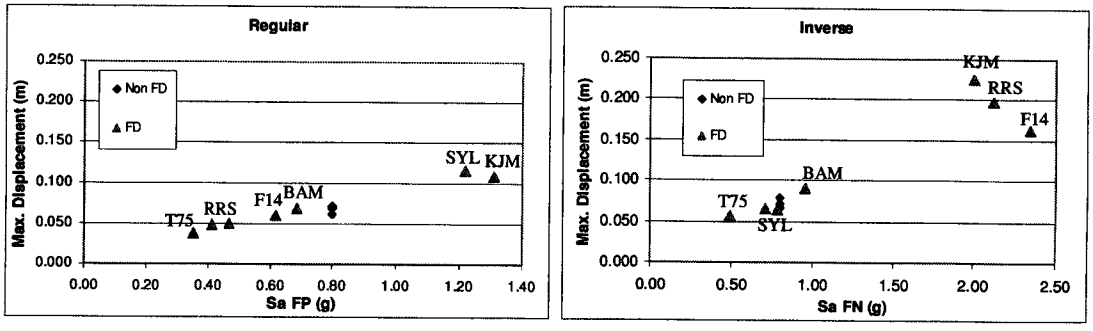

Figure 36. Bridge 405 max longitudinal relative displacement, S_a's at $T_1 = 0.65$ sec.

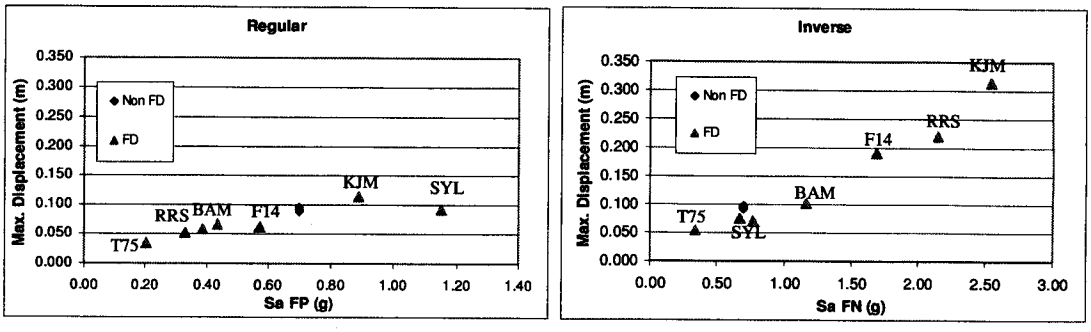

Figure 37. Bridge 520 max longitudinal relative displacement, S_a's at $T_1 = 0.80$ sec.

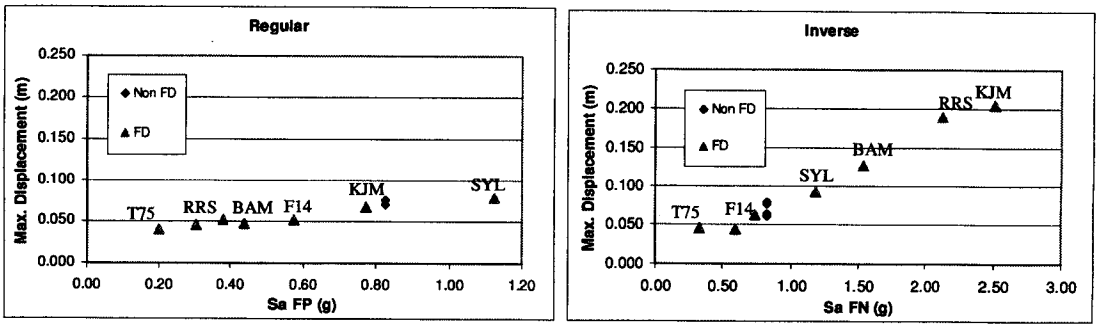

Figure 38. Bridge 90 max longitudinal relative displacement, S_a's at $T_1 = 0.82$ sec.

The column's maximum base shear increases slightly with the spectral acceleration due to the strain hardening effect after the column has yielded. A similar trend is seen for maximum column displacements, but its effect is more pronounced. Since the column behaves plastically, the displacements increase rapidly in the plastic plateau region. The maximum displacements for the FDGMs can be significantly higher than those for the non-FDGMs due to their high relative value of spectral acceleration at this period. The FD effect is seen in the intermediate period range for the selected motions ($0.5s < T < 1s$) of the FN GM component ("Inverse" plots). The range of spectral acceleration value is smaller for the FP component since the FD effect is less pronounced.

The energy dissipated by plastic deformation in the system often increases abruptly during a FDGM, as shown on Figures 39, 40, and 41. It is interesting to note that the level of damage is highly dependent upon the period of the bridge versus that of the forward directivity pulse. Table 7 summarizes the different fundamental bridge periods and velocity pulse periods of the FN ground motion component. When the two periods are close, most of the damage occurs during the pulse, as in the KJM Inv, RRS Inv, and F14 Inv earthquakes. For cases in which there is no pulse or the pulse period does not match the fundamental period of the bridge, the damage is much lower and it increases gradually. The damage curve for the KJM Inv and RRS Inv ground motions for Bridge 90 did not reach a very high level since one of the columns failed during the first seconds of the record, which made the finite element analysis terminate.

Table 7. Fundamental bridge periods and FDGM's velocity pulse periods (T_v)

Period (sec)	Bridge 405	Bridge 520	Bridge 90
$T_{longitudinal}$	0.66	0.80	0.82
$T_{transverse}$	0.18	0.17	0.47

FDGM	T_v (sec)
BAM	2.065
F14	0.75
KJM	1
RRS	1.25
Sylmar	2.32
T75	2.5
LCN	5.5

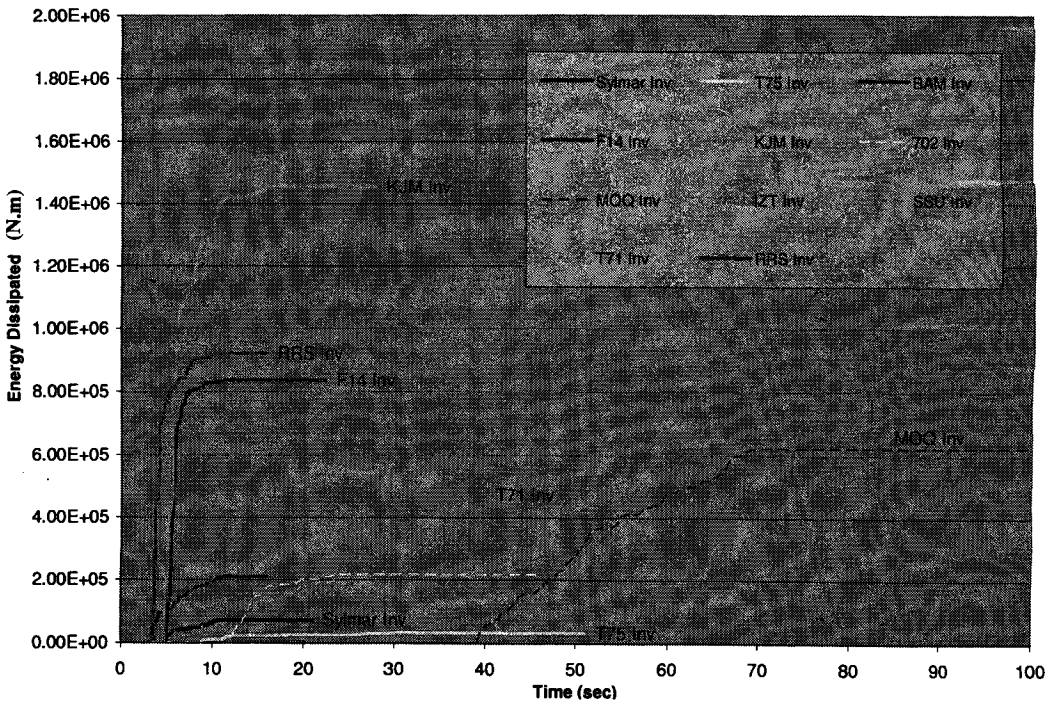

Figure 39. Bridge 405 energy dissipated by plastic deformation for the non-FD (dashed) and FDGM's (solid).

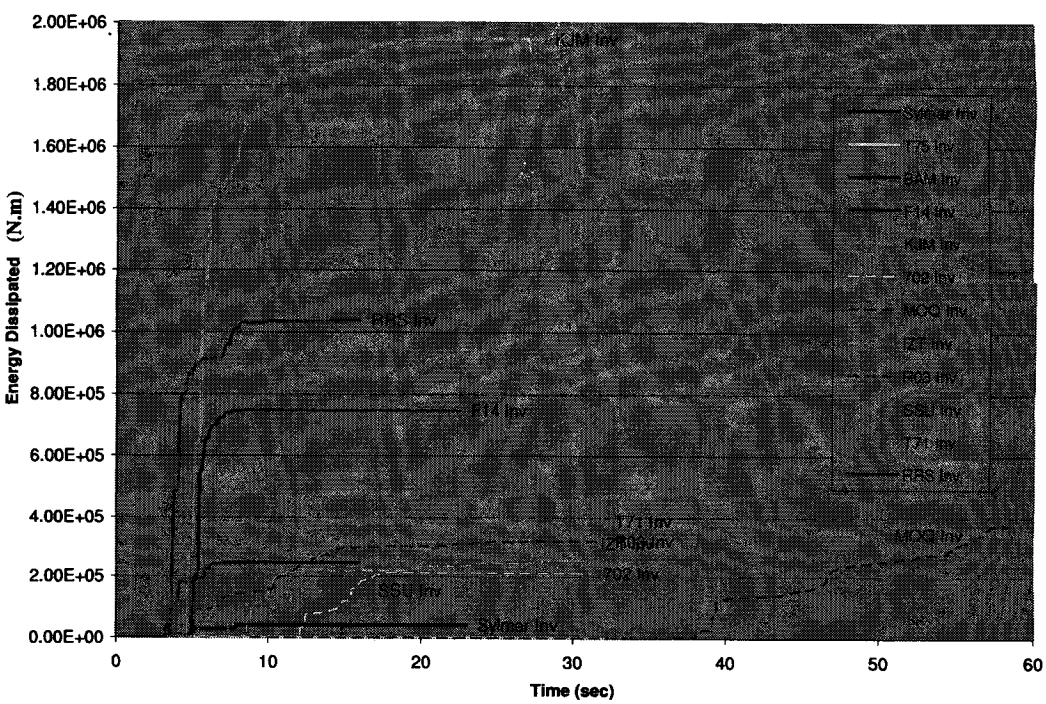

Figure 40. Bridge 520 energy dissipated by plastic deformation for the non-FD (dashed) and FDGM's (solid).

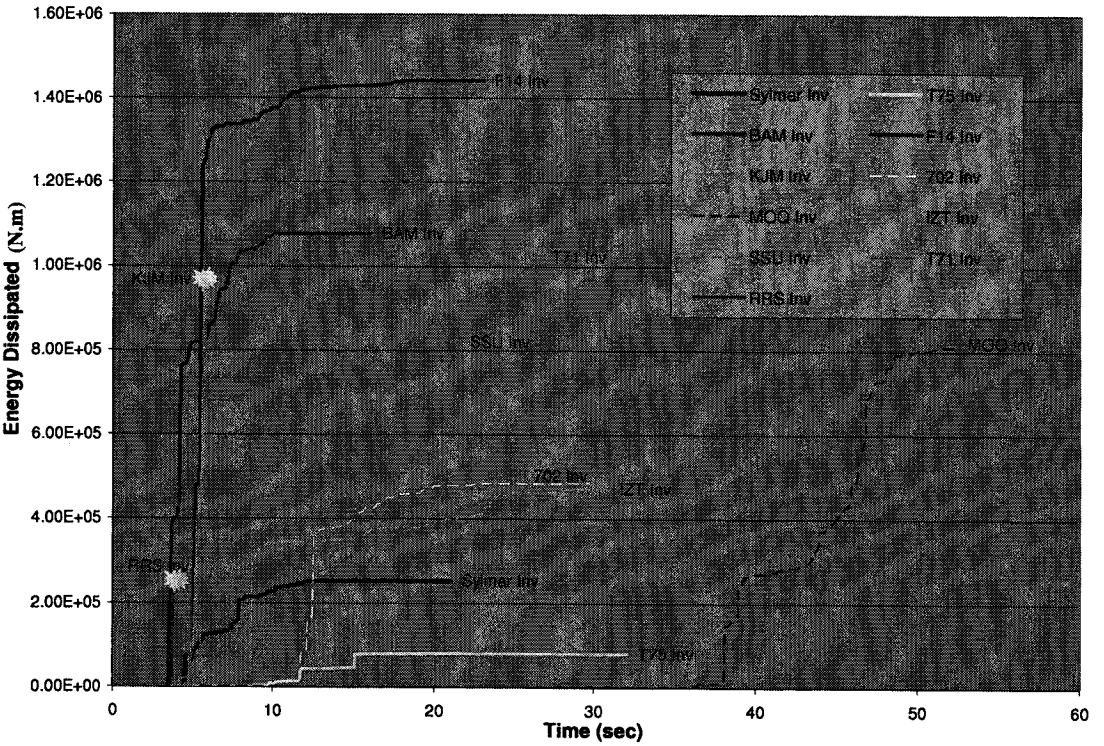

Figure 41. Bridge 90 energy dissipated by plastic deformation for the non-FD (dashed) and FDGM's (solid). Column failure noted for KJM Inv and RRS Inv records.

Plots of force versus displacement and moment versus curvature are shown in Figure 42 for the most damaging ground motion considered on Bridge 405. The hysteretic curves show the expected pinching behavior and decreased column stiffness and strength due to the double-sided velocity pulse of the FDGM. From the plots, one can see that the majority of plasticity and damage results from only a few large cycles.

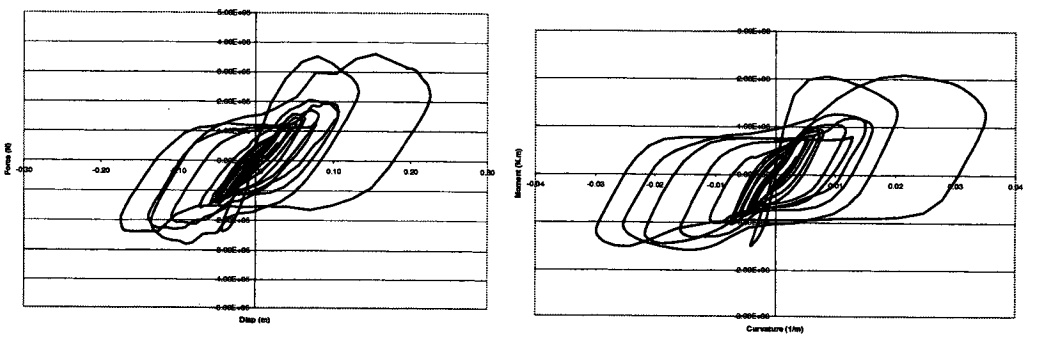

Figure 42. Bridge 405 Force-Displacement and Moment-Curvature hysteresis curve from the FD KJM GM, in the longitudinal direction.

A plot of moment versus curvature is shown in Figure 43 for the most damaging ground motion considered for Bridge 90. In dashed red, the backbone curve was computed from the cross-section analysis. The end of the curve indicates the failure of the column cross-section. The peak spectral acceleration closely matched the longitudinal fundamental period of vibration of the structure. This ground motion induced the bending failure of the shortest column (C_4). ABAQUS stopped the analysis when the maximum material capacity was reached at the top of the column. It does not indicate the overall failure of the bridge but, rather, a local failure. One can note that the column did not fail when it reached its first maximum curvature at the end of the cross-section analysis curve, but the second time. The maximum curvature capacity from ABAQUS was slightly higher than that from the cross-section analysis. A plot of force versus displacement is shown in Figure 44. The column reached its maximum displacement capacity of approximately 20 cm (8 in). In dashed green, the shear capacity envelope proposed by Kowalsky and Priestley (2000) is shown. The column shear capacity is shown to be higher than its bending capacity for any displacement level.

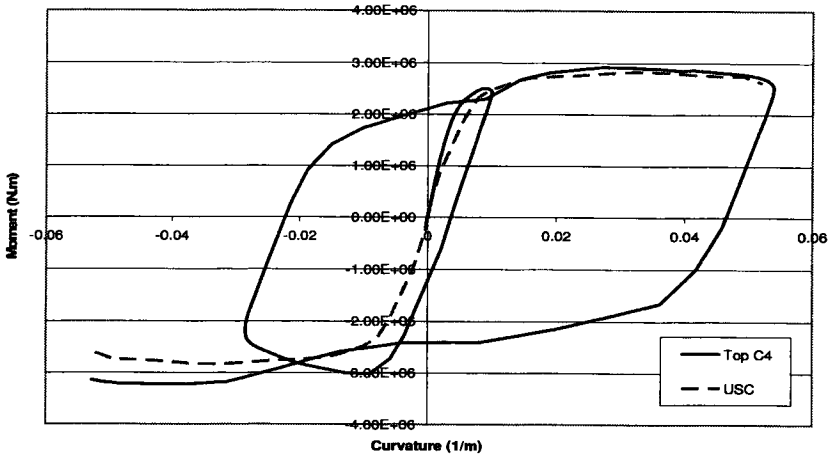

Figure 43. Bridge 90 Moment-Curvature hysteresis curve of column C_4 from the FD KJM ground motion, in the longitudinal direction.

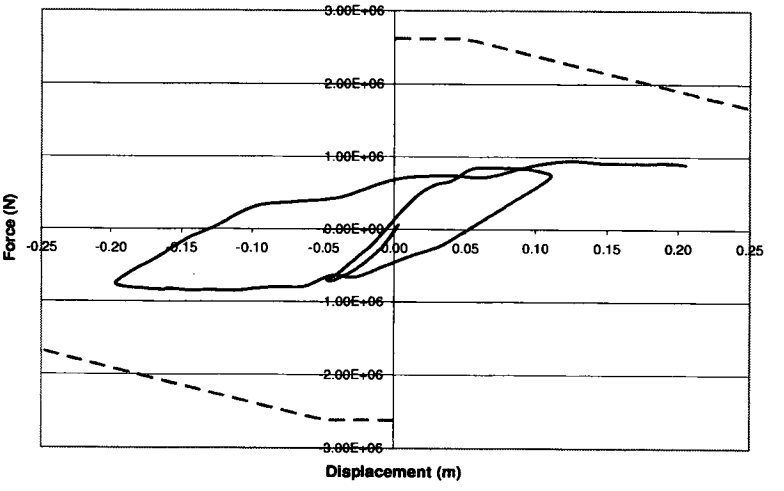

Figure 44. Bridge 90 Force – Displacement hysteresis curve of column C_4 from the FD KJM ground motion, in the longitudinal direction. Column shear capacity is shown in dashed green.

Tables 8, 9, and, 10 summarize the response of the abutments during the earthquakes. "Pounding" indicates that the gap closed, "# max pressure" is the number of times the abutment reached its maximum allowable pressure force, and "Deformation" is the maximum plastic deformation in the springs. For Bridge 405, the non-FDGM's did not induce any damage in the abutments, but the FDGM BAM, Sylmar, F14, and KJM did. Again, note that pounding only occurred once or twice, indicating that it results from the forward directivity pulse. For Bridge 520, the non-FDGMs SSU and T71 induced four to five repeated poundings of the abutments, but the level of damage was small. On the other hand, the FDGMs KJM Inv and RRS Inv induced during only one pounding (even though they touched twice) a much larger plastic deformation caused by the pulse. The abutments of Bridge 405 and Bridge 520 behaved differently since their geometry and, subsequently, their strength capacity were unique. The bearing pads displacement capacity, never reached, of 50 cm (20 in) was the same, however. For Bridge 90, the non-FDGMs induced repeated poundings of the abutments with varying levels of damage. On the other hand, the FDGMs KJM Inv and RRS Inv induced during only one pounding a much larger plastic deformation of 33 cm caused by the pulse.

Table 8. Bridge 405 Abutment pounding

		Regular			Inverse		
Type (M_w)	GM	Pounding	# max pressure	Deformation (m)	Pounding	# max pressure	Deformation (m)
Non FD	702	yes	0	0	yes	0	0
	IZT	yes	0	0	yes	0	0
	MOQ	yes	0	0	yes	0	0
	SSU	yes	0	0	yes	0	0
	T71	yes	0	0	yes	0	0
FD (6.9)	KJM	yes	1	0.014	**yes**	**2**	**0.16**
FD (6.5)	BAM	yes	0	0	yes	1	0.017
FD (6.2)	LCN	yes	0	0	yes	0	0
FD (6.0)	F14	yes	0	0	yes	2	0.09
FD (6.7)	RRS	yes	0	0	**yes**	**1**	**0.13**
FD (7.2)	Sylmar	yes	2	0.04	yes	0	0
	T75	yes	0	0	no	0	0

Table 9. Bridge 520 Abutment pounding

		Regular			Inverse		
Type (M_w)	GM	Pounding	# max pressure	Deformation (m)	Pounding	# max pressure	Deformation (m)
Non FD	702	yes	2	0.03	yes	1	0.014
	IZT	yes	2	0.03	yes	2	0.024
	SSU	yes	4	0.03	yes	2	0.012
	T71	yes	4	0.034	yes	5	0.036
FD (6.9)	KJM	yes	1	0.056	**yes**	**2**	**0.18**
FD (6.5)	BAM	yes	1	0.004	yes	2	0.043
FD (6.2)	LCN	yes	0	0	yes	1	0.015
FD (6.0)	F14	yes	1	0.001	yes	2	0.014
FD (6.7)	RRS	yes	0	0	**yes**	**1**	**0.17**
FD (7.2)	Sylmar	yes	3	0.03	yes	2	0.011
	T75	yes	0	0	yes	0	0

Table 10. Bridge 90 Abutment pounding

		Regular			Inverse		
Type (M_w)	GM	Pounding	# max pressure	Deformation (m)	Pounding	# max pressure	Deformation (m)
Non FD	702	yes	3	0.09	yes	2	0.08
	IZT	yes	5	0.1	yes	2	0.08
	MOQ	yes	8	0.08	yes	7	0.1
	SSU	yes	4	0.065	yes	4	0.1
	T71	yes	2	0.09	yes	3	0.1
FD (6.9)	KJM	yes	1	0.065	**yes**	**1**	**0.33**
FD (6.5)	BAM	yes	2	0.005	yes	1	0.11
FD (6.2)	LCN	yes	3	0.007	yes	1	0.07
FD (6.0)	F14	yes	3	0.04	**yes**	**1**	**0.19**
FD (6.7)	RRS	yes	4	0.007	**yes**	**1**	**0.33**
FD (7.2)	Sylmar	yes	4	0.06	yes	2	0.027
	T75	yes	1	0.001	yes	4	0.02

Transverse Response

Figures 45 to 50 show the effect of the spectral acceleration on the column response in the transverse direction. The column's maximum base shears and displacements increase nearly linearly with S_a. The bridge response is mainly governed by the frequency content of the ground motion. The transverse fundamental periods of Bridges 405 and 520 are around 0.2 sec. At this short period range ($0 < T < 0.5s$), the Forward Directivity "bump" effect does not appear in the ARS and the non-FDGMs had a greater spectral acceleration value. Consequently, the non-FDGMs often induced higher maximum base shears and displacements.

As in the longitudinal direction, the maximum column responses were governed by the ARS value but, in the transverse direction, those values were generally higher for the non-FDGMs than those for the FDGMs because the fundamental bridge periods were different. For the "Regular" plots (on the figure's left), the FN ground motion component was applied to the bridge transverse direction, and for the "Inverse" plots (on the figure's right), the FP ground motion component was applied to the bridge transverse direction.

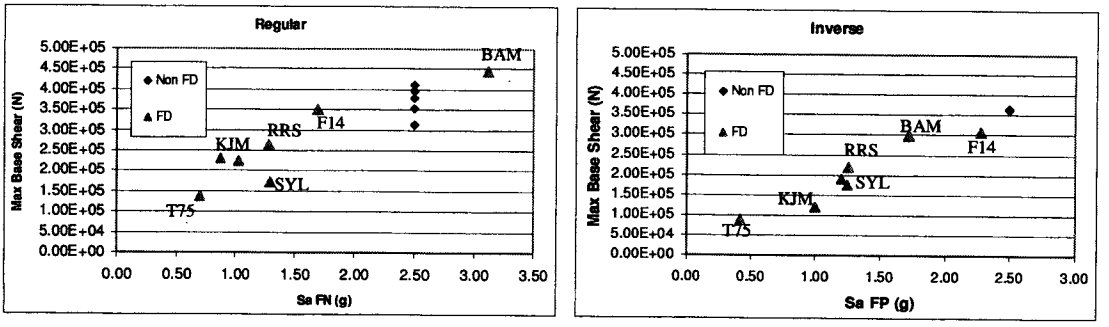

Figure 45. Bridge 405 Max Transverse Base Shear, S_a's at $T_t = 0.18$ s.

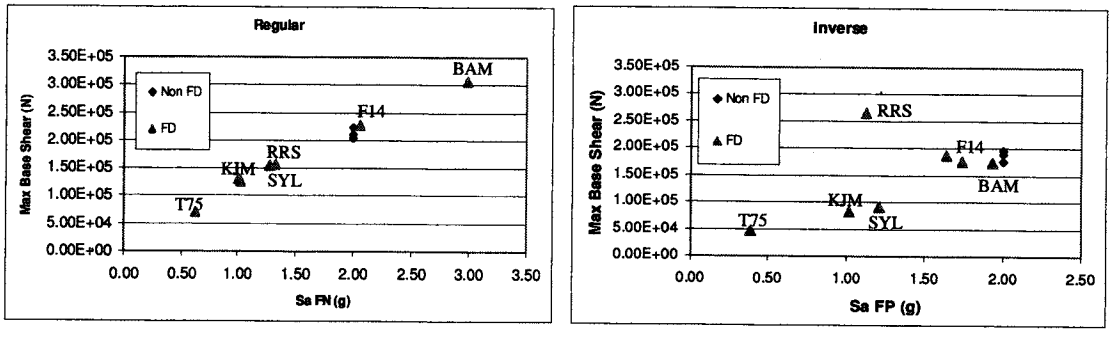

Figure 46. Bridge 520 Max Transverse Base Shear, S_a's at $T_t = 0.17$ s.

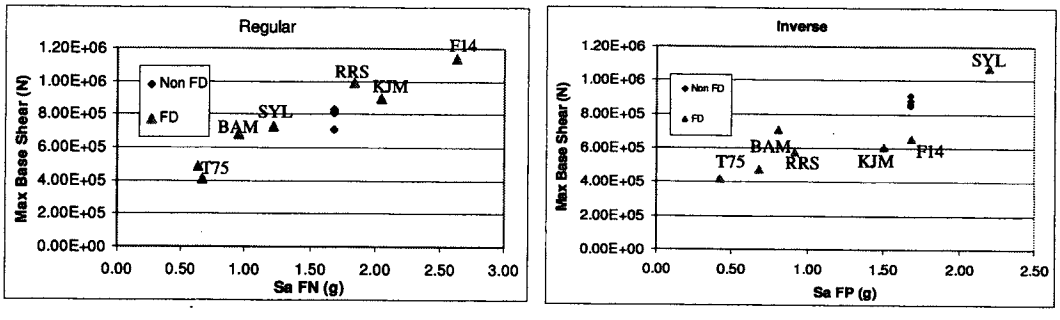

Figure 47. Bridge 90 Max Transverse Column (C_4) Shear, S_a's at $T_t = 0.47$ s.

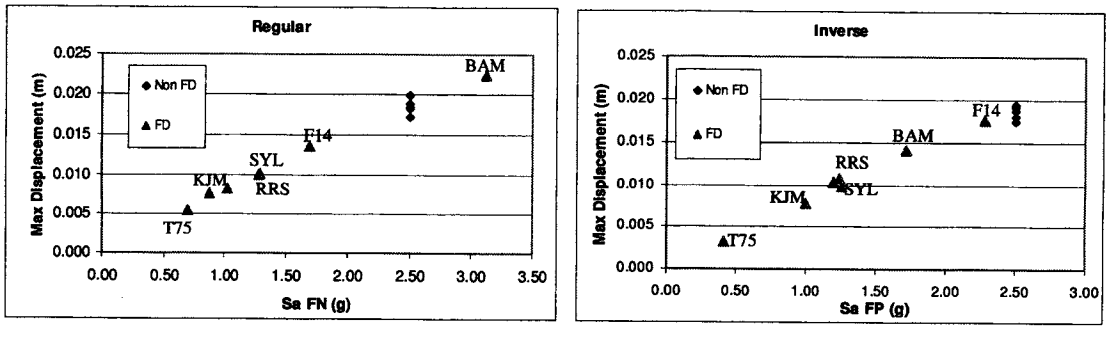

Figure 48. Bridge 405 Max Transverse relative Displacement, S_a's at $T_t = 0.18$ s.

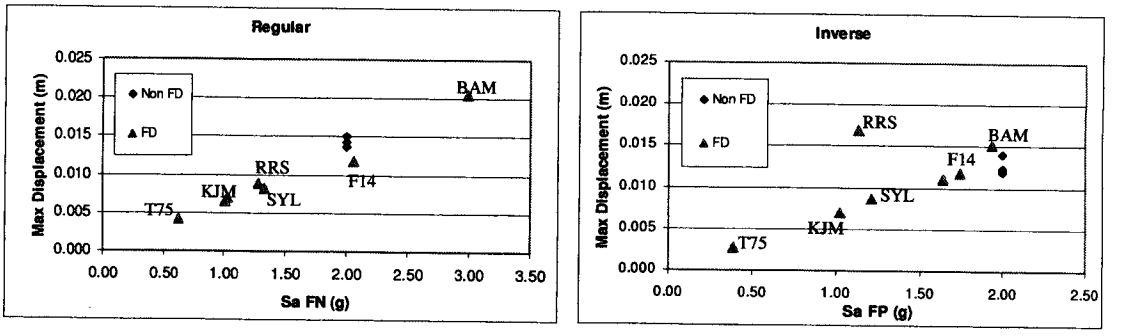

Figure 49. Bridge 520 Max Transverse relative Displacement, S_a's at $T_t = 0.17$ s.

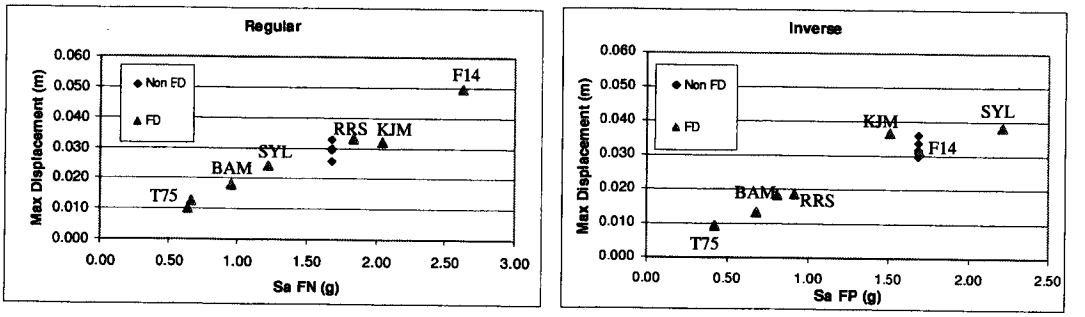

Figure 50. Bridge 90 Max Transverse Column (C_4) relative Displacement, S_a's at $T_t = 0.47$ s.

VELOCITY PULSE PERIOD EFFECT

The effect of the velocity pulse period was investigated. A plot of maximum longitudinal displacement from the FN component of the FDGMs versus velocity pulse period is shown on Figure 51. One can see that the maximum displacement in the governing columns is much higher when the velocity pulse period is close to the fundamental longitudinal periods (in dashed red in the Figures) of the bridges. These results were expected and agree with earlier results since the "bumps" seen in the FN FDGM response spectra correspond to their pulse period, or periods (Somerville et al. 1997). The pulse period range that is the most influential on the bridge response does not exceed $^{+}/_{-}$ 0.5 sec from the fundamental bridge period. The severity of the demand was controlled by the ratio of the pulse period to system period.

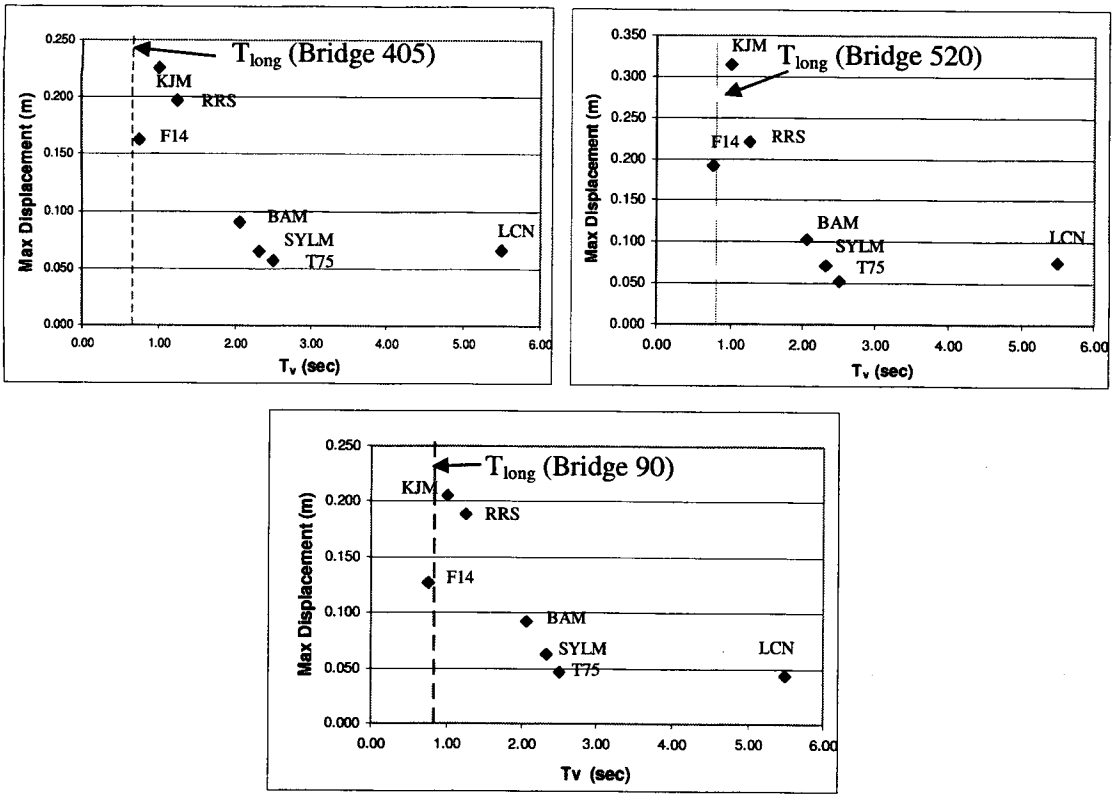

Figure 51. Bridge 405 (left), Bridge 520 (right), and Bridge 90 (down) Max Displacement Vs. Velocity Pulse Period

The FDGM pulse period is proportional to the earthquake magnitude, lengthening as the earthquake magnitude increases (Somerville 1998, Rodriguez-Marek 2000, and Alavi and Krawinkler 2000; see Equation 1). As a result, damage due to smaller magnitude earthquakes can be more significant for short period structures than damage due to larger magnitude earthquakes, since the near-fault pulse period is closer to the fundamental period of the structure in the smaller magnitude earthquake. Such was the case in this research. The KJM ground motion recorded from the magnitude 6.9 Kobe earthquake induced significantly higher damage to the columns than that from the LCN ground motion recorded from a magnitude 7.3 earthquake. The uncertainty associated with the pulse period determination is very high, however. At the current state of knowledge on the FDGMs, it is hard to predict the velocity pulse period. The probability of occurrence of a FDGM with a specific velocity pulse period is also difficult to predict. To be conservative, a designer may choose to consider a FD ground motion with a velocity pulse period matching the fundamental bridge period. However, such a choice could be greatly conservative. Since the

bridge response is mainly governed by the first velocity pulse, a simple ground motion consisting of a single pulse may be sufficient to evaluate bridge performance for forward directivity ground motions.

COMPARISON WITH A SDOF SYSTEM

Gillie (2005) utilized time-stepping Newmark's method to compute the nonlinear response of a SDOF system when subjected to the fault normal ground motion component. All near-fault ground motions were run using a Wen (1976) hysteretic relationship calibrated to a typical concrete hysteresis loop. A comparison of the multi-degree-of-freedom (MDOF) models of Bridge 520 and Bridge 405 was made to the nonlinear SDOF analyses by Gillie (2005). The comparison to nonlinear SDOF analyses was not possible for Bridge 90 because its column yielding force was significantly different from those of the SDOF models. The comparison was also not possible for the bridge transverse responses because the nonlinear SDOF system did not show realistic results at low period values. The analyses were conducted for unscaled motions. The SDOF maximum displacements were those computed in the case where the SDOF natural period matches the longitudinal bridge mode of vibration. Being able to accurately evaluate the modes of vibration of a structure is a key aspect to predicting its response using a nonlinear SDOF analysis. Figures 52 and 53 show the comparison, for each ground motion, of the maximum displacements found from the following models: nonlinear SDOF in pink circles, nonlinear MDOF (ABAQUS) including SSI in red diamonds, and nonlinear MDOF (ABAQUS) without SSI in blue squares. The SDOF maximum displacements are always unconservative with regard to the ones computed with the ABAQUS bridge models for the non-FDGMs, while the results for the FDGMs were mixed. The use of a simple SDOF system to predict the response of a complex structure under forward directivity ground motions is not recommended since the results were not consistent. The variation of the axial load on the column is not taken into account in the SDOF system and the P-Delta effect is not included. Moreover, the SDOF hysteretic model could not match the one in ABAQUS. There was also a slight uncertainty concerning the determination of the SDOF model yielding force.

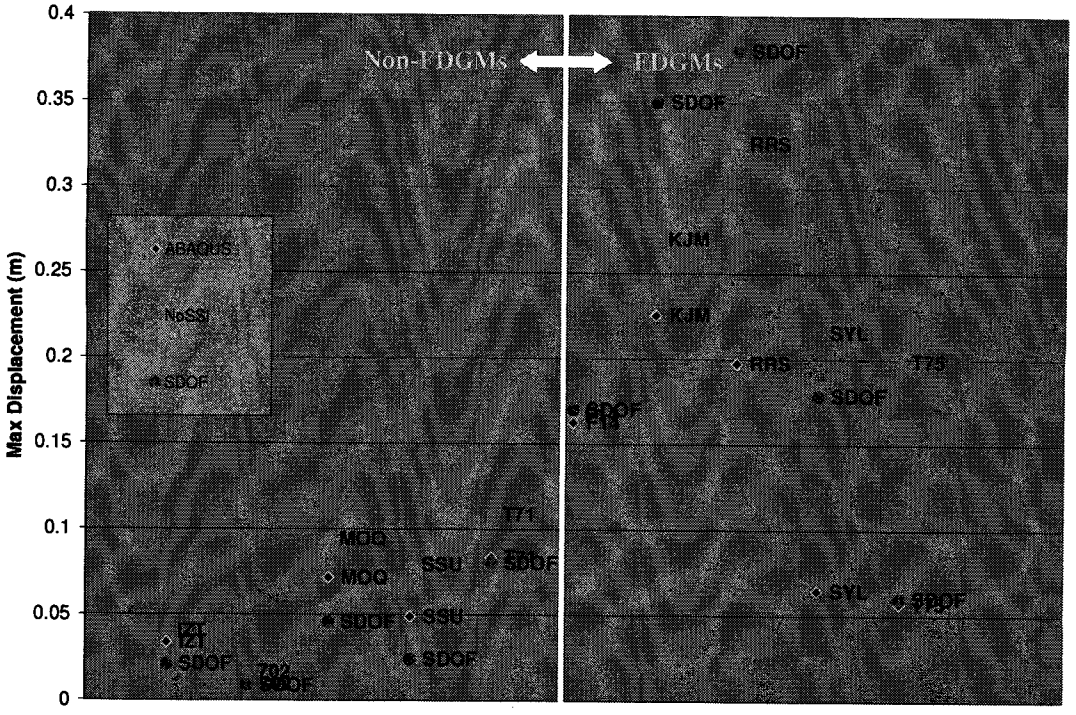

Figure 52. (Bridge 405) Maximum SDOF displacement compared to the longitudinal ABAQUS model response

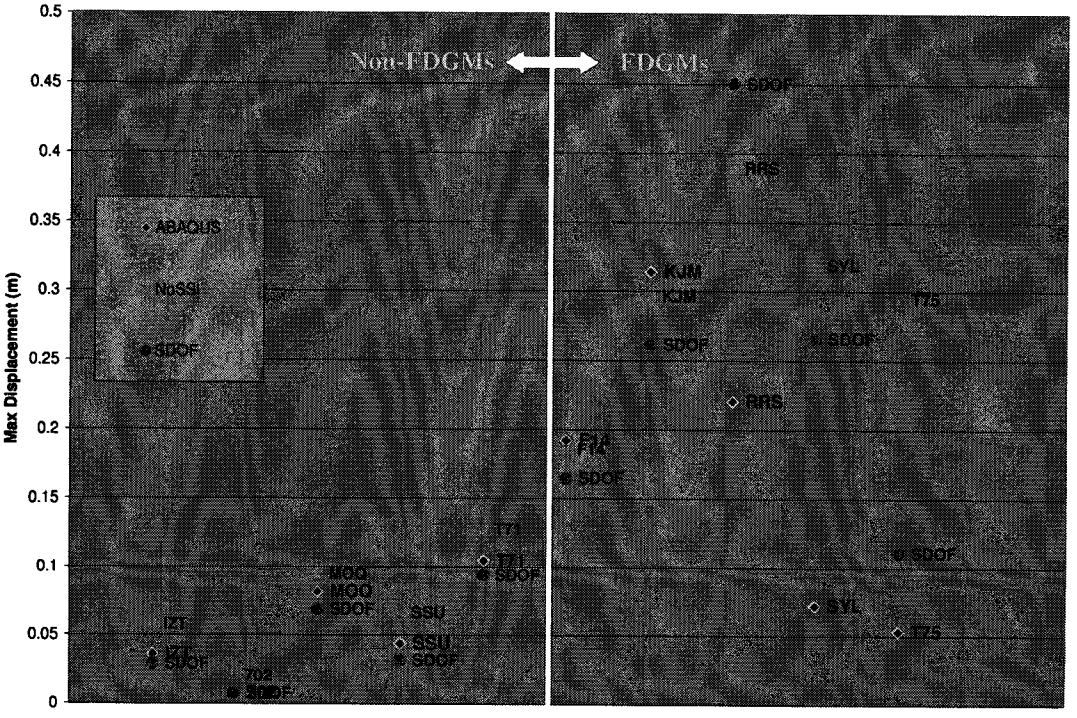

Figure 53. (Bridge 520) Maximum SDOF displacement compared to the longitudinal ABAQUS model response

AASHTO PREDICTION COMPARISON

Bridges in the United States are usually designed using the *Standard Specifications for Highway Bridges*, which was written by the American Association of State Highway and Transportation Officials (AASHTO). Following the AASHTO (LRFD Bridge Design Specifications 2004) procedure, the maximum base shear was computed and compared to those of the finite element model. A multimode linear response spectrum analysis was performed to obtain an approximate upper bound to the peak significant response (column maximum base shear, column max. relative displacement) of the WSDOT bridges to a user-supplied input spectrum as a function of period (given by the WSDOT). Figures 30 to 32 show the ARS of the FN and FP component of the non-FD and FD ground motions for each bridge. Moreover, the figures show the target ARS found from the PSHA (Gillie 2005) and the AASHTO ARS used by the WSDOT. One can see that the AASHTO curve was lower than the target ARS. The AASHTO procedure uses an outdated acceleration coefficient map created in 1988 by the United States Geological Survey (USGS). Moreover, the USGS PSHA (Gillie 2005) was based on 2 percent probability of exceedance in 50 years which corresponds to a collapse protection, rare but possible. On the other hand, the AASHTO contour maps of the acceleration coefficient were based on 10 percent probability of exceedance in 50 years which corresponds to the design level. Figure 54 shows the ARS for 2 and 10% probability of exceedance. A factor of 1.5 that is used in the building codes to compute the collapse level from the design spectrum was applied to the AASHTO ARS.

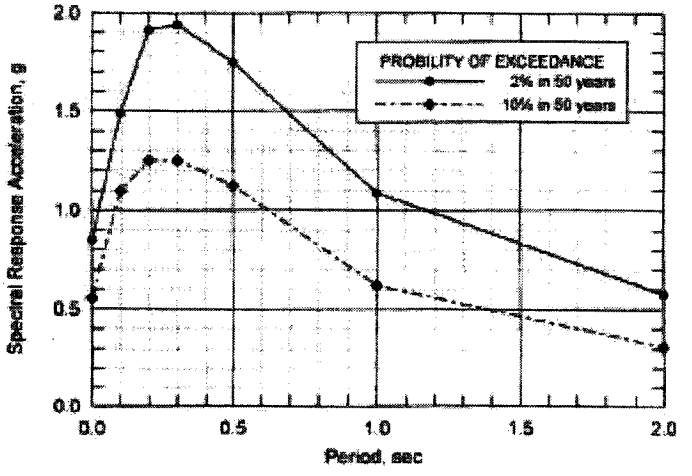

Figure 54. Uniform hazard response spectra for 2% and 10% probability of exceedance in 50 years for San Francisco, California

The maximum base shear comparisons are shown in Figures 55 to 57 for each bridge. A Response Modification factor to take into account the inelastic effect of 3.5 for multiple columns per bent and 2.0 for single column was subsequently applied to the AASHTO maximum base shears assuming that the bridges were of the "essential" importance category. The AASHTO predicted maximum base shears were always unconservative in comparison to the non-FDGMs and FDGMs for Bridges 405 and 520, and were always conservative for Bridge 90. Figure 58 shows the comparison between the FEM displacements and the design AASHTO displacements. AASHTO (2004) results are found to be unconservative in that respect, predominantly for the FDGMs. This is expected since AASHTO requires that bridges near faults use a site specific ground motion assessment.

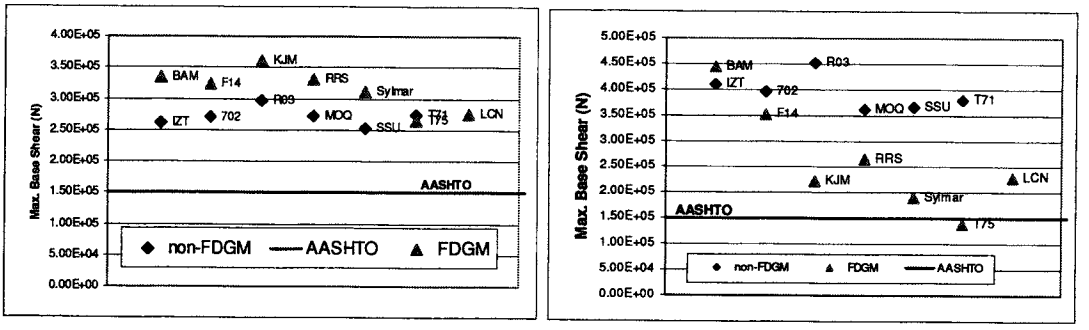

Figure 55. Bridge 405 Maximum longitudinal (left) and transverse (right) governing column base shears compared to the AASHTO (2004) design prediction

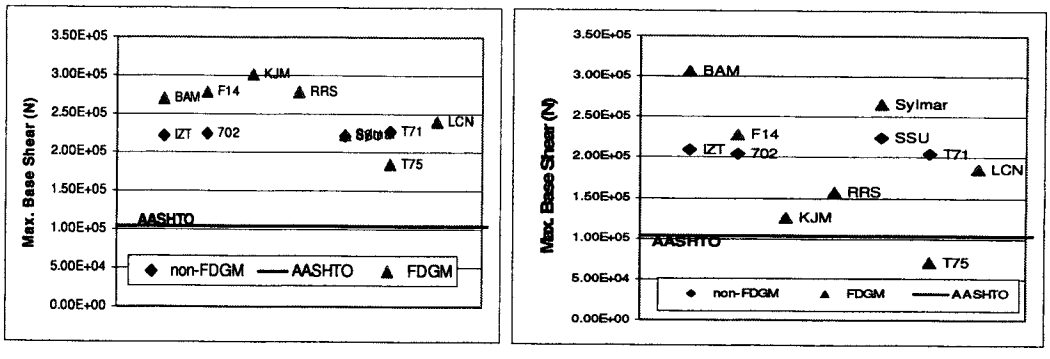

Figure 56. Bridge 520 Maximum longitudinal (left) and transverse (right) governing column base shears compared to the AASHTO (2004) design prediction

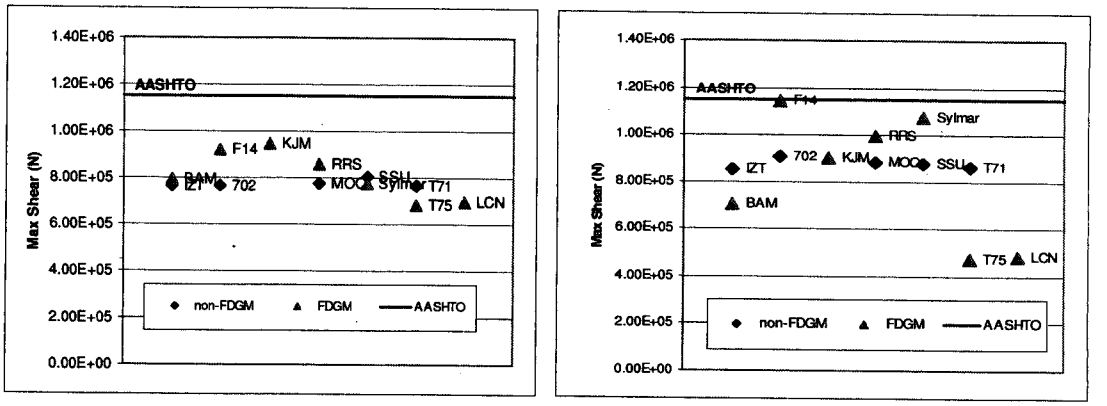

Figure 57 Bridge 90 Maximum longitudinal (left) and transverse (right) column shears (column C_4) compared to the AASHTO (2004) design prediction

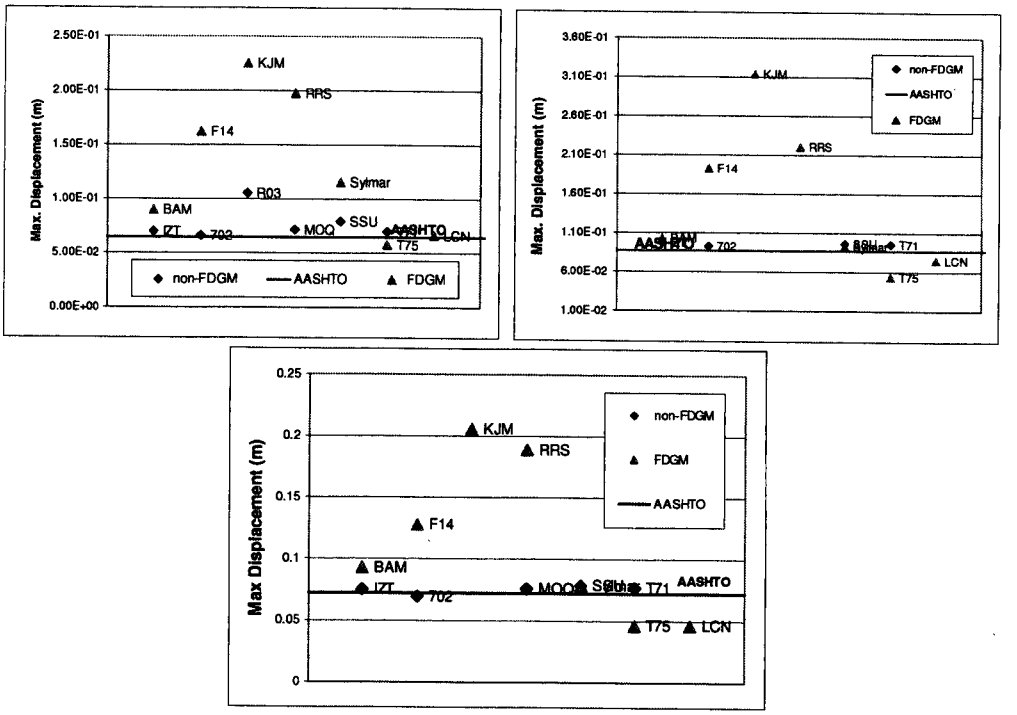

Figure 58 Bridge 405 (left), Bridge 520 (right) and Bridge 90 (down) maximum governing column displacements compared to the AASHTO (2004) design prediction

CONCLUSIONS AND RECOMMENDATIONS

Three typical post-1990 Washington State Department of Transportation (WSDOT) monolithic concrete bridges were chosen for nonlinear seismic evaluation under both forward directivity (FD) and non-FD ground motions (GM). Additionally, comparisons with results of a nonlinear and linear single-degree-of-freedom (SDOF) analysis and those of the American Association of State Highway and

Transportation Officials (AASHTO) design provisions were made. The effects of soil-structure interaction (SSI) were investigated as well.

Significant seismic damage may occur if the structural response is in tune with the velocity pulse of the FDGM. This velocity pulse is a result of fault propagation effects in the near-fault, and occurs when the direction of slip and rupture propagation coincide. The period of the velocity pulse is proportional to the magnitude of the earthquake (Eq. 2). The response of bridges to FDGMs is highly dependent upon the period of this velocity pulse. If this period is close to one of the bridge fundamental periods, significant damage can occur during a few cycles of motion. The severity of the demand is controlled by the ratio of the pulse period to bridge fundamental periods. As a consequence of this, damage in a bridge with moderate periods (T=0.1s to 1.0s) may be more significant in smaller magnitude earthquakes where the pulse period is closer to the fundamental period of the structure. This was the case for both the MDOF and SDOF analyses of all three bridges in this research. The results showed also that the occurrence of high PGA and/or PGV is only one of several conditions that can cause high demand on the bridges.

The nonlinear time history analyses results from ABAQUS showed that most of the damage in the bridge columns during FDGMs occurred at the beginning of the record in response to the double-sided velocity pulse. Therefore, a simple ground motion consisting of a sinusoidal single pulse may be sufficient to evaluate bridge performance for FDGMs.

The three bridges considered, Bridge 90, Bridge 405, and Bridge 520, all typical concrete overpasses ranging from 50 m (162 ft) to 91 m (298 ft) in length, generally survived the earthquake motions with only minor damage to their columns. However, column flexural failure was predicted for the Bridge 90 model when subjected to two of the forward directivity ground motions. The maximum curvature capacity of one of the four columns was reached. The bridge models often indicated distress at the abutments, including pounding, violation of abutment strength limits, and significant movement at the bearing pads. The risk of the deck exceeding the abutment bearing pad displacement capacity was high for Bridge 90 under forward directivity ground motion. The abutment strength limit was often reached, corresponding to an excessive pressure from the abutment on its surrounding soil.

The effect of Soil-Structure-Interaction (SSI) was studied through the response of the ABAQUS bridge models that included foundation flexibility. When the SSI was not included in the bridge models, the bridge maximum displacements in both directions increased significantly as well. This increase was particularly over-conservative for the FDGMs which already had a high displacement demand, in many cases.

The use of the acceleration response spectra to compute the expected response of the bridges in terms of maximum base shears and relative displacements was found to yield mixed responses for non-FD and FDGMs. Care must be taken in the choice of the response modification factor (or R-Factor) to include the inelasticity effect on the maximum base shear in the columns. The performance of the nonlinear SDOF bridge models were always slightly unconservative compared to that of the full bridge models under non-FDGM. The results of a simple SDOF bridge model to predict the response of a bridge under FDGM ranged from very conservative for some ground motions, to slightly unconservative for other GM. Therefore, nonlinear SDOF analyses are specifically not recommended in the case of FDGM since the results were not consistent. A more detailed MDOF model should be used to assess bridge seismic performance so that SSI and the interaction of the longitudinal and transverse responses of the bridges can be included, particularly if a performance based design or assessment of the bridge is required.

The AASHTO (2004) bridge design procedure using the ATC-6 collapse level acceleration response spectra, assuming that the bridges were categorized as "essential", was very unconservative for Bridge 405 and 520 with regard to the predicted maximum base shears in comparison to the nonlinear time history results for the non-FDGM and the FDGMs. The predicted AASHTO maximum base shears were found to be slightly conservative for Bridge 90 for both sets of motions. The maximum AASHTO displacements for the non-FDGMs were found to be close to those from the nonlinear time history analyses. However, the maximum displacements from the AASHTO procedure were found to be unconservative for all three bridges for most of the FDGMs. This was expected since AASHTO requires that bridges near faults use a site-specific ground motion assessment to assess the uncertainty in the FDGMs. Due to the variation in acceleration response spectra with period in the FDGM, modifications to the elastic design spectra does not provide a reliable basis for representing FDGMs.

Depending on the importance of the bridge being designed or assessed, the appropriate approach taken with FDGMs should be carefully considered by the designer. To follow the current AASHTO code provisions may lead to unconservative displacement ductility demand unless the required site-specific analysis is performed. On the other hand, design for a FDGM with a velocity pulse period matching the fundamental bridge period will require the bridge to resist very large demands. It must be kept in mind that the predicted velocity pulse period is still subject to significant uncertainty. Therefore, it is difficult from the current state of knowledge to include FDGM parameters within a probabilistic seismic hazard analysis.

REFERENCES

ABAQUS (2004). ABAQUS Software & Documentation, Version 6.5-1, ABAQUS, Inc.

Abrahamson, N. A. (1998). "Non-stationary spectral matching program RSPMATCH," PG&E Internal Report, February.

Abrahamson, N. A. and Silva, W. J. (1997). "Empirical Response Spectral Attenuation Relationships for Shallow Crustal Earthquakes." Seismological Research Letters, 68(1): 94-127.

Alavi, B. and Krawinkler, H. (2000). "Consideration of near-fault ground motion effects in seismic design." Proceedings, 12th World Conference on Earthquake Engineering, Auckland, New Zealand, Paper No. 2665.

Alavi, B. and Krawinkler, H. (2004). "Behavior of moment-resisting frame structures subjected to near-fault ground motions," Earthquake Engineering and Structural Dynamics; 33:687–706 (DOI: 10.1002/eqe.369)

Bertero, V. V. et al. (1976). "Establishment of design earthquakes: evaluation of present methods." Proceedings, International Symposium On Earthquake Structural Engineering, St. Louis, 1: 551-580.

Bray, J. D. and Rodriguez-Marek, A. (2004). "Characterization of forward-directivity ground motions in the near-fault region." Soil Dynamics and Earthquake Engineering, 24: 815-828.

Brocher, T. M., Blakely, R. J., and Wells, R. E. (2004). "Interpretation of the Seattle Uplift, Washington, as a passive-roof duplex." Bulletin of the Seismological Society of America, 94(4): 1379–1401.

ENSOFT, Inc. (2002). L-Pile Plus 4.

Gillie J.L. (2005). *Nonlinear Response Spectra of Forward-Directivity Ground Motions.* M.S. Thesis, Washington State University.

Hall, J. B., and Othberg, K. L. (1974) "Thickness of unconsolidated sediments, Puget Lowland, Washington." Washington State Division Geology and Earth Resources Geologic Map, GM-12.

Johnson, S.Y., Dadisman, S.V., Childs, J.R., and Stanley, W.D. (1999). "Active tectonics of the Seattle Fault and Central Puget Sound, Washington : Implications for earthquake hazards." Geological Society of America Bulletin, 111(7): 1042-1053.

Kowalsky, M.J., Priestley, M.J.N. (2000). "Improved Analytical Model for Shear Strength of Circular Reinforced Concrete Columns in Seismic Regions," ACI Structural Journal, 97(3), 388-397.

Krawinkler, H. and Alavi, B. (1998). "Development of improved design procedures for near-fault ground motions." Proceedings, SMIP98 Seminar on Utilization of Strong Motion Data Oakland, CA: 21-41.

Makley, B. (2001). "Seismic behavior of bridge shear columns subjected to near-field pulse loading." M.S. Thesis, University of California at San Diego, La Jolla, CA.

Mavroeidis, G. P. and Papageorgiou, A. S. (2003). "A mathematical representation of near-fault ground motions." Bulletin of the Seismological Society of America, 93(3): 1099-1131.

Pacific Earthquake Engineering Research Center (PEER). (2000). PEER Strong Motion Database [Online]. <http://peer.berkeley.edu/smcat/>

Pratt, T. L., S. Y. Johnson, C. J. Potter, W. J. Stephenson, and C. A. Finn (1997). "Seismic reflection images beneath Puget Sound, western Washington State: the Puget Lowland thrust sheet hypothesis," J. Geophys. Res., 102, 27,469–27,489.

Priestley, M. J. N. (2003) Myths and fallacies in earthquake engineering, revisited: The Malley-Milne lecture. Rose School, Collegio Allessandro Volta, Pavia, Italy.

Rodriguez-Marek, A. (2000) Near-Fault Seismic Site Response Ph. D. Dissertation. University of California at Berkeley, Berkeley, CA.

Roger Lowe Associates, Inc. (1980). Report of Geotechnical Studies SR 90 Tunnel Project Mercer Island, Washington. [Report to the Washington State Department of Transportation]. June 30,1980.

Somerville, P. G. (2003). "Magnitude Scaling of the Near Fault Rupture Directivity Pulse." Physics of the Earth and Planetary Interiors, 137: 201-212.

Somerville, P. G., Smith, N. F., Graves, R. W., and Abrahamson, N. A. (1997). "Modification of empirical strong ground motion attenuation relations to include the amplitude and duration effects of rupture directivity." Seismological Research Letters, 68(1):199-222.

Washington State Department of Transportation (WSDOT). (1990a). "SR-405, C. S. 1745, XL-0549 NE 8th to Northup I/C HOV Improvement Geotechnical Report." Intra-Departmental Communication. From Finkle, R. G. and Harrison, T. L. to Walley, A. H. October 11, 1990.

Washington State Department of Transportation (WSDOT). (1990b). "CS 1745, SR-405, XL-0549 NE 8th to Northup I/C NE Ramp/116th Ave NE O'ing Foundation requirements." Intra-Departmental Communication. From Finkle, R. G. to Walley, A. H. October 22, 1990.

Welch, R. C. and Reese, L. C. (1972). "Laterally loaded behavior of drilled shafts Research Report 3-5-65-89," Center for Highway Research, University of Texas, Austin.

Wen, Y. (1976). "Method for random vibration of hysteretic systems." Journal of the Engineering .Mechanics Division ASCE, 102(EM2): 249-263.

APPENDIX A

Ground Motion Database

Table A1. Earthquakes included in the Bray and Rodriguez-Marek forward-directivity database (1 through 13) and those added by Gillie (2005) (14 through 17).

Event #	Earthquake	Date	Moment magnitude	Mechanism[a]	Strike	Dip
1	Parkfield	6/27/66	6.1	SS	317	90
2	San Fernando	2/9/71	6.6	R	290	50
3	Imperial valley	10/15/79	6.5	SS	143	90
4	Morgan Hill	4/24/84	6.2	SS	154	90
5	Superstition hills (B)	11/24/87	6.6	SS	127	90
6	Loma Prieta	10/17/89	7	OB	128	70
7	Erzincan, Turkey	3/13/92	6.7	SS	300	86
8	Landers	6/28/92	7.3	SS	351[b]	90
9	Northridge	1/17/94	6.7	R	122	40
10	Kobe	1/17/95	6.9	SS	50	85
11	Kocaeli	8/17/99	7.4	SS	90	90
12	Chi-Chi	9/21/99	7.6	R	0[c]	30
13	Duzce	11/12/99	7.1	SS	90	90
14	Palm Springs	7/8/86	6.0	OB	300	45
15	Denali	11/3/02	7.9	SS	105[d]	90
16	Bam	12/26/03	6.5	SS	175	90
17	Parkfield	9/28/04	6.0	SS	137	90

[a] SS, Strike-slip, R, reverse, OB, oblique-slip, T/R, thrust/reverse. Fault parameters are obtained from Somerville et al. (1997) when available.

[b] The Landers earthquake occurred on a fault with multiple segments. The Lucerne record was rotated to the indicated strike that corresponded to the highest fault normal peak ground velocity.

[c] The strike of the fault changes drastically in the northern end of the fault. An average north-south orientation near the epicenter was used for the strike orientation. The fault-normal orientation of records near the northern end of the fault is selected to match the orientation of the velocity pulse.

[d] Denali earthquake ruptured three different faults. Strike/dip provided for the Denali fault, which ruptured near PS10. (Wright et al. 2005).

Table A2. Ground motions from the Bray and Rodriguez-Marek (2004) database.

Station	Agency	Station #	Event[a]	R[b] (km)	RDI[c]	Site[d]	PGA (g)	PGV (cm/s)	$PGV_{P/N}$ [e]	T_v (s)	T_{v-p} (s)
Cholame #2	CDMG	1013	1	0.1	1.08	s	0.47	75	–[f]	0.67	0.66
Temblor	CDMG	1438	1	9.9	1.08	r	0.29	17.5	1.07	0.44	0.4
Pacoima dam	CDMG	279	2	2.8	1.04	r	1.47	114	0.33	1.44	1.15
Brawley airport	USGS	5060	3	8.5	1.48	s	0.21	36.1	0.99	2.56	3.11
EC County center	CDMG	5154	3	7.6	1.48	s	0.22	54.5	0.79	3.78	3.44
EC Meloland overpass	CDMG	5155	3	0.5	1.48	s	0.38	115	0.24	2.82	2.86
El Centro array #10	USGS	412	3	8.6	1.48	s	0.23	46.9	0.84	3.93	3.82
El Centro array #3	USGS	5057	3	9.3	1.48	s	0.27	45.4	1.10	4.5	4.27
El Centro array #4	USGS	955	3	4.2	1.48	s	0.47	77.8	0.52	4.31	4.00
El Centro array #5	USGS	952	3	1.0	1.48	s	0.53	91.5	0.54	3.37	3.25
El Centro array #6	USGS	942	3	1.0	1.48	s	0.44	112	0.58	3.65	3.41
El Centro array #7	USGS	5028	3	0.6	1.48	s	0.46	109	0.41	3.73	3.31
El Centro array #8	USGS	5159	3	3.8	1.48	s	0.59	51.9	1.07	3.98	4.00
El Centro diff array	USGS	5165	3	5.3	1.48	s	0.44	59.6	0.86	4.18	3.02
Holtville Post Office	USGS	5055	3	7.5	1.48	s	0.26	55.1	0.78	4.28	4.2
Westmorland fire sta	CDMG	5169	3	15.1	1.48	s	0.1	26.7	0.28	3.93	4.71
Coyote lake dam	CDMG	57217	4	0.1	1.17	r	1.00	68.7	1.02	0.73	0.71
Gilroy array #6	CDMG	57383	4	11.8	1.17	r	0.61	36.5	0.29	1.00	1.16
El Centro Imp co. cent	CDMG	1335	5	13.9	1.48	s	0.31	51.9	0.70	1.85	1.25
Parachute test site	USGS	5051	5	0.7	1.48	s	0.42	107	0.43	2.11	1.86
Gilroy—Gavilan coll.	CDMG	47006	6	11.6	1.48	r	0.41	30.8	0.86	1.16	0.38

Station	Agency	Station #	Event[a]	R[b] (km)	RDI[c]	Site[d]	PGA (g)	PGV (cm/s)	$PGV_{P/N}$ [e]	T_v (s)	T_{v-p} (s)
Gilroy—historic bldg.	CDMG	57476	6	12.7	1.48	s	0.29	36.8	0.65	1.33	1.47
Gilroy array#1	CDMG	47379	6	11.2	1.48	r	0.44	38.6	0.74	1.16	0.4
Gilroy array#2	CDMG	47380	6	12.7	1.48	s	0.41	45.6	0.61	1.36	1.46
Gilroy array#3	CDMG	47381	6	14.4	1.48	s	0.53	49.3	0.69	1.46	0.48
LGPC	UCSC	16	6	6.1	1.48	r	0.65	102	0.50	2.14	0.79
Saratoga - Aloha Ave	CDMG	58065	6	13	1.48	s	0.38	55.5	0.78	2.31	1.55
Saratoga—W Valley Coll.	CDMG	58235	6	13.7	1.48	s	0.04	71.3	0.84	1.71	1.14
Erzincan		95	7	2	1.23	s	0.49	95.5	0.48	2.27	2.23
Lucerne	SCE	24	8	1.1	1.48	r	0.78	147	0.21	5.39	4.3
Jensen filter plant	USGS	655	9	6.2	1.14	s	0.62	104	0.90	1.99	2.86
LA dam	USGS	–	9	2.6	1.14	r	0.58	77	0.25	1.24	1.3
Newhall—fire Sta.	CDMG	24279	9	7.1	1.16	s	0.72	120	0.42	0.95	0.71
Newhall—W. Pico Cyn. Rd	USC	90056	9	7.1	1.15	s	0.43	87.7	0.85	2.19	2.03
Pacoima dam (downstr)	CDMG	24207	9	8	1.16	r	0.48	49.9	0.46	0.61	0.44
Pacoima dam (upper left)	CDMG	24207	9	8	1.16	r	1.47	107	0.43	0.89	0.73
Rinaldi receiving Sta	DWP	77	9	7.1	1.13	s	0.89	173	0.29	1.31	1.06
Sylmar—converter Sta	DWP	74	9	6.2	1.14	s	0.8	130	0.72	2.87	1.1
Sylmar—converter Sta E.	DWP	75	9	6.1	1.14	s	0.84	116	0.67	2.64	2.92
Sylmar—olive view FF	CDMG	24514	9	6.4	1.16	s	0.73	123	0.44	1.76	2.42
KJMA (Kobe)		–	10	0.6	1.14	r	0.85	96	0.56	1.91	0.86
Kobe University	CEOR	–	10	0.2	1.48	r	0.32	42.2	0.92	1.59	1.33
OSAJ		–	10	8.5	1.48	s	0.08	19.9	0.86	3.83	1.18

Station	Agency	Station #	Event[a]	R[b] (km)	RDI[c]	Site[d]	PGA (g)	PGV (cm/s)	$PGV_{P/N}$[e]	T_v (s)	T_{v-p} (s)
Port Island (0 m)	CEOR	–	10	2.5	1.12	s	0.38	84.3	0.30	1.91	1.3
Arcelik Kandilli		–	11	17	1.03	r	0.21	42.3	0.31	6.82	5.24
Duzce	ERD	–	11	12.7	1.48	s	0.37	52.5	0.82	1.92	1.37
Gebze	ERD	–	11	17	1.03	r	0.26	40.7	0.84	5.04	4.62
TCU052g	CWB	–	12	0.2	–[h]	s	0.35	159	0.75	3.14	4.48
TCU068g	CWB	–	12	1.1	–[h]	s	0.57	295.9	0.37	2.41	4.06
TCU075	CWB	–	12	1.5	–[h]	s	0.33	88.3	0.43	2.3	2.03
TCU101	CWB	–	12	2.9	–[h]	s	0.2	67.9	0.73	5.35	8.62
TCU102	CWB	–	12	1.8	–[h]	s	0.3	112.4	0.69	3.85	2.52
TCU103	CWB	–	12	4	–[h]	s	0.13	61.9	0.42	9.52	7.19
Bolu	ERD	–	13	17.6	1.48	s	0.82	62.1	1.1	0.79	0.57

[a] See Table A1.

[b] Closest distance to the fault plane Somerville et al. 1997

[c] Ratio of fault normal to fault parallel at 3 s spectral period from [8].

[d] Soil (s) or rock (r).

[e] Ratio of peak velocity in the fault parallel to the peak velocity in the fault normal direction.

[f] The Cholame #2 record in the Parkfield earthquake triggered only in one direction (158 from the fault normal direction).

[g] The fault normal direction for these records was assumed to be the direction oriented with the largest velocity pulse (N1228 for TCU052 and N1998 for TCU068).

[h] The complex rupture pattern for the Chi-Chi earthquake precludes a single estimate of RDI. For the stations analyzed, the RDIs vary from 0.91 to 1.48 depending on whether the RDI is computed as a dip-slip or as a strike-slip fault. Chi et al. [19] report both fault mechanisms acting at different locations along the fault rupture.

Table A3. Records fulfilling all forward-directivity requirements that were added to the Bray and Rodriguez-Marek (2004) database.

Station	Agency/ Station #	EQ[f]	R[a] (km)	RDI[b]	Site[c]	PGA	PGV	$PGV_{N/P}$[d]	$S_{a\ N/P}$[e] 1 sec	$S_{a\ N/P}$ 3 sec	T_p[g]
Cabazon Post Office	USGS/ 5073	14	8.4	1.36	s	0.23	17.5	0.43	2.00	2.10	1.40
Desert Hot Springs	CSMIP/ 12149	14	6.8	1.37	s	0.34	26.8	1.30	2.43	2.10	0.72
N. Palm Springs Pst Off	USGS/ 5295	14	3.4	1.03	s	0.71	73.2	2.00	3.03	1.80	1.38
PS10	TAPS/ 10	15	3.0	1.29	s	0.33	108	0.67	0.92	1.60	2.76
Bam	BHRC/ BAM	16	4.8	1.19	s	0.81	134	1.15	0.95	2.30	1.68
Coalinga - Slack Canyon	CSMIP/ CE46175	17	10.0	1.48	r	0.33	42.1	1.16	0.73	2.00	0.72
Fault Zone 9	CSMIP/ CE36443	17	1.1	1.16	r	0.14	26.1	3.53	2.52	4.10	1.56
Fault Zone 12	CSMIP/ CE36138	17	1.2	1.19	s	0.25	57.4	3.69	5.00	3.20	1.36
Fault Zone 14	CSMIP/ CE36456	17	0.1	1.46	s	0.99	84.7	1.13	1.64	1.90	0.88
Fault Zone 15	CSMIP/ CE36445	17	0.6	1.48	s	0.21	28.1	1.18	1.55	2.00	1.68
Middle Mountain	USGS/ MFU	17	2.0	1.48	s	0.32	32.3	2.30	2.00	2.80	1.48
Vineyard Canyon 1E	CSMIP/ CE36455	17	6.5	1.48	r	0.32	34.6	1.62	1.85	1.90	1.56
Vineyard Cyn 1W	CSMIP/ CE36448	17	2.1	1.48	r	0.14	21.1	2.25	3.35	1.30	0.40
Vineyard Cyn 2W	CSMIP/ CE36447	17	17.0	1.48	r	0.61	30.2	2.28	1.28	1.17	1.94

[a] Closest distance to the fault plane.
[b] Predicted ratio of fault normal to fault parallel at 3 s spectral period from Somerville et al. (1997).
[c] Soil (s) or Rock (r).
[d] Ratio of peak ground velocity of the fault normal (FN) component divided by the peak ground velocity in the fault parallel (FP) component. Note that this is the reciprocal of the PGV ratio presented in Table A2
[e] Spectral ratio between the FN and FP components.
[f] Refer to Table A1
[g] Pulse period
[h] Period of maximum spectral velocity.

Table A4 – Group 2: Parkfield 2004 records having RDI less than 1.0 with directivity effects.

Station	Station #	EQ	R (km)	RDI	Site	PGA	PGV	$PGV_{(N/P)}$	$S_{a\ N/P}$ 1 sec	$S_{a\ N/P}$ 3 sec	T_p[f]	T_{RSV}[g]
Cholame 1E	CSMIP/ CE36452	17	6.5	0.80	s	0.47	52.6	1.80	2.94	4.15	1.16	1.10
Cholame 2E	CSMIP/ CE36230	17	7.3	0.79	s	0.51	22.6	1.84	2.03	3.20	0.92	0.19
Cholame 3E	CSMIP/ CE36450	17	7.6	0.78	s	0.65	34.3	1.60	2.02	1.88	0.84	0.83
Cholame 3W	CSMIP/ CE36410	17	7.2	0.80	r	0.44	43.2	2.80	2.30	3.30	0.52	0.42
Cholame 4AW	CSMIP/ CE36412	17	8.4	0.80	s	0.28	38.1	0.70	2.64	1.45	1.20	0.58
Cholame 4W	CSMIP/ CE36411	17	7.5	0.79	s	0.57	17.4	1.40	2.94	3.07	0.92	0.68
Cholame 5W	CSMIP/ CE36227	17	10.0	0.77	s	0.21	19.6	1.37	1.02	0.94	0.80	0.59
Cholame 6W	CSMIP/ CE36451	17	10.0	0.75	s	0.41	21.5	1.38	1.44	1.09	1.20	0.85
Cholame 12W	CSMIP/ CE36228	17	6.7	0.80	s	0.50	63.3	1.20	1.57	1.80	0.84	0.48
Eades	USGS/ EFU	17	1.7	0.99	s	0.43	36.1	3.30	2.04	2.85	1.24	1.11
Fault Zone 1	CSMIP/ CE36407	17	3.4	0.80	s	0.45	63.8	1.22	1.26	2.20	1.28	1.20
Fault Zone 6	CSMIP/ CE36454	17	0.8	0.90	s	0.18	21.2	3.40	2.08	2.13	1.20	0.53
Fault Zone 7	CSMIP/ CE36431	17	1.2	0.85	r	0.24	28.1	2.20	1.55	2.55	0.48	0.30
Fault Zone 11	CSMIP/ CE36453	17	3.4	0.90	s	0.80	25.0	1.99	0.99	1.30	0.84	0.43
Stone Corral 1E	CSMIP/ CE36419	17	3.3	0.78	s	0.86	43.2	1.30	1.80	2.70	1.23	0.91

[a] Closest distance to the fault plane.
[b] Predicted ratio of fault normal to fault parallel at 3 s spectral period from Somerville et al. (1997).
[c] Soil (s) or Rock (r).
[d] Ratio of peak velocity of the fault normal (FN) component divided by the peak velocity in the fault parallel (FP) component.
[e] Spectral ratio between the FN and FP components.
[f] Pulse period
[g] Period of maximum spectral velocity.

Table A5. Ground motions included in the non-FD database (see Gillie 2005 for details).

Station	Agency	Station #	Event[a]	R[b] (km)	Site[c]	PGA	PGV	$PGV_{N/P}$[d]	T_{RSV}[e]
Cholame – Shandon Array #5	CDMG		1	9.58	s	0.35	15.3	0.96	0.35
Lake Hughes #12	USGS	128	2	19.30	r	0.27	13.1	0.51	0.24
LA – Hollywood Stor FF	CDMG	24303	2	22.77	s	0.38	11.8	0.98	0.53
Pasadena – Old Seismo Lab	USGS	266	2	21.50	r	0.45	26.4	0.75	0.32
Bonds Corner	USGS	5054	3	2.68	s	0.40	26.4	0.87	0.86
Chihuahua	UNAMUCSD	6621	3	7.29	s	0.37	35.5	1.26	0.68
Cerro Prieto	UNAMUCSD	6604	3	15.19	r	0.18	9.8	1.61	1.09
Calexico Fire Station	USGS	5053	3	10.45	s	0.78	47.5	0.98	0.54
SAHOP Casa Flores	UNAMUCSD	6619	3	9.64	s	0.63	53.3	1.49	0.72
Anderson Dam (Downstream)	USGS	1652	4	3.26	r	0.28	21.3	1.28	0.45
Gilroy – Gavilan Coll.	CDMG	47006	4	14.84	r	0.27	28.9	0.51	0.26
Gilroy Array #2	CDMG	47380	4	13.69	s	0.12	10.9	0.61	0.71
Gilroy Array #3	CDMG	47381	4	13.02	s	0.11	3.7	1.33	0.51
Gilroy Array #4	CDMG	47382	4	11.54	s	0.15	19.2	1.48	1.09
Hollister Diff Array #1	USGS	1656	4	22.6	s	0.28	11.3	1.07	1.16
Hollister Diff Array #4	USGS	1656	4	26.43	s	0.19	11.7	2.08	1.14
Brawley Airport	USGS	5060	5	17.03	s	0.55	30.5	0.83	1.02
Superstition Mtn Camera	USGS	286	5	5.61	r	0.25	32.0	2.44	0.60
Wildlife Liquef. Array	USGS	5210	5	23.85	s	0.25	29.3	1.23	1.29
BRAN	UCSC	13	6	10.72	r	0.54	38.3	0.90	0.49
Capitola	CDMG	47125	6	15.23	s	0.22	28.0	1.29	0.64
Corralitos	CDMG	57007	6	3.85	r	0.29	31.8	0.83	0.75

Station	Agency	Station #	Event[a]	R[b] (km)	Site[c]	PGA	PGV	$PGV_{N/P}$[d]	T_{RSV}[e]
UCSC Lick Observatory	CDMG	15	6	18.41	r	0.23	29.2	0.64	0.36
Sunnyvale – Colton Ave.	USGS	1695	6	24.23	s	0.51	45.4	1.09	1.29
UCSC	UCSC	58135	6	18.51	r	0.17	18.3	1.58	0.16
WAHO	UCSC	14	6	17.47	r	0.29	23.5	0.97	0.23
Joshua Tree	CDMG	22170	8	11.03	r	0.15	16.5	0.78	1.12
Morongo Valley	USGS	5071	8	17.32	s	0.36	23.8	0.96	0.60
Arleta – Nordhoff Fire Sta	CDMG	24087	9	8.66	s	0.11	10.7	1.14	0.71
Monte Nido Fire Station	USGS	5080	9	25.59	r	0.10	10.5	1.01	0.39
LA – Century City CC North	CDMG	24389	9	23.41	s	0.39	23.6	1.03	1.12
LA – Chalon Rd	USC	90015	9	20.45	r	0.14	8.1	1.18	0.62
N Hollywood – Coldwater Can	USC	90009	9	12.51	r	0.30	45.5	1.57	1.20
LA – N Faring Rd	USC	90016	9	20.81	r	1.07	51.4	1.37	0.62
Sunland – Mt Gleason Ave	USC	90058	9	13.35	r	0.37	16.9	1.34	1.04
Glendale – Las Palmas	USC	90063	9	22.21	r	0.51	19.4	0.91	0.24
LA – Hollywood Stor FF	CDMG	24303	9	24.03	s	0.21	38.5	0.96	0.82
Burbank – Howard Rd		90059	9	16.88	r	0.17	21.4	1.41	0.64
Simi Valley – Katherine Rd	USC	90055	9	13.42	r	0.21	19.0	0.76	0.62
Pacoima Kagel Canyon	CDMG	24088	9	7.26	r	0.53	56.0	1.51	0.69
Sun Valley – Roscoe Blvd	USC	90006	9	10.05	s	0.18	10.5	0.71	1.01
Santa Susana Ground	USGS	5108	9	16.74	r	0.39	32.7	0.79	0.69
Santa Monica City Hall	CDMG	24538	9	26.45	s	0.38	30.2	1.87	1.42
Pacific Palisades – Sunset	USC	90049	9	24.08	s	0.34	20.1	1.22	0.28
Topanga – Fire Sta	USGS	5081	9	22.28	r	0.74	35.8	0.75	0.22

Station	Agency	Station #	Event[a]	R[b] (km)	Site[c]	PGA	PGV	$PGV_{N/P}$[d]	T_{RSV}[e]
Big Tujunga, Angeles Nat F	USC	90061	9	19.74	r	0.48	30.9	2.05	0.64
LA – UCLA Grounds	CDMG	24688	9	22.49	r	0.86	43.1	0.74	2.30
Hollywood – Willoughby Ave	USC	90018	9	23.07	s	0.22	50.8	0.50	0.91
CHY028	CWB	-	12	3.14	s	0.82	72.8	1.09	0.62
CHY029	CWB	-	12	10.97	s	0.28	35.3	0.86	0.67
CHY035	CWB	-	12	12.65	s	0.25	45.5	1.21	1.28
CHY080	CWB	-	12	2.69	s	0.97	107.7	1.05	0.88
CHY006	CWB	-	12	9.77	s	0.36	55.5	1.30	1.81
TCU055	CWB	-	12	6.36	s	0.24	51.3	0.51	2.15
TCU070	CWB	-	12	19.02	s	0.26	62.2	0.84	5.10
TCU071	CWB	-	12	5.31	s	0.65	69.4	0.64	0.56
TCU072	CWB	-	12	7.03	s	0.49	72.1	1.28	0.88
TCU074	CWB	-	12	13.46	s	0.60	73.4	1.79	1.47
TCU079	CWB	-	12	10.97	s	0.74	61.2	1.26	0.60
TCU089	CWB	-	12	8.88	s	0.33	31.1	0.99	5.42
Fun Valley	USGS	5071	14	14.24	s	0.25	13.6	0.99	0.74
Morongo Valley	USGS	5069	14	12.07	s	0.41	19.9	0.71	1.64
Vineyard Canyon	USGS	VFU	17	4.2	s	0.26	21.5	0.71	0.49

[a] See Table A1.

[b] Closest distance to the fault plane Somerville et al. 1997

[c] Soil (s) or rock (r).

[d] Ratio of peak velocity in the fault normal to the peak velocity in the fault parallel direction.

[e] Period of maximum spectral velocity.

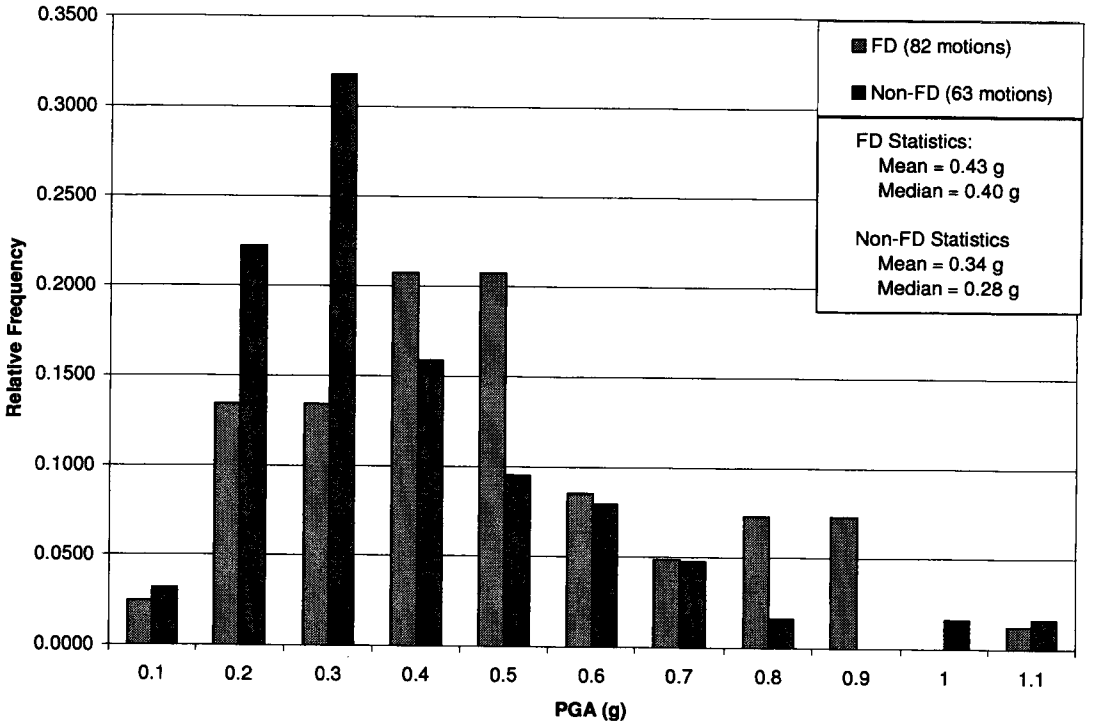

Fig.A1a. Comparison of normalized distribution of PGA for FD and Non-FD records.

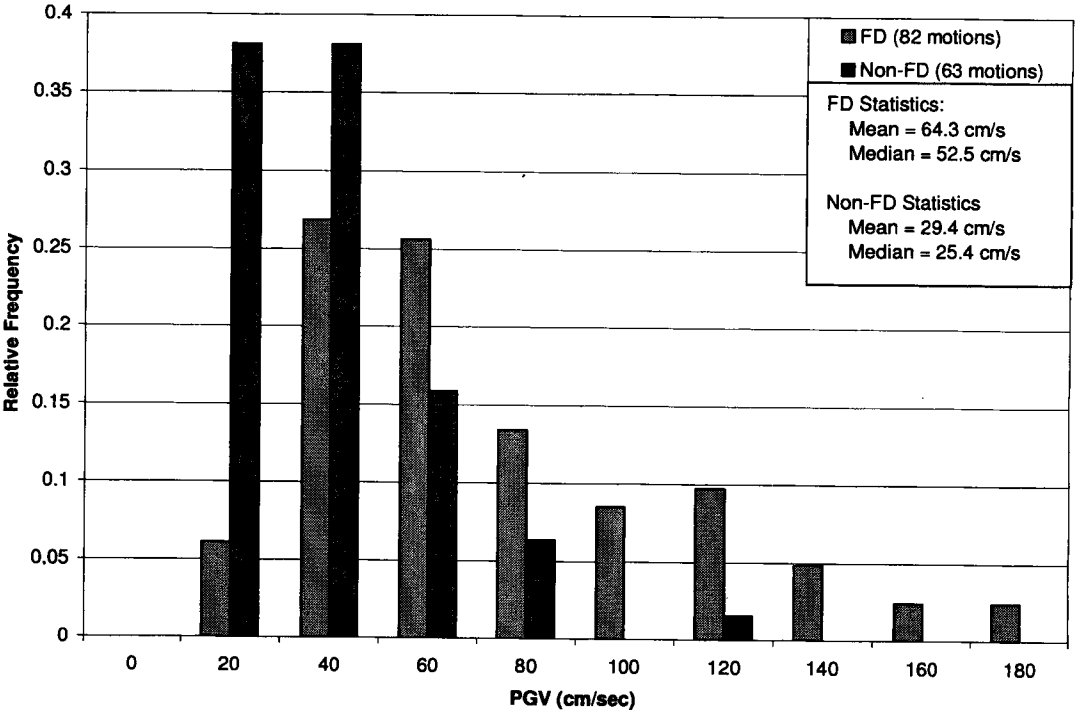

Fig. A1b. Comparison of normalized distribution of PGV for FD and Non-FD records.

APPENDIX B

Borehole data at the bridge sites

Table B1. SPT correlations for 90 26A bridge site

					Seed et al. 1983		Seed et al. 1986		Imai & Tonouchi 1982		
Depth	Soil	N_m[b]	γ[c]	σ'_{vo}[d,e]	V_s[f]		V_s[g]		G_{max}[h]	V_s[i]	
(ft)	Unit[a]	(blows/ft)	(pcf)	(psf)	(ft/sec)	(m/s)	(ft/sec)	(m/s)	(kip/ft^2)	(ft/sec)	(m/s)
0		--	102	0	--	--	--	--	--	--	--
5	1	100	102	510	664.1	202.4	2000.0	609.6	7445.3	1533.1	467.3
10	1	100	128	1150	762.8	232.5	2000.0	609.6	7445.3	1368.6	417.1
15	1	90	116	1730	812.6	247.7	1897.4	578.3	6930.6	1387.0	422.8
20	1	50	110	2280	778.8	237.4	1414.2	431.1	4647.1	1166.3	355.5
25	1	60	122	2890	840.0	256.0	1549.2	472.2	5260.5	1178.3	359.2
30	1	42	110	3440	820.0	249.9	1296.1	395.1	4127.6	1099.2	335.0
35	2	--	100	3940	--	--	--	--	--	--	--
40	2	50	110	4490	894.7	272.7	1414.2	431.1	4647.1	1166.3	355.5
45	2	20	110	4879	783.9	238.9	894.4	272.6	2492.2	854.1	260.3
50	2	40	112	5278	900.7	274.5	1264.9	385.5	3992.9	1071.4	326.6
55	2	20	110	5667	816.0	248.7	894.4	272.6	2492.2	854.1	260.3
60	2	26	110	6056	868.2	264.6	1019.8	310.8	2979.0	933.8	284.6
65	2	20	111	6450	843.7	257.2	894.4	272.6	2492.2	850.3	259.2
70	2	40	110	6839	963.4	293.6	1264.9	385.5	3992.9	1081.1	329.5
75	3	24	90	7128	895.5	273.0	979.8	298.6	2821.2	1004.7	306.2
80	3	40	85	7392	989.4	301.6	1264.9	385.5	3992.9	1229.9	374.9
85	3	20	90	7681	890.2	271.3	894.4	272.6	2492.2	944.3	287.8
90	3	24	80	7920	928.8	283.1	979.8	298.6	2821.2	1065.6	324.8
95	3	40	90	8209	1024.0	312.1	1264.9	385.5	3992.9	1195.2	364.3
100	3	28	90	8498	973.7	296.8	1058.3	322.6	3132.9	1058.7	322.7

[a] Soil Units:
(1) very hard, medium dark gray, sandy silt with occasional gravel and cobbles, identified as Vashon Glacial Till
(2) hard to very hard, medium dark gray, silt to silty clay with traces of sand, gravel, and cobbles, identified as Glacio-Lacustrine Drift
(3) medium dark gray, very stiff to very hard, silty clay to clay that is massive or laminated

[b] SPT blow counts obtained from Roger (1980).
[c] Unit weights obtained from Roger (1980).
[d] Overburden computed using unit weights.
[e] Ground water level: approximately 40 ft (Roger 1980).
[f] Seed et al. 1983: $V_s = 220*N_{60}^{0.17}D^{0.2}$
[g] Seed et al. 1986: $V_s = 200*SQRT(N_{60})$
[e] Imai and Tonouchi 1982: $G_{max} = 325*N_{60}^{0.68}$
[f] $G_{max} = \rho*Vs^2$

Table B2. SPT correlations for 405 46NE bridge site

					Seed et al. 1983		Seed et al. 1986		Imai & Tonouchi 1982		
Depth	Soil	N_m[b]	γ[c]	σ'_{vo}[d]	V_s[e]		V_s[f]		G_{max}[g]	V_s[h]	
(ft)	Unit[a]	(blows/ft)	(pcf)	(psf)	(ft/sec)	(m/s)	(ft/sec)	(m/s)	(kip/ft^2)	(ft/sec)	(m/s)
0	1	--	120	0	--		--		--	--	
5	1	58	120	600	555.0	169.2	1179.8	359.6	3632	987.2	300.9
10	1	115	120	1200	716.2	218.3	1661.3	506.4	5785	1245.9	379.8
15	1	122	120	1800	784.5	239.1	1711.1	521.6	6022	1271.2	387.5
20	1	67	120	2400	750.5	228.8	1268.1	386.5	4006	1036.8	316.0
25	1	45	120	3000	733.4	223.5	1039.2	316.8	3056	905.6	276.0
30	2	300	120	3600	1050.1	320.1	2683.3	817.9	11104	1726.1	526.1
35	3	140	140	4156	951.4	290.0	1833.0	558.7	6613	1233.3	375.9
38	3	240	140	4389	1060.0	323.1	2400.0	731.5	9540	1481.3	451.5

[a] Soil Units
(1) dense to very dense, brown and gray, gravelly, silty to very silty sand
(2) dense to very dense and hard, gray sandy silt, very silty sand and silty clay
(3) very dense, gray, silty, sand and gravel

[b] SPT blow counts obtained from WSDOT (1991?).

[c] Unit weights obtained from WSDOT (1991?).

[d] Overburden computed using unit weights (WSDOT 1991?).

[e] Ground water level: approximately 33.5 ft

[f] Seed et al. 1983: $V_s = 220*N_{60}^{0.17}D^{0.2}$

[g] Seed et al. 1986: $V_s = 200*SQRT(N_{60})$

[e] Imai and Tonouchi 1982: $G_{max} = 325*N_{60}^{0.68}$

[f] $G_{max} = \rho*Vs^2$

Table B3. SPT correlations for 520 19EN bridge site

					Seed et al. 1983		Seed et al. 1986		Imai & Tonouchi 1982		
Depth	Soil	N_m[b]	γ[c]	σ'_{vo}[d]	V_s[e]		V_s[f]		G_{max}[g]	V_s[h]	
(ft)	Unit[a]	(blows/ft)	(pcf)	(psf)	(ft/sec)	(m/s)	(ft/sec)	(m/s)	(kip/ft^2)	(ft/sec)	(m/s)
0	1	--	120	0	--	--	--	--	--	--	--
5	1	82	120	600	588.2	179.3	1399.4	426.5	4581.2	1108.7	337.9
10	1	57	120	1200	635.6	193.7	1169.6	356.5	3589.4	981.4	299.1
15	1	35	120	1800	634.5	193.4	916.5	279.4	2576.3	831.4	253.4
20	1	48	120	2400	709.1	216.1	1073.3	327.1	3193.5	925.7	282.2
25	2	55	120	3000	758.9	231.3	1148.9	350.2	3503.3	969.6	295.5
30	2	48	120	3444	769.0	234.4	1073.3	327.1	3193.5	925.7	282.2
35	3	200	140	3782	1010.9	308.1	2190.9	667.8	8428.0	1392.3	424.4
40	3	70	140	4170	868.5	264.7	1296.1	395.1	4127.6	974.3	297.0
45	3	100	140	4558	944.8	288.0	1549.2	472.2	5260.5	1100.0	335.3

[a] Soil Units:

(1) dense to very dense, well graded, gray and brown, silty to very silty, gravelly sand with cobbles
in places and is considered glacial till

(2) very stiff to hard, gray, laminated silt, sandy silt and silty clay and is interpreted to be advance
outwash sediments

(3) very dense, sandy gravel and gravelly sand

[b] SPT blow counts obtained from WSDOT (1991?).

[c] Unit weights obtained from WSDOT (1991?).

[d] Overburden computed using unit weights.

[e] Ground water level: approximately 27.5 ft (WSDOT 1991?)

[f] Seed et al. 1983: $V_s = 220*N_{60}^{0.17}D^{0.2}$

[g] Seed et al. 1986: $V_s = 200*SQRT(N_{60})$

[e] Imai and Tonouchi 1982: $G_{max} = 325*N_{60}^{0.68}$

[f] $G_{max} = \rho*Vs^2$

APPENDIX C

Dynamic Response Parameters of Each Bridge

Table C1. Summary of the GM characteristics and the Bridge 405 column response parameters

Earthquake							Regular			Inverse		
Type	GM	PGA (g) FP	PGA (g) FN	Sa FN	Sa FP	Direction	Max. Base Shear (N)	Max. Disp. (m)	Plastic Energy	Max. Base Shear (N)	Max. Disp. (m)	Plastic Energy
Non FD	IZT	0.764	0.773	0.80	0.80	Longi.	2.452E+05	0.0702	5.13E+04	2.618E+05	0.0657	5.48E+04
	IZT	0.764	0.773	2.50	2.50	Transv.	4.104E+05	0.0184	5.13E+04	3.634E+05	0.0175	5.48E+04
	702	0.846	0.942	0.80	0.80	Longi.	2.708E+05	0.0615	5.42E+04	2.621E+05	0.0664	5.36E+04
	702	0.846	0.942	2.50	2.50	Transv.	3.965E+05	0.0183	5.42E+04	3.645E+05	0.0181	5.36E+04
	MOQ	0.668	1.042	0.80	0.80	Longi.	3.126E+05	0.0173	1.70E+05	2.727E+05	0.0714	1.55E+05
	MOQ	0.668	1.042	2.50	2.50	Transv.	2.688E+05	0.0684	1.70E+05	3.624E+05	0.0192	1.55E+05
	SSU	0.725	0.828	0.80	0.80	Longi.	2.523E+05	0.0717	4.85E+04	2.522E+05	0.0791	5.52E+04
	SSU	0.725	0.828	2.50	2.50	Transv.	3.537E+05	0.0188	4.85E+04	3.659E+05	0.0188	5.52E+04
	T71	0.730	0.840	0.80	0.80	Longi.	2.737E+05	0.0701	6.91E+04	2.685E+05	0.0667	1.21E+05
	T71	0.730	0.840	2.50	2.50	Transv.	3.798E+05	0.0199	6.91E+04	3.643E+05	0.0194	1.21E+05
FD (6.5)	BAM	0.647	0.880	0.95	0.69	Longi.	2.748E+05	0.0689	1.92E+04	3.353E+05	0.0903	3.90E+04
	BAM	0.647	0.880	3.12	1.72	Transv.	4.444E+05	0.0224	1.92E+04	2.993E+05	0.0142	3.90E+04
FD (6.0)	F14	0.857	1.015	2.34	0.62	Longi.	2.497E+05	0.0605	1.71E+04	3.237E+05	0.1625	7.76E+04
	F14	0.857	1.015	1.69	2.28	Transv.	3.518E+05	0.0136	1.71E+04	3.061E+05	0.0177	7.76E+04
FD (6.9)	KJM	0.548	0.854	2.00	1.31	Longi.	3.126E+05	0.1087	6.10E+04	3.613E+05	0.2254	1.26E+05
	KJM	0.548	0.854	1.03	1.00	Transv.	2.234E+05	0.0083	6.10E+04	1.210E+05	0.0078	1.26E+05
FD (6.7)	RRS	0.390	0.887	2.12	0.47	Longi.	2.591E+05	0.0495	9.78E+03	3.305E+05	0.1976	7.86E+04
	RRS	0.390	0.887	1.28	1.24	Transv.	2.643E+05	0.0101	9.78E+03	1.764E+05	0.0108	7.86E+04

Earthquake							Regular			Inverse		
Type	GM	PGA (g) FP	PGA (g) FN	Sa FN	Sa FP	Direction	Max. Base Shear (N)	Max. Disp. (m)	Plastic Energy	Max. Base Shear (N)	Max. Disp. (m)	Plastic Energy
FD (6.7)	Sylmar	0.595	0.733	0.79	1.22	Longi.	3.120E+05	0.1151	6.43E+04	2.609E+05	0.0645	1.83E+04
	Sylmar	0.595	0.733	1.30	1.20	Transv.	1.733E+05	0.0102	6.43E+04	1.915E+05	0.0105	1.83E+04
FD (7.6)	T75	0.278	0.314	0.50	0.41	Longi.	2.481E+05	0.0477	2.34E+03	2.663E+05	0.0574	7.91E+03
	T75	0.278	0.314	0.70	0.42	Transv.	1.393E+05	0.0054	2.34E+03	8.702E+04	0.0032	7.91E+03
FD (7.3)	LCN	0.783	0.728	0.71	0.35	Longi.	2.312E+05	0.0374	4.19E+00	2.763E+05	0.0659	8.49E+03
	LCN	0.783	0.728	0.88	1.26	Transv.	2.293E+05	0.0076	4.19E+00	2.184E+05	0.0099	8.49E+03

Table 4.2 Summary of the GM characteristics and the Bridge 520 column response parameters

Earthquake							Regular			Inverse		
Type	GM	PGA (g) FP	PGA (g) FN	S_a FN	S_a FP	Direction	Max Base Shear (N)	Max Disp (m)	Plastic Energy	Max Base Shear (N)	Max Disp (m)	Plastic Energy
Non FD	IZT	0.764	0.773	0.70	0.70	Longi.	2.140E+05	0.0970	2.77E+04	2.212E+05	0.0971	2.92E+04
	IZT	0.764	0.773	2.00	2.00	Transv.	2.097E+05	0.0151	2.77E+04	1.969E+05	0.0123	2.92E+04
	702	0.846	0.942	0.70	0.70	Longi.	2.238E+05	0.0892	2.94E+04	2.161E+05	0.0926	2.72E+04
	702	0.846	0.942	2.00	2.00	Transv.	2.040E+05	0.0142	2.94E+04	1.770E+05	0.0123	2.72E+04
	SSU	0.725	0.828	0.70	0.70	Longi.	2.211E+05	0.0957	2.16E+04	2.211E+05	0.0933	1.23E+04
	SSU	0.725	0.828	2.00	2.00	Transv.	2.237E+05	0.0136	2.16E+04	1.962E+05	0.0119	1.23E+04
	T71	0.730	0.840	0.70	0.70	Longi.	2.266E+05	0.0934	4.35E+04	2.271E+05	0.0953	6.59E+04
	T71	0.730	0.840	2.00	2.00	Transv.	2.046E+05	0.0137	4.35E+04	1.895E+05	0.0141	6.59E+04
FD (6.5)	BAM	0.647	0.880	1.16	0.43	Longi.	2.200E+05	0.0656	4.26E+02	2.707E+05	0.1027	1.88E+04
	BAM	0.647	0.880	2.39	1.78	Transv.	3.065E+05	0.0205	4.26E+02	1.764E+05	0.0118	1.88E+04
FD (6.0)	F14	0.857	1.015	1.69	0.57	Longi.	2.013E+05	0.0625	2.79E+02	2.787E+05	0.1922	5.21E+04
	F14	0.857	1.015	1.94	1.71	Transv.	2.282E+05	0.0118	2.79E+02	1.746E+05	0.0152	5.21E+04
FD (6.9)	KJM	0.548	0.854	2.54	0.89	Longi.	2.449E+05	0.1155	3.47E+04	3.018E+05	0.3140	1.64E+05
	KJM	0.548	0.854	0.98	1.02	Transv.	1.261E+05	0.0070	3.47E+04	8.270E+04	0.0070	1.64E+05
FD (6.7)	RRS	0.390	0.887	2.15	0.38	Longi.	1.935E+05	0.0589	1.52E+01	2.786E+05	0.2206	7.92E+04
	RRS	0.390	0.887	1.20	1.03	Transv.	1.573E+05	0.0083	1.52E+01	9.117E+04	0.0086	7.92E+04
FD (6.7)	Sylmar	0.595	0.733	0.76	1.15	Longi.	2.226E+05	0.0921	1.99E+04	2.161E+05	0.0717	1.53E+03
	Sylmar	0.595	0.733	1.25	1.07	Transv.	1.539E+05	0.0088	1.99E+04	2.648E+05	0.0169	1.53E+03
FD	T75	0.278	0.314	0.34	0.20	Longi.	1.336E+05	0.0346	0.00E+00	1.837E+05	0.0533	0.00E+00

Earthquake							Regular			Inverse		
Type	GM	PGA (g) FP	PGA (g) FN	S_a FN	S_a FP	Direction	Max Base Shear (N)	Max Disp (m)	Plastic Energy	Max Base Shear (N)	Max Disp (m)	Plastic Energy
(7.6)	T75	0.278	0.314	0.67	0.35	Transv.	7.139E+04	0.0042	0.00E+00	4.756E+04	0.0026	0.00E+00
FD (7.3)	LCN	0.783	0.728	0.67	0.33	Longi.	2.157E+05	0.0514	0.00E+00	2.399E+05	0.0749	6.20E+02
	LCN	0.783	0.728	1.21	1.78	Transv.	1.314E+05	0.0065	0.00E+00	1.862E+05	0.0111	6.20E+02

Table C3. Summary of the GM characteristics and the Bridge 90 column response parameters.

Earthquake							Regular			Inverse		
Type	GM	PGA (g) FP	PGA (g) FN	S_a FN	S_a FP	Direction	Max Base Shear (N)	Max Disp (m)	Plastic Energy	Max Base Shear (N)	Max Disp (m)	Plastic Energy
Non FD	IZT	0.764	0.773	0.83	0.83	Longi.	7.638E+05	0.0753	1.96E+05	7.295E+05	0.0609	1.54E+05
	IZT	0.764	0.773	1.68	1.68	Transv.	8.295E+05	0.0300	1.96E+05	8.510E+05	0.0318	1.54E+05
	702	0.846	0.942	0.83	0.83	Longi.	7.640E+05	0.0695	2.28E+05	7.455E+05	0.0641	1.12E+05
	702	0.846	0.942	1.68	1.68	Transv.	8.121E+05	0.0297	2.28E+05	9.084E+05	0.0336	1.12E+05
	MOQ	0.668	1.042	0.83	0.83	Longi.	7.773E+05	0.0753	2.23E+05	7.773E+05	0.0758	2.60E+05
	MOQ	0.668	1.042	1.68	1.68	Transv.	8.166E+05	0.0258	2.23E+05	8.818E+05	0.0298	2.60E+05
	SSU	0.725	0.828	0.83	0.83	Longi.	7.791E+05	0.0702	1.24E+05	8.049E+05	0.0788	1.83E+05
	SSU	0.725	0.828	1.68	1.68	Transv.	7.060E+05	0.0329	1.24E+05	8.788E+05	0.0359	1.83E+05
	T71	0.730	0.840	0.83	0.83	Longi.	7.647E+05	0.0704	1.89E+05	7.537E+05	0.0764	3.25E+05
	T71	0.730	0.840	1.68	1.68	Transv.	7.081E+05	0.0296	1.89E+05	8.605E+05	0.0311	3.25E+05
FD (6.5)	BAM	0.647	0.880	1.18	0.44	Longi.	7.398E+05	0.0466	1.28E+04	7.949E+05	0.0921	1.61E+05
	BAM	0.647	0.880	0.95	0.81	Transv.	6.776E+05	0.0178	1.28E+04	7.070E+05	0.0184	1.61E+05
FD (6.0)	F14	0.857	1.015	1.54	0.58	Longi.	6.674E+05	0.0509	5.74E+04	9.239E+05	0.1274	1.40E+05
	F14	0.857	1.015	2.63	1.69	Transv.	1.142E+06	0.0494	5.74E+04	6.574E+05	0.0314	1.40E+05
FD (6.9)	KJM	0.548	0.854	2.51	0.77	Longi.	7.049E+05	0.0677	1.19E+05	9.454E+05	0.2053	5.29E+02
	KJM	0.548	0.854	2.04	1.51	Transv.	8.997E+05	0.0320	1.19E+05	6.061E+05	0.0366	5.29E+02
FD (6.7)	RRS	0.390	0.887	2.13	0.38	Longi.	6.455E+05	0.0515	2.61E+04	8.586E+05	0.1887	3.81E+04
	RRS	0.390	0.887	1.84	0.91	Transv.	9.938E+05	0.0333	2.61E+04	5.770E+05	0.0186	3.81E+04
FD	Sylmar	0.595	0.733	0.74	1.13	Longi.	7.749E+05	0.0783	1.09E+05	7.016E+05	0.0623	7.12E+04

Earthquake							Regular			Inverse		
Type	GM	PGA (g) FP	PGA (g) FN	S_a FN	S_a FP	Direction	Max Base Shear (N)	Max Disp (m)	Plastic Energy	Max Base Shear (N)	Max Disp (m)	Plastic Energy
(6.7)	Sylmar	0.595	0.733	1.22	2.20	Transv.	7.307E+05	0.0241	1.09E+05	1.072E+06	0.0383	7.12E+04
FD (7.6)	T75	0.278	0.314	0.33	0.20	Longi.	6.680E+05	0.0402	4.18E+03	6.816E+05	0.0461	1.48E+04
	T75	0.278	0.314	0.67	0.68	Transv.	4.080E+05	0.0125	4.18E+03	4.729E+05	0.0132	1.48E+04
FD (7.3)	LCN	0.783	0.728	0.59	0.30	Longi.	6.988E+05	0.0462	6.64E+03	6.883E+05	0.0439	7.95E+03
	LCN	0.783	0.728	0.64	0.42	Transv.	4.829E+05	0.0102	6.64E+03	4.156E+05	0.0092	7.95E+03